Aalto-yliopisto
Insinööritieteiden
korkeakoulu

Mikko Tuohino

Application of the NTNU Frozen and Unfrozen Soil model to modelling effects of freeze-thaw on low-volume roads

Thesis submitted for examination for the degree of Master of Science in Technology.

Espoo 20.09.2019
Supervisor: Assistant Professor Wojciech Solowski
Advisors: D. Sc. Ayman Abed, M. Sc. Kirsi Koivisto,
D. Sc. Xiaoqin Lei

Aalto University
School of Engineering

Aalto University, P.O. BOX 11000, 00076 AALTO
www.aalto.fi

Abstract of master's thesis

Author Mikko Tuohino

Title of thesis Application of the NTNU Frozen and Unfrozen Soil model to modelling effects of freeze-thaw on low-volume roads

Degree programme Master's Programme in Geoengineering

Major/minor Geoengineering **Code** ENG23

Thesis supervisor Assistant Professor Wojciech Solowski

Thesis advisor(s) D. Sc. Ayman Abed, M. Sc. Kirsi Koivisto, D. Sc. Xiaoqin Lei

Date 20.09.2019 **Number of pages** 74 **Language** English

Abstract

Freezing and thawing of soil must be considered in design of infrastructure in seasonally cold regions. Cycles of freezing-thawing can affect the performance of thinly paved low-volume roads especially severely, causing frost heave during the winter and thaw weakening in the spring.

Freezing of soils entails many complex phenomena, necessitating advanced analysis tools such as numerical modelling. This Master's thesis studies the numerical modelling of deformation of low-volume road structures caused by freezing and thawing with the Frozen and Unfrozen Soil model for the finite element program Plaxis 2D. The research was carried out as a literature review, a laboratory study and by modelling a case study of frost heave of a road on dry crust clay in Vesilahti, Finland.

The Vesilahti test site monitoring results of frost heave, temperature and groundwater level were used in this study to simulate the frost heave of a pavement with shallow structural layers. In addition, soil sampling and laboratory tests were performed for the Vesilahti dry crust clay properties at the Aalto University. These were combined to simulate the frost heave and thaw settlement measured on the site. The road deformation at the measurement time intervals was matched qualitatively well and the model performed mostly according to expectations. The complexity and the black box nature of the model implementation make evaluation of calculation errors tough and time-consuming however, and in its current state the model is too complex for standard infrastructure design use.

Keywords freeze-thaw of soils, numerical methods, NTNU Frozen and Unfrozen Soil model, low-volume roads, pavement deformations

Aalto-yliopisto
Insinööritieteiden
korkeakoulu

Aalto-yliopisto, PL 11000, 00076 AALTO
www.aalto.fi

Diplomityön tiivistelmä

Tekijä Mikko Tuohino

Työn nimi NTNU Frozen and Unfrozen Soil -mallin käyttö jäätymissulamisen vaikutusten mallintamiseen alemman tieverkon teissä

Koulutusohjelma Master's Programme in Geoengineering

Pää-/sivuaine Geotekniikka **Koodi** ENG23

Työn valvoja Apulaisprofessori Wojciech Solowski

Työn ohjaaja(t) TkT Ayman Abed, DI Kirsi Koivisto, TkT Xiaoqin Lei

Päivämäärä 20.09.2019 **Sivumäärä** 74 **Kieli** englanti

Tiivistelmä

Suunniteltaessa infrastruktuuria kausittaisesti kylmillä alueilla täytyy ottaa huomioon maan jäätyminen ja sulaminen. Jäätymissulamissyklit voivat vaikuttaa ohutpäällysteisten alemman tieverkon teiden toimintaan erityisen vakavasti, aiheuttaen routanousua talvella ja kelirikkoa keväällä.

Maan jäätyminen käsittää monia monimutkaisia ilmiöitä, vaatien edistyneitä analyysimenetelmiä, kuten numeerista mallintamista. Tämä diplomityö tutkii jäätymisen ja sulamisen aiheuttaman muodonmuutoksen numeerista mallintamista alemman tieverkon tierakenteissa Frozen and Unfrozen Soil -mallilla Plaxis 2D -elementtimenetelmäohjelmassa. Tutkimus toteutettiin kirjallisuusselvityksenä, laboratoriotutkimuksena ja mallintamalla tapaustutkimuksena Vesilahdella sijaitsevan kuivakuorisavelle perustetun tien routanousu.

Vesilahden koekohteen routanousu-, lämpötila- ja pohjavesiseurantatuloksia käytettiin tässä tutkimuksessa kevytrakenteisen tien routanousun mallintamiseen. Lisäksi suoritettiin näytteenotto ja laboratoriokokeita maaparametrien määrittämiseksi Aalto-yliopistossa. Nämä yhdistettiin tien mitatun routanousun ja sulamispainuman mallintamiseksi. Tien muodonmuutos mittausajankohtina toisinnettiin laadullisesti hyvin ja mallin tulokset vastasivat pääosin odotettua. Mallin monimutkaisuus ja toteutuksen musta laatikko -luonne tekevät kuitenkin laskentavirheiden arvioinnista vaikeaa ja aikaa vievää, ja mallin nykytilassa se on liian monimutkainen tavalliseen infrastruktuurin suunniteluun.

Avainsanat maan jäätyminen ja sulaminen, numeeriset menetelmät, NTNU Frozen and Unfrozen Soil -malli, alemman tieverkon tiet, päällysteen muodonmuutokset

Preface

This study analyses the use of the Frozen and Unfrozen Soil model in simulation of frost heave in low-volume roads. The work was performed at Aalto University under supervision of Assistant Professor Wojciech Solowski. The study was financially supported by Aalto University and Ramboll Finland Oy.

In the thesis guidance group participated:

- *Wojciech Solowski, Aalto University (thesis supervisor)*
- *Ayman Abed, Aalto University (thesis advisor)*
- *Kirsi Koivisto, Ramboll Finland Oy (thesis advisor)*
- *Xiaoqin Lei, Aalto University (thesis advisor)*
- *Juha Forsman, Ramboll Finland Oy*
- *Henry Gustavsson, Aalto University*

I would like to thank all participants of the guidance group for their help and support with this research. Also, thanks to Matti Ristimäki for assisting me in the sampling and laboratory testing of the Vesilahti clay. Special thanks to my wife Irene, my parents, my brother and my friends for their support during the thesis process and my studies. All good things come to an end, even a Master's thesis.

Espoo, 20.09.2019

Mikko Tuohino

Contents

Symbols

a_j		Coefficients for the melting pressure equation
b		Empirical parameter based on the grain size distribution
$\boldsymbol{b}$	N	Body force
b_j		Exponents for the melting pressure equation
c_s	J/kg/K	Specific heat capacity
d_{cl}	mm	Particle size limit of clay
d_g	mm	Geometric mean of the soil particle diameter
d_{sa}	mm	Particle size limit of sand
d_{si}	mm	Particle size limit of silt
e		Void ratio
e_0		Initial void ratio
E_f	N/m^2	Frozen soil Young's modulus
$E_{f,ref}$	N/m^2	Frozen soil Young's modulus at a reference temperature
$E_{f,inc}$	$N/m^2/K$	Rate of change in Young's modulus with temperature
F_1		Yield criterion due to variation of solid phase stress
F_2		Yield criterion due to variation of cryogenic suction
G	N/m^2	Soil shear modulus
G_0	N/m^2	Soil shear modulus in unfrozen state
g_n		Fitting parameter of rate of water extraction
g_a		Fitting parameter related to air entry value of soil
g_l		Fitting parameter for relative soil permeability
K	N/m^2	Soil bulk modulus
K_W	N/m^2	Water bulk modulus
k	m/s	Hydraulic conductivity
k_{sat}	m/s	Unfrozen saturated hydraulic conductivity
k_t		Rate of change in apparent cohesion with suction
L	J/kg	Latent heat of fusion for water
M		Slope of the critical state line
m		Yield surface parameter
m_{cl}		Clay mass fraction
m_{sa}		Sand mass fraction
m_{si}		Silt mass fraction
n		Porosity
p^*	N/m^2	Solid phase mean stress
p_{at}	N/m^2	Atmospheric pressure
p_c^*	N/m^2	Reference stress
p_{ice}	N/m^2	Ice pressure
p_{ref}	N/m^2	Reference pressure
p_w	N/m^2	Pore water pressure
p^*_y	N/m^2	Pseudo preconsolidation stress for a frozen soil
$(p^*_{y0})_{in}$	N/m^2	Initial preconsolidation stress for unfrozen soil
p^*_{y0}	N/m^2	Preconsolidation stress for unfrozen soil
$\boldsymbol{Q}$	$W/m/m^3$	Heat flux per unit volume
Q_1		Plastic potential function
q^*	N/m^2	Deviatoric stress
r		Coefficient related to the maximum soil stiffness
s_c	N/m^2	Cryogenic suction
$s_{c,seg}$	N/m^2	Segregation threshold
$(s_{c,seg})_{in}$	N/m^2	Initial segregation threshold
S_{ice}		Ice saturation

S_{res}		Residual saturation
S_{sat}		Saturation in saturated conditions
S_{uw}		Unfrozen water saturation
SSA	m^2/g	Specific surface area
t	s	Time
T	K	Temperature
T_f	K	Freezing/melting temperature
T_{ref}	K	Reference temperature
$\boldsymbol{v}_w$	m/s	Water velocity relative to the soil skeleton
dV	m^3	Change in volume
w_u		Unfrozen water content
z	m	Depth
α	1/K	Thermal expansion coefficient
α		Constant parameter for freezing/thawing temperature
β	m^2/N	Rate of change in soil stiffness with suction
$d\epsilon$		Increment of strain
$d\epsilon^m$		Increment of strain due to solid phase stress variation
$d\epsilon^{me}$		Increment of elastic strain due to solid phase stress variation
$d\epsilon^{mp}$		Increment of plastic strain due to solid phase stress variation
$d\epsilon^p$		Increment of plastic strain
$d\epsilon^s$		Increment of strain due to suction variation
$d\epsilon^{se}$		Increment of elastic strain due to suction variation
$d\epsilon^{sp}$		Increment of plastic strain due to suction variation
$d\epsilon_q^e$		Increment of elastic shear strain
$d\epsilon_v^e$		Increment of elastic volumetric strain
γ		Plastic potential parameter
γ_{sat}	N/m^3	Saturated unit weight
γ_{unsat}	N/m^3	Unsaturated unit weight
κ		Elastic compressibility coefficient for frozen soil
κ_s		Elastic compressibility coefficient for suction variation
κ_0		Elastic compressibility coefficient for unfrozen soil
λ		Elasto-plastic compressibility coefficient for frozen soil
λ	W/m/K	Thermal conductivity
λ_0		Elasto-plastic compressibility coefficient for unfrozen soil
$d\lambda_1$		Plastic multiplier regarding the loading-collapse yield surface
$d\lambda_2$		Plastic multiplier regarding the grain segregation yield surface
λs		Elasto-plastic compressibility coefficient for suction variation
λ_r		Unfrozen water saturation fitting parameter
ν_f		Frozen soil Poisson's ratio
$\boldsymbol{\Phi}$	J/m^3	Heat content per unit volume
ρ_b	kg/m^3	Bulk density of unfrozen soil
ρ_r		Unfrozen water saturation fitting parameter
ρ_s	kg/m^3	Specific gravity of unfrozen soil
$\boldsymbol{\sigma}$		Net stress
$\boldsymbol{\sigma^*}$		Solid phase stress
σ_g		Geometric standard deviation
θ_{ice}		Volumetric ice content
θ_{sat}		Volumetric water content of fully saturated soil
θ_{uw}		Volumetric unfrozen water content
θ_w		Volumetric water content

Abbreviations

BBM	*Barcelona Basic model*
MCC	*Modified Cam Clay model*
NTNU	*Norwegian University of Science and Technology*
THM	*Thermo-Hydro-Mechanical*
TUT	*Tampere University of Technology*
USDA	*United States Department of Agriculture*

1 Introduction

Considering the effects of frost in infrastructure design is extremely important in cold, seasonally frozen regions. With the onset of climate change, freezing-thawing cycles are likely to become even more common in Finland, presenting further challenge for low-volume roads that are susceptible to frost effects.

Freezing and thawing soils present complex geotechnical problems requiring simultaneous analysis of their thermal, hydrological and mechanical behavior. This makes numerical methods a necessity for an in-depth analysis of frozen soils, as field studies and laboratory tests are often very expensive and time-consuming endeavors.

Past decades have seen much research on frozen soils and development of comprehensive constitutive models for frozen soils has gained speed in recent years. One prospect is the Frozen and Unfrozen Soil model (Ghoreishian Amiri et al., 2016b) of Norwegian University of Science and Technology (NTNU) which is available as a user-defined model in the common geotechnical finite element program Plaxis 2D. The NTNU model for fully saturated, isotropic and elasto-plastic soils is based on the Barcelona Basic model (BBM) and can replicate many features of frozen soils, including frost heave and thaw settlement.

In the initial publication by Aukenthaler (2016) the NTNU model has been tested on pipe frost heave and footing settlement problems and initial model parameters have been defined for clay, silt and sand soil types. However, pavement deformations have not previously been modelled with the NTNU model. Frost action related damage is common in low-volume roads in seasonally frozen areas, so being able to comprehensively analyze frost related behavior of pavements with the most up-to-date tools is important for infrastructure design practice.

The objective of this thesis is to study the deformation of pavements using the NTNU Frozen and Unfrozen Soil model. The subject will be approached with the following research questions:

- What kind of experimental data would be most suitable for deriving clay model parameters?
- What kind of uncertainties or difficulties are there related to model parameter definition for clays?
- How does the model perform in replication of experimental data based on the selected parameters?
- How does the pavement deform upon freezing and thawing based on simulations with the NTNU model?
- What are the factors affecting the behavior of pavement upon freezing and thawing?
- What factors have the most significant influence on the pavement behavior during the thaw season?

The thesis will detail the frozen ground theory and investigate how frost heave and thaw affect settlements. It will also describe THM coupled analysis and constitutive models for frozen soils theoretically.

A case study using site measurement data from road 2983 in Vesilahti, Finland will be used to verify performance of the model and chosen parameters.

The analysis will focus on deformation of paved low-volume roads on clay subgrade. It is assumed that the granular road material does not take part in frost heave. The road subgrade is assumed to be fully saturated and the road structure partially saturated. The road construction materials modelled will be common granular Finnish road construction materials. Traffic loading is modelled as an even, concentrated standard load to represent heavy truck axial load. Dynamic loading is not modelled.

Other constitutive models in addition to the NTNU model are briefly discussed in the Numerical modelling of freezing and thawing section of the thesis, but they are not applied in this study.

2 Frost

2.1 Frozen ground

Andersland and Ladanyi (2004) define frozen ground when soil (or rock) reaches temperature below 0 °C, the freezing point of clear water. The principal heat transportation mechanism in soil is conduction (Saarelainen, 1992). According to Andersland and Ladanyi (2004) ice in coarse soil acts as a bonding agent that holds adjacent soil particles together, increasing strength and decreasing permeability of frozen soil. The ice in a frozen ground can be found in different forms ranging from coating on individual soil particles to lenses of a few centimeters thickness and massive deposits of hundreds of meters in permafrost areas (Andersland and Ladanyi, 2004).

Frozen ground can be divided top-down into zones of frozen soil, ice lenses, frozen fringe and unfrozen soil, which is represented in Figure 1. The frozen fringe is a region, where soil pores are partially filled with ice, impeding flow of water. In the frozen fringe, liquid water exists in an equilibrium state with the ice at a temperature below the freezing point of water. Ice lenses are clear ice interlayered in the surrounding soil. The soil skeleton in the frozen fringe will expand when the pressure in the ice exceeds the soil overburden pressure and the required pressure to initiate separation in the skeleton, and a new ice lens can form in the residual void. During slow freezing the temperature profiles in frozen fringe and unfrozen soil are near steady state (Andersland and Ladanyi, 2004).

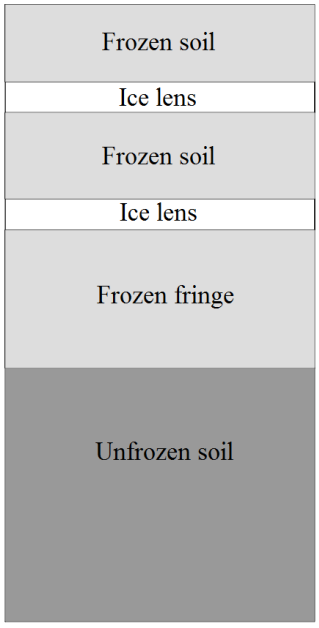

Figure 1 Schematic representing different parts of frozen soil (after Thomas et al., 2009).

When the frost front advance and temperature decrease are rapid, the heat flow is unsteady and the permeability of the frozen fringe will decrease, reducing water flow into the ice lens. This variation of heat and water flow results in finer ice lenses near the surface where freezing is fast and in thicker lenses at greater depths, where the temperature gradient is smaller (Andersland and Ladanyi, 2004).

The physical properties of frozen ground depend on the freezing and thawing process and the time-dependent temperature variation. The freezing process happens when the water in soil voids freezes as temperature is lowered below the freezing point. Thawing means

melting of the accumulated ice with rising temperature and is usually associated with thaw weakening and thaw settlement. Temperature variation in ground depends on the air and ground surface temperatures, heat flow from the interior of earth and soil thermal properties (Andersland and Ladanyi, 2004).

The freezing process is dependent on the soil type. For sand or gravel, the pore water freezes in situ causing volume expansion. Water expands by 9 % when freezing, but in sand or gravel freezing does not always lead to the expansion of voids by 9 %, as water may also expel during freezing in partly saturated conditions due to the large void size of these soils (Andersland and Ladanyi, 2004).

For silt and silty sand, the process depends on the rate of temperature change. Rapid cooling causes in situ pore water freezing. However, more gradual cooling gives time for water to flow into the frozen fringe, resulting in the ice condensing into ice lenses accumulating parallel to the freezing surface. As such, natural frozen silt or silty sand usually consists of a mix of layers of frozen soil and ice. Ice lenses only develop in fine grained soils, where continuous water flow to the frozen fringe is possible. In clays the formation of ice lenses is reduced due to the low permeability limiting the water migration (Andersland and Ladanyi, 2004).

2.2 Frost heave

It has been observed that frozen soils expand in volume far more than what could be accounted for with the water phase change. With normal soil void ratios and water content, an overall expansion of 2 to 3 % of original soil mass should be expected, corresponding to around 2 to 3 centimeters vertical expansion, but vertical expansion of 20 to 50 centimeters is quite common in low-volume roads. This major additional expansion called frost heave results from the migration of water from the unfrozen soil below to the frozen fringe and the formation of distinct ice lenses in the soil, which is known as ice segregation (Andersland and Ladanyi, 2004).

Frost heave will occur, if the following factors are present: the soil is frost-susceptible, the ground is frozen and there is a sufficient source of water to initiate and keep up the growth of ice lenses. Freezing air temperature causes a thermal gradient in the soil that induces upward heat flow. Freezing in the soil is then initiated as the heat is extracted into the air and ice crystals start coalescing into ice lenses. When there is water available from the unfrozen soil below, the ice lenses continue growing and the soil above is displaced forcing the soil grains out of contact with each other (Anderson et al., 1984).

Soils are classified to frost-susceptible and non-frost-susceptible soils. Frost-susceptible soils tend to increase in volume during freezing, which in this case manifests as heave of soil surface. There are many criteria for frost susceptibility, but most common is the grain-size distribution. Normally frost-susceptible soils are fine-grained, but in laboratory conditions ice segregation can be produced in even coarse-grained gravels (Saarelainen, 1992).

The capillary flow of pore water up toward the lower temperature ice-water interface results from the cryogenic suction induced by thermal and pressure gradient in the freezing soil. This induced force causing pore water flow can be determined based on thermodynamics with the Clausius-Clapeyron equation (2). Ice segregation occurs if a threshold value of cryogenic suction or pore pressure depending on the definition is exceeded and

a new ice lens forms in the direction of heat removal (Thomas et al., 2009; Aukenthaler, 2016).

Frost heave is usually uneven as the variability in underlying soils permeability results in varying available water flow (Andersland and Ladanyi, 2004). Other factors causing uneven frost heave are differences in the freezing process due to the variability of soil and environmental conditions, the variable frost susceptibility characteristics of subgrade soil and the variability of the ground thermal conditions and topography or geometry of the surface and earth structure (Dore and Zubeck, 2009). Thus, road structures in the frost-heave zone will usually experience surface roughness and bumps and in some cases even frost heave cracking. In moderate winter climates, pavement surface frost heave of 15 centimeters is not uncommon (Andersland and Ladanyi, 2004).

2.3 Thaw

On soil thawing, the ice melts and the soil skeleton adapts to a new equilibrium void ratio, causing settlement and the soil stiffness is reduced as shown in Figure 2. The altered water retaining capacity of the soil skeleton may be exceeded by the melting water, and the water content of the soil increases. In the fine-grained soils with low permeabilities, the excess pore water pressure may develop until drainage is completed. If the thawing happens faster than the melted water can drain, the soil can be transformed into a slurry of soil and water, unable to support almost any load at all. Along with this thaw weakening, volume change will also result from the phase change of water and from the flow of the excess water out of the soil. This is referred to as thaw settlement (Andersland and Ladanyi, 2004; Kangas et al., 2000).

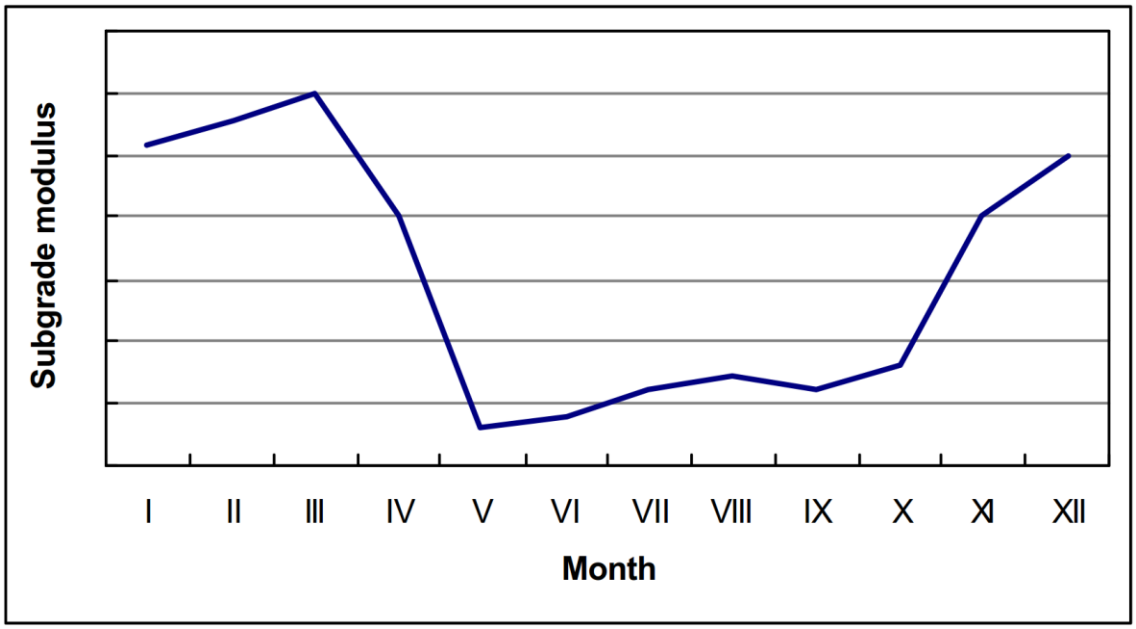

Figure 2 General representation of seasonal subgrade stiffness modulus variation in Finland (Kangas et al., 2000).

Usually the moisture content of frozen silts and clays exceeds their natural unfrozen moisture content considerably. When these soils are thawed under drained conditions, they will undergo volume change and settlement under their own weight. The total thaw settlement comes from three factors: phase change, settlement under own weight and settlement under applied load. As such, consideration of thawing is very important in designing road structures (Andersland and Ladanyi, 2004).

Frost action describes the detrimental effect of the combination of frost heave during downward movement of the frozen fringe followed by thaw weakening as the soil defrosts. Major engineering concerns regarding pavements are the damaging effects of ice lens growth at the frozen fringe, heave of pavement surface and thaw weakening of subgrade. The pavement is most susceptible to damage during the thaw of subgrade (Andersland and Ladanyi, 2004).

2.4 Seasonally frozen ground

Cold regions may be defined in a number of ways, but in the context of frozen ground, the most important factors are temperature and frost penetration. The 0 °C isotherm (the depth of freezing) of mean temperature during the coldest month of a year in the Northern Hemisphere is one definition for the southern boundary of cold regions. A similar and generally accepted criterion for the southern boundary is the seasonal frost penetration of 300 mm once in 10 years. The cold regions are divided into continuous and discontinuous permafrost and seasonally frozen ground. The division between seasonally frozen and discontinuous permafrost is the -5 °C isotherm at the depth of zero annual temperature amplitude (Andersland and Ladanyi, 2004). Finland mostly lies within the seasonally frozen region, except for a few locations of discontinuous permafrost in northern Lapland, which is illustrated in Figure 3 (Seppälä, 1997).

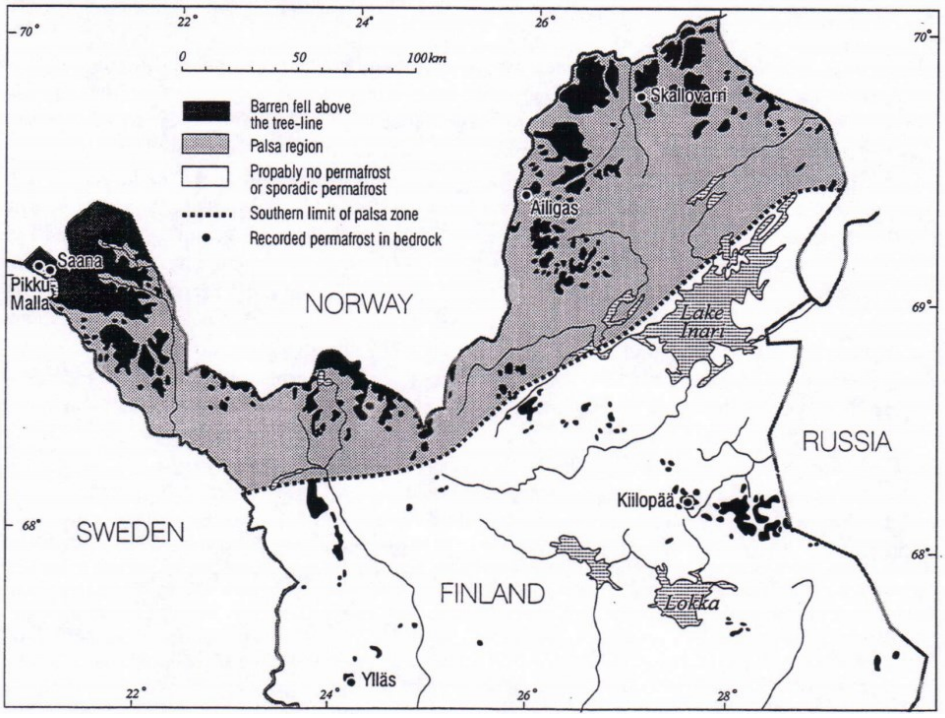

Figure 3 Potential permafrost locations in northern Finland (Seppälä, 1997).

2.5 Frost depth

The layer of ground where temperature fluctuates above and below 0 °C during a year is defined by Andersland and Ladanyi (2004) as the active layer, which can also be called seasonally frozen ground, seasonal frost or annually thawed layer. Depth of the active layer or depth of frost depends on the local winter temperatures, soil type and moisture content, cover by surface vegetation, structures and snow, drainage conditions and slope of the soil (Andersland and Ladanyi, 2004). Maximum frost depths occurring in 50 years used in Finnish road design are shown in Figure 4 (Liikennevirasto, 2018).

In geotechnical engineering. foundations are generally built below frost depth to mitigate adverse effects of freezing ground. Most state highway agencies recommend using non-frost-susceptible granular materials to mitigate effects of the freeze and thaw on pavements (Rajaei and Baladi, 2015).

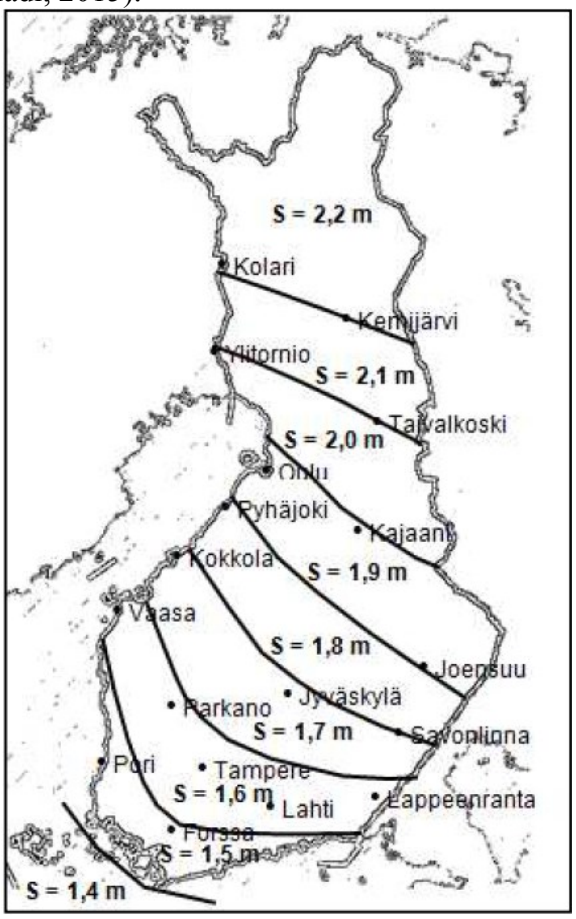

Figure 4 Design frost depths for Finnish roads (Liikennevirasto, 2018).

3 Numerical modelling of freezing and thawing

3.1 THM coupled analysis of frozen soil

THM coupled analysis of frozen soil involves complex simultaneous thermal, hydraulic and mechanical processes as the ground freezes and thaws as illustrated in Figure 5. Nishimura et al. (2009) used as an example the phase change of pore fluid caused by temperature variation, which changes the hydraulic regime of the freezing soil, which induces mechanical deformation. Conversely changes in the hydraulic and mechanical state of the soil also affect the thermal state via advection and changes in the ice and water content (Nishimura et al., 2009).

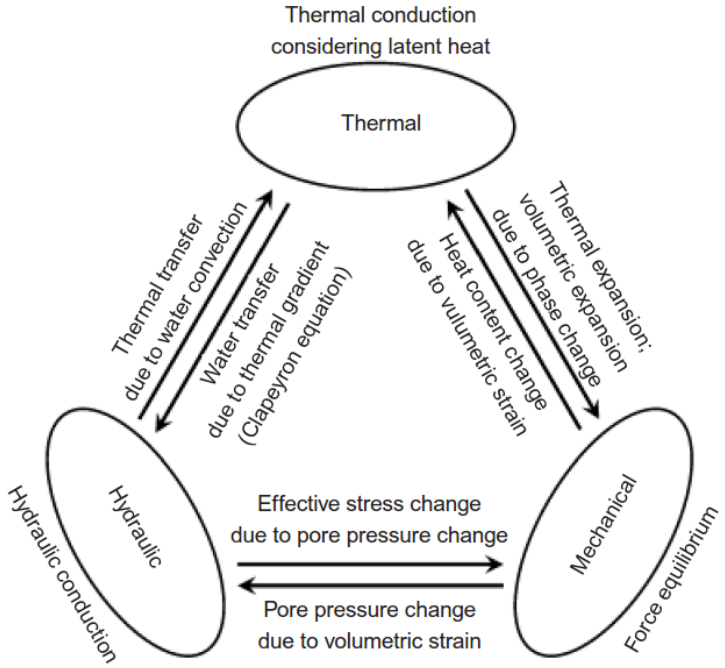

Figure 5 THM coupled interaction in frozen soils (Thomas et al., 2009).

The basic algorithms for simulating multiple physical processes such as thermal, hydraulic and mechanical are one-way, loose and fully coupled (Minkoff et al., 2003). The earliest method is the one-way coupling where equations for processes are solved independently in each step and information is passed as input to other processes without reciprocally returning information back to the other processes. This is easy and computationally less costly and provides good results for problems where one process dominates the others. One-way coupling does not take into account the mutual effect of the processes on each other. Full coupling by simultaneously solving a set of equations yields best results in problems where processes are linked, but it is computationally costly and can result in a huge matrix for the coupling equations. Loose coupling is a middle solution between these two, as equations for different processes are solved independently and information is passed sequentially between the processes. Results are not as accurate as fully coupled method, but calculation is much faster (Zhang, 2014).

Early research (Harlan, 1973, Jame and Norum, 1980) into THM modelling freezing and thawing of porous media such as rock, concrete and soil built the fundamental governing equations and numerical methods required to solve the partial differential equations. Lack of adequate computational tools slowed the initial progress into practice and from the late 1990s onward the THM method has become widely used both in research and practice

(Zhang, 2014). According to Nishimura et al. (2009) numerical methods are practically a must-use tool to solve THM coupled problems due to the non-linearity of the governing equations of frozen soils (Nishimura et al., 2009).

3.2 Constitutive models for frozen soils

Ghoreishian Amiri et al. (2016b) stated in their study that constitutive modelling of frozen soils has been tightly linked with finding correct stress measures to describe the stress-strain behavior of frozen soils. Total stress-based models have been widely used and most historic models for frozen soils have utilized total stress-based mechanical approaches (Nishimura et al., 2009). The total stress-based approaches have however proven to be unable to simulate deformation under varying ice content and temperature in freezing and thawing. Additionally, the effect of unfrozen water presents significant difficulties for these models in describing soil behavior (Ghoreishian Amiri et al., 2016b).

Effective stress-based models have been implemented with different definitions of pore pressure. Some (Li et al., 2008, Nicolsky et al., 2008) have used a combination of unfrozen water and ice pressure, and some (Nixon, 1991, Thomas et al., 2009) have switched between water and ice pressure in partially and fully-frozen states (Ghoreishian Amiri et al., 2016b). Issues in representing change of pore pressure due to phase change of freezing water have risen with these models and various approaches have been introduced to counter this. Thomas et al. (2009) for example assume that in partially-frozen soil the pore ice is not continuous and is unable to exert mechanical pressure, but in a fully-frozen soil pore ice is continuous and pore pressure in essence represents the mechanical pressure exerted by ice (Thomas et al., 2009).

The two-stress-state-variable approach by employing net stress and cryogenic suction was first proposed by Nishimura et al. (2009). In their model the increase of ice pressure results in zero or negative net mean stress, causing grain segregation and softer behavior of soil. In unfrozen state the model reduces to the effective stress-based critical state model similar to Modified Cam-Clay model, allowing simulation of thaw consolidation (Nishimura et al., 2009, Ghoreishian Amiri et al., 2016b). The NTNU Frozen and Unfrozen Soil model studied in this thesis is based on this approach by implementing solid phase stress and cryogenic suction as the two stress state variables. These models differentiate between the water and ice pressure in the equilibrium equation by using the Clausius-Clapeyron equation (2) to determine the balance between the pressures.

4 Pavement deformation due to frost action

4.1 Pavement deterioration mechanisms

According to Dore and Zubeck (2009), main deterioration mechanisms for pavements in cold regions can be divided into those acting on the bituminous materials and those acting on the unbound structural layers and subgrade soil. Mechanisms acting on bituminous materials are thermal cracking, fatigue, crack deterioration, rutting, aging, disintegration of pavement and potholes. Mechanisms acting on unbound layers and subgrade soils are differential volume change by frost heave and bearing capacity loss due to spring thaw, which are described in the following chapter 4.2, and frost destructuration of sensitive clays (Dore and Zubeck, 2009).

Thermal cracking is often divided into low temperature cracking and thermal fatigue cracking. Low temperature cracking occurs when temperature quickly decreases below -16 to -35 °C and thermal stresses in the pavement exceed its tensile strength. For low temperature cracking to happen the decrease of temperature needs to be sufficiently fast and large, and the bituminous layer must be restricted from contracting. Thermal fatigue cracking is more common in regions where such low temperatures do not occur, since it happens due to daily temperature cycle (Dore and Zubeck, 2009).

Fatigue is one of the most common pavement distress forms, which occurs due to repeated application of tensile strains less than the tensile strength of the pavement. Microscopic flaws in the bituminous layer grow and concentrate under load repetitions, finally manifesting as visible flaws of cracks. Effect of fatigue is aggravated by poorly drained and thus weakened pavement, which is an important factor in spring thaw weakening discussed in chapter 4.2 (Dore and Zubeck, 2009).

Cracks initiated by other damage mechanisms accelerate pavement deterioration. Layer stiffness decreases in proximity of the crack as it allows water to flow through it, weakening the unbound layers. Secondary cracks are initiated due to weakened state of the pavement and traffic load repetitions cause spalling and widening of the crack faces (Dore and Zubeck, 2009).

Rutting means depression of wheel paths as the result of traffic loads. The layer under the traffic load compresses and plastic flow begins: bituminous material moves to the sides of the wheel path forming upheavals. Rutting poses a risk to traffic safety because of its effect on lateral maneuverability of vehicles and possibility of hydroplaning due to water ponding in the depression. Ruts harm the pavement structural capacity as they decrease layer thickness and change their properties. Rutting in cold regions has a few sources. Rutting of the bituminous layer is caused either by permanent deformation of the layer as described above or by studded tire wear. Studded tire rutting happens as the studs scratch and detach particles from the surface. Rutting in unbound layers or in the subgrade usually happens due to spring thaw weakening and compression of these layers (Dore and Zubeck, 2009). Effect of rutting, fatigue and cracking is illustrated in Figure 6.

Figure 6 Rutted road, where pavement has also suffered fatigue and cracked around ruts (Saarenketo et al., 2012).

Aging hardens bituminous material and makes it brittle (Dore and Zubeck, 2009). It happens due to chemical processes in the bituminous layer, evaporation of volatile components, exuding or separation of the bitumen from cements and physical hardening due to reorganization of the binder microstructure (Johansson et al., 1998). Aging improves resistance against rutting due to plastic deformation, but makes the material more susceptible to cracking, potholes and wear by studded tires (Dore and Zubeck, 2009).

Disintegration means breakup of pavement structure. It can take the form of raveling, stripping or potholes. Raveling happens from top down as binder separates from aggregate and particles come loose on the surface. Stripping is the loss of bond in the aggregate and cement in presence of moisture and typically progresses upwards from bottom (Roberts et al., 1996).

Potholes are circular or elongated cavities resulting from local disintegration of the pavement surface in presence of breaches in the surface, water and traffic load. They are extreme manifestations of pavement deterioration such as cracking and raveling. Damage in pavement surface with water weakening the underlying structure and redistributing loads causes drastic increase in the disintegration process and formation of potholes (Dore and Zubeck, 2009).

Cryogenic suction causes intense stress in frost-susceptible subgrade soils. Undisturbed sensitive clays that have not been previously subjected to frost action are thus likely to be mechanically altered. Stresses induced by cryogenic suction break the cementation between clay particles resulting in reduction of volume and moisture content consolidating them (Dore and Zubeck, 2009). Roy et al. (1995) have reported in such clays a 30 % reduction of volume and moisture content in the first freeze-thaw cycle and an additional 6 % reduction in volume during subsequent cycles (Roy et al., 1995).

4.2 Effects of freezing and thawing on pavement deformations

In cold regions pavements are seasonally exposed to a significant variation of temperature and moisture conditions. During winter the pavement freezes and frost heave can occur, and during spring the pavement thaws and both settles and weakens. The mechanical properties of pavement are greatly affected by these changes (Simonsen, 1999). During cold periods frost penetrates pavement materials and subgrade soil. Frost causes pore water to expand and can cause ice segregation in the unbound granular pavement materials and frost heave on the surface, though these are generally insignificant in comparison to natural subgrade soil. The unbound layers may however become looser. When the freezing front reaches the subgrade, water begins to be sucked up and forms ice lenses, causing notable frost heave (Dore and Zubeck, 2009).

In winter the stiffness of unbound road layers is increased due to a bonding effect of pore ice and ice lensing, and the stiffness of bituminous layers is increased due to stiffening of the binder. The increase of overall bearing capacity of pavement during winter can be beneficial, but the functional performance of the pavement may suffer due to uneven frost heave and pavement cracking (Simonsen, 1999). Uniform frost heave is not damaging for pavement, but as noted before, uneven frost heave can damage the pavement and cause major surface roughness and driving discomfort during winter (Dore and Zubeck, 2009).

Variations of thermal conditions on the transverse section of the pavement structure can cause frost heave cracking. Snow on the sides of the road decreases frost penetration so frost penetration at the center of the pavement structure is much deeper. As frost heave is dependent on the frost penetration, this causes differential heave along the transverse section that manifests as a bending moment and tensile stresses on the bituminous surface, cracking the pavement longitudinally as represented in Figure 7. This usually does not initially affect the user service performance of the pavement, but can be highly detrimental to the structural performance of the road as water seeps through the cracked surface into the pavement structure, exposing it to further damage in the future (Dore and Zubeck, 2009).

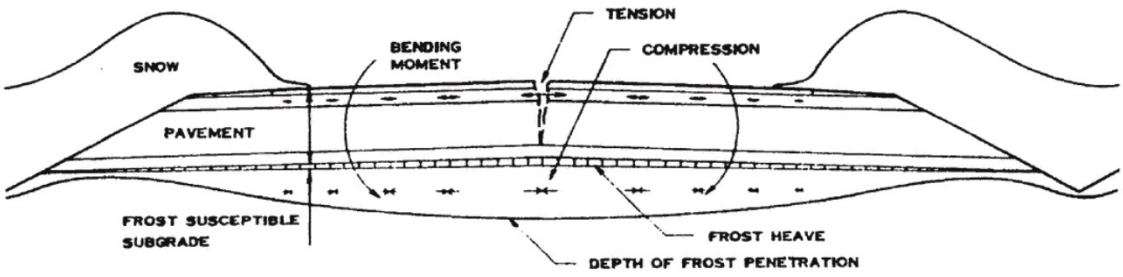

Figure 7 Longitudinal cracking of pavement due to differential frost heave (Nordal and Refsdal, 1989).

During spring thaw, the pavement structure may become saturated by accumulation of pore water due to thawing ice. This can result in a significant reduction of pavement bearing capacity and during thaw weakening even a single heavy-vehicle pass can cause severe damage to the pavement. The effect of the accumulating water and traffic load is shown in Figure 8. Thaw usually progresses downwards from the pavement surface and may be hindered by insulating snow cover on the shoulders of the road. Consequently, the still frozen layers below and frozen shoulders of the road can restrict drainage of the pavement and prolong the thaw weakening period (Simonsen, 1999). As the pavement

structure gradually drains over time, the bearing capacity is recovered (Dore and Zubeck, 2009). Due to the effects of thaw weakening the Finnish pavement design is based around accommodating the spring thaw period (Kangas et al., 2000).

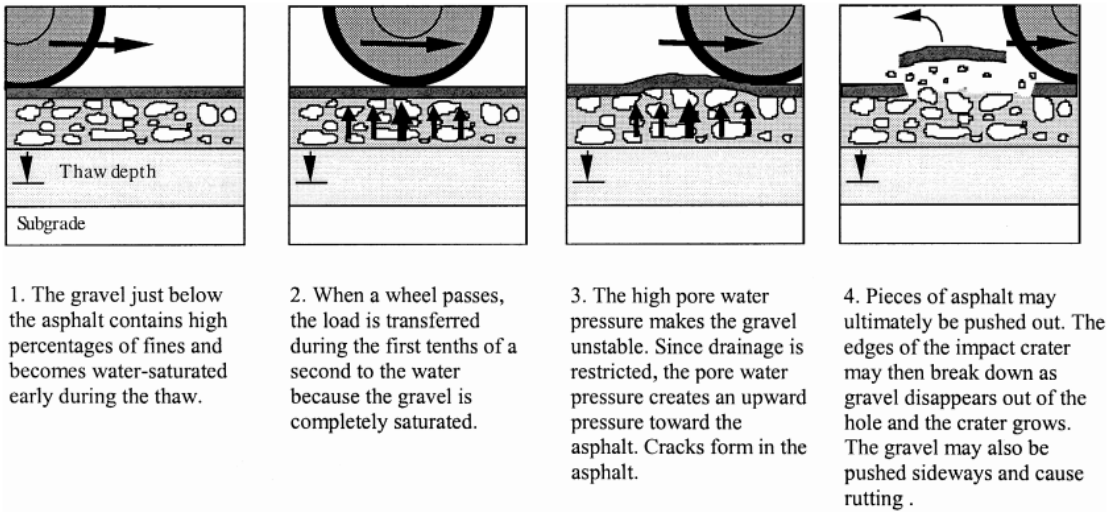

Figure 8 Damage to the pavement with a poorly drained structure (Simonsen, 1999).

The extent of thaw weakening depends mostly on the subgrade soil type, permeability, drainage conditions and the rate of thaw, which is the most important factor according to Simonsen (1999). The rate of thaw influences the generation of excess pore pressure and thus the shear strength of soil. The effect of thaw is not limited to the spring time as permanent structural changes can occur in the subgrade: if the degree of consolidation increases, soil strength can increase too, and in contrast highly cemented and overconsolidated clays can lose strength (Simonsen, 1999).

During spring thaw, rut and crack formation may occur in paved low-volume roads. The ruts are generally wider than on higher-quality roads due to weaker pavement layers as materials used in low-volume roads may be of varying quality. Water can accumulate in the subbase and subgrade layers if they are frost-susceptible and poorly drained, and they will weaken during thaw (Simonsen, 1999). This is especially harmful to roads with thin bituminous layers, as a weak layer close to the surface causes flexing of the surface and extensive tensile stresses to the bottom of the bituminous material (Gandahl, 1987). This is illustrated in Figure 9.

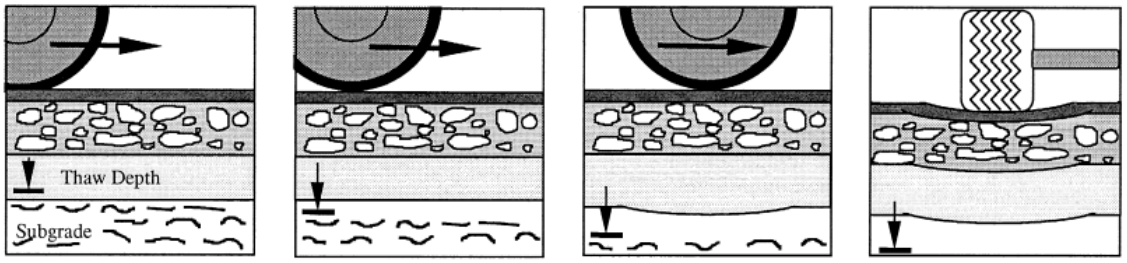

1. Damage development during thaw when the pavement is too thin and the subgrade is frost-susceptible. As long as the thaw depth has not reached the subgrade (with ice formations), the bearing capacity is high.

2. When the subgrade begins to thaw, the excess water may cause a significant drop in strength.

3. The weak subgrade is pressed aside due to wheel loading and settlements migrate towards the asphalt surface.

4. After many passages, the deformations may become quite large. Such damage occurs relatively late in the thaw.

Figure 9 Damage to the pavement with a thin bituminous layer (Simonsen, 1999).

5 Frozen and Unfrozen Soil model

5.1 Theory

The model assumes fully saturated, isotropic and elasto-plastic soil behavior. The frozen soil is a natural material composed of solid soil grains, solid pore ice and unfrozen liquid pore water, which are all assumed to be incompressible. Fully-frozen soil is composed of only soil grains and pore ice, whereas unfrozen soil only contains soil grains and pore water. Partially-frozen soil is a mixture of these two extreme cases. The Frozen and Unfrozen Soil model was published in its initial form by Ghoreishian Amiri et al. (2016b). In his Master's thesis (2016), Aukenthaler implemented the model to be used within Plaxis 2D (Brinkgreve et al., 2017) as a user-defined soil model and modified some parts such as the yield surface definition (Aukenthaler, 2016).

The model considers frozen soil as analogous to unsaturated soil by assuming that the flow of water in pores is hindered by ice in a way similar to air. Using this analogy, the model borrows ideas from the Barcelona Basic model (BBM) for unsaturated soils (Alonso et al., 1990) to model the behavior of frozen saturated soil, such as the yield condition definitions, linear increase of cohesion with suction, parameters describing virgin loading in isotropic stress states and the definition of suction-induced elastic strain (Aukenthaler, 2016). In a fully-unfrozen state the model reduces to the Modified Cam-Clay (MCC) model (Schofield and Wroth, 1968).

5.2 Thermodynamic equilibrium

Each component of the soil composite is assumed to have the same temperature at each point of soil implying a local thermal equilibrium. The thermodynamic equilibrium of frozen soil is essentially the equilibrium of liquid water and ice, which according to Thomas et al. (2009) can be represented by the Clausius-Clapeyron equation (1):

$$\frac{p_{ice}}{\rho_{ice}} - \frac{p_w}{\rho_w} = -L \ln\left(\frac{T}{T_f}\right) \tag{1}$$

Here p_{ice} and p_w are ice and pore water pressures, ρ_{ice} and ρ_w are densities of ice and pore water, L is the latent heat of fusion, and T is the prevailing temperature and T_f is the freezing/melting temperature at prevailing pressure. The latent heat of fusion L is the required heat energy for water to change phase from liquid to solid ice in constant temperature.

The cryogenic suction is an important factor in describing the water migration in frozen soil. It is a negative pressure that draws pore water from the unfrozen soil to the frozen fringe, which is induced by the temperature and pore pressure difference between unfrozen and frozen soil. As described in chapter 2.1, frozen fringe is a zone between fully-frozen and unfrozen soil, where the phase change between water and ice occurs. Fully-frozen soil means soil, where nearly all pore water has frozen. For temperature higher than the freezing/melting temperature of the soil, the cryogenic suction is zero and the model becomes the Modified Cam Clay model (Aukenthaler, 2016).

Using the Clausius-Clapeyron equation it is possible to derive the equation for cryogenic suction (4) as the pressure difference between pore ice and pore water:

$$s_c = p_{ice} - p_w \tag{2}$$

$$s_c = \rho_{ice}\left(\frac{p_w}{\rho_w} - L\ln\left(\frac{T}{T_f}\right)\right) - p_w \tag{3}$$

Assuming ice and water density are close in value, the equation reduces to:

$$s_c \approx -\rho_{ice} L \ln\left(\frac{T}{T_f}\right) \tag{4}$$

The freezing point of water is dependent on prevailing pressure. When pressure increases, the freezing/melting temperature of water decreases and vice versa. Two approaches are presented in the Plaxis model manual (Ghoreishian Amiri et al., 2016a) for estimating the soil freezing/thawing temperature. The approach used by Ghoreishian Amiri et al. (2016b) relates the temperature T_f to ice pressure as:

$$T_f = T_{ref}\left(\frac{p_{ice}}{-p_{ref}} + 1\right)^{\frac{1}{\alpha}} \tag{5}$$

Where T_{ref} is the reference temperature 273.16 K, p_{ref} is the reference pressure of -395 MPa and α is a constant parameter between 7 and 9.

Aukenthaler (2016) adopted the equation (6) by Wagner et al. (2011) to represent the pressure dependency of the soil freezing/melting temperature and combines it with the cryogenic suction as follows:

$$\frac{s_c + p_w}{611.657\ Pa} = 1 + \sum_{1}^{3} a_j\left(1 - \left(\frac{T_f}{273.16\ K}\right)^{b_j}\right) \tag{6}$$

In equation (6) the temperature 273.16 K refers to the vapor-liquid-solid triple point temperature and the pressure 611.657 Pa to the triple-point pressure respectively. The coefficients a_j and exponents b_j for freezing/melting temperature in equation (6) are represented below in Table 1 with variable *j* having values from 1 to 3:

Table 1 Coefficients and exponents for freezing/melting point pressure dependency equation.

j	a_j	b_j
1	$0.119539337 \cdot 10^7$	$0.300000 \cdot 10$
2	$0.808183159 \cdot 10^5$	$0.257500 \cdot 10^2$
3	$0.333826860 \cdot 10^4$	$0.103750 \cdot 10^3$

Thus, with the equation (6) a decrease in the freezing/melting temperature corresponds to a decrease in cryogenic suction and an increase in pore water pressure. By inserting the definition of the cryogenic suction (4) into the pressure dependency equation of the freezing/melting temperature, it is possible to first compute the freezing/melting temperature and then the cryogenic suction by just inputting the current temperature and pore water pressure (Aukenthaler, 2016).

5.3 Unfrozen water content

All pore water in a freezing soil does not freeze at the same temperature. The water in the middle of soil voids tends to freeze first, while the water remains unfrozen in the gaps between ice and the soil grains. According to Ghoreishian Amiri et al. (2016b) there are two main phenomena affecting this, which are known as the curvature-induced premelting and interfacial premelting illustrated in Figure 10.

Curvature-induced premelting happens due to the surface tension of the water between soil grains and acts by bonding these grains together, which Ghoreishian Amiri et al. (2016b) stated to be an effect very similar to capillary suction. The interfacial premelting on the other hand is a result of repulsion forces between the ice and the soil grains, and acts as a disjoining pressure that widens the gaps between ice and grains while sucking in more water (Aukenthaler, 2016). The gap between the ice and soil grains acts as a capillary space, where the water is kept unfrozen as high pore water pressure in a small space lowers the water freezing temperature.

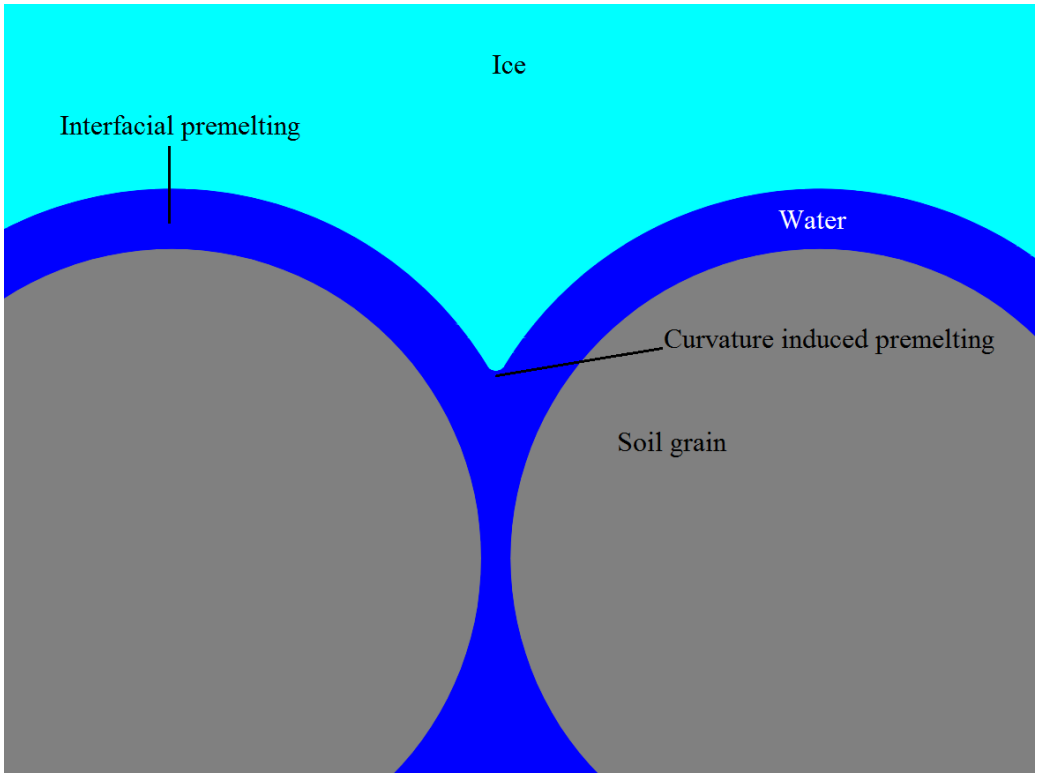

Figure 10 Curvature induced and interfacial premelting effects illustrated (after Ghoreishian Amiri et al., 2016b).

To calculate the unfrozen water remaining in the soil in relation to the temperature, two approaches are again represented in the model manual by Ghoreishian Amiri et al. (2016a). The unfrozen water saturation S_{uw} can be calculated and fitted to the experimental results using the van Genuchten model (van Genuchten, 1980) based formulation by Nishimura et al. (2009) as:

$$S_{uw} = \left(1 + \left(\frac{S_c}{\rho_r}\right)^{\frac{1}{1-\lambda_r}}\right)^{-\lambda_r} \tag{7}$$

Where ρ_r and λ_r are constants for fitting the unfrozen water saturation.

Aukenthaler (2016) calculates the unfrozen water saturation using an empirical equation (8) based on publication by Anderson and Tice (1972), which takes the soil specific surface area SSA, the bulk density of the soil ρ_b and its temperature as inputs. This method is also implemented in Plaxis (Brinkgreve et al., 2017). Three examples for soil freezing characteristic curves calculated with this method are represented in Figure 11. This equation calculates the volumetric unfrozen water content θ_{uw} as:

$$\theta_{uw} = \frac{\rho_w}{\rho_b} \exp(0.2618 + 0.5519 \ln(SSA) - 1.4495(SSA)^{-0.2640} \ln(T_f - T)) \quad (8)$$

The unfrozen water saturation of the soil is calculated from the volumetric unfrozen water content using soil porosity n:

$$S_{uw} = \frac{\theta_{uw}}{n} \quad (9)$$

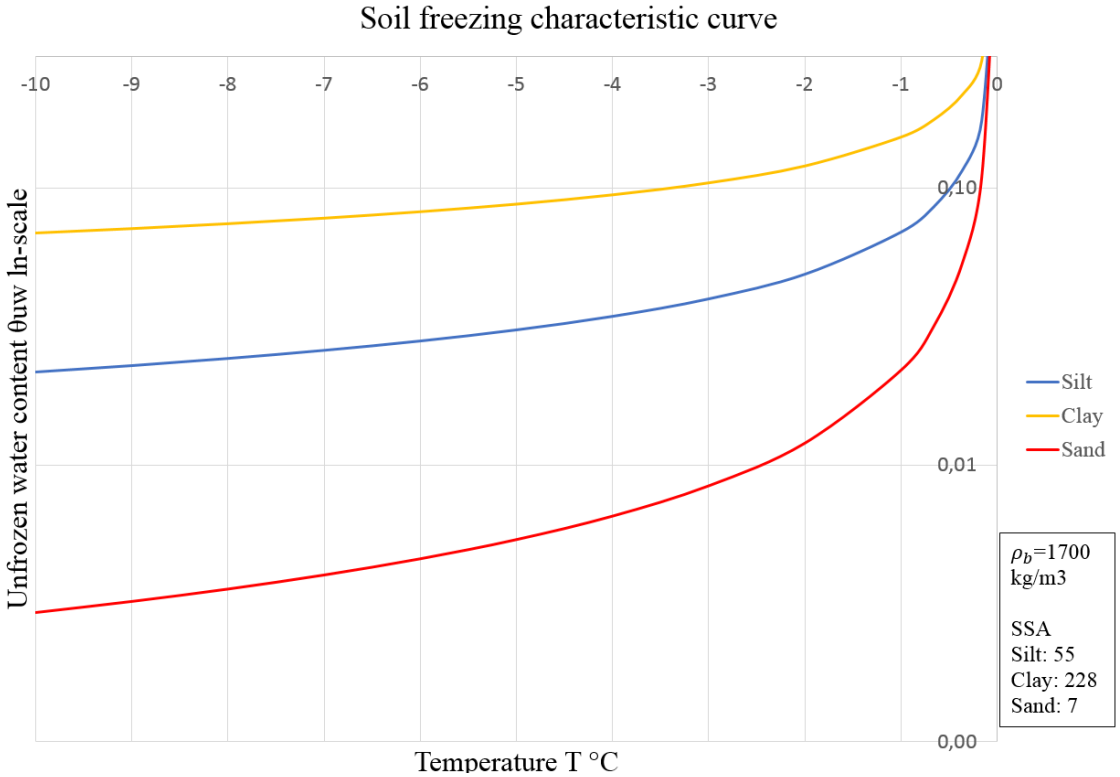

Figure 11 Examples of soil freezing characteristic curves for silt, clay and sand, calculated with the Anderson and Tice (1972) method (unfrozen water content in logarithmic scale).

The specific surface area SSA is the sum of surface areas of soil particles per unit mass. In this model it is estimated using an empirical predictive power function (10) by Sepaskhah et al. (2010) that is defined with the geometric mean of soil particle diameter.

$$SSA = 3.89 \cdot d_g^{-0.905} \quad (10)$$

The geometric mean of soil particle diameter d_g is calculated based on publication by Shirazi and Boersma (1984) using particle size limits in the United States Department of Agriculture (USDA) soil classification system and assuming there is a lognormal particle

size distribution within these classification limits. The geometric mean of soil particle diameter is defined as:

$$d_g = \exp(m_{cl}\ln d_{cl} + m_{si}\ln d_{si} + m_{sa}\ln d_{sa}) \tag{11}$$

Here m_{cl}, m_{si}, and m_{sa} are the mass fractions of clay, silt and sand respectively, and d_{cl} = 0.001mm, d_{si} = 0.026mm and d_{sa} = 1.025mm the particle size limits according to the USDA soil classification system

5.4 Moisture transfer

The law of mass conservation of moisture in freezing soils states that the sum of changes in masses of water and ice fractions and the mass flux of pore water is zero, which can be represented as:

$$\frac{\partial(\rho_w\theta_w)}{\partial t} + \frac{\partial(\rho_{ice}\theta_{ice})}{\partial t} + \rho_w\nabla\boldsymbol{v}_w = 0 \tag{12}$$

Here θ_w and θ_{ice} are the volumetric water and ice contents, t is time and $\boldsymbol{v}_w$ is the pore water velocity vector relative to the soil skeleton. Adopting Darcy's law, Thomas et al. (2009) propose the following equation to represent the pore water flow in freezing soil:

$$\boldsymbol{v}_w = -\frac{k}{\gamma_w}\left(\nabla(p_w - \gamma_w z) + \frac{\rho_{ice}L}{T_f}\nabla T\right) \tag{13}$$

Here k is the frozen soil hydraulic conductivity, γ_w is water unit weight and z is the depth.

The hydraulic conductivity of frozen soils is complicated to determine and measure (Aukenthaler, 2016). Based on the assumption that hydraulic conductivity of partially frozen soils behaves like that of unsaturated soils, Aukenthaler (2016) represents the following model by Campbell (1985) to calculate hydraulic conductivity of partially frozen soil:

$$k = k_{sat}\left(\frac{\theta_{uw}}{\theta_{sat}}\right)^{2b+3} = k_{sat}(S_{uw})^{2b+3} \tag{14}$$

Here θ_{uw} and θ_{sat} are the volumetric unfrozen water and saturated soil water content respectively and k_{sat} is the unfrozen saturated soil hydraulic conductivity. In a fully saturated soil the volumetric water content θ_{sat} is equal to porosity.

The hydraulic conductivity of unfrozen saturated soil k_{sat} can be estimated with an empirical equation (15) represented by Tarnawski and Wagner (1996) as:

$$k_{sat} = 4\cdot 10^{-5}\left(\frac{0.5}{1-\theta_{sat}}\right)^{1.3b}\exp(-6.88\,m_{cl} - 3.63\,m_{si} - 0.025) \tag{15}$$

The parameter b is an empirical parameter based on grain size distribution and is calculated as:

$$b = d_g^{-0.5} + 0.2\,\sigma_g \tag{16}$$

Here d_g is the geometric mean of soil particle diameter (11) and σ_g is geometric standard deviation of soil particle diameter defined as:

$$\sigma_g = \exp\left(\sum_{n=1}^{3} m_i(\ln d_i)^2 - (\sum_{n=1}^{3} m_i \ln d_i)\text{^}2\right)^{0.5} \tag{17}$$

According to Rostami (2017) and Cicchetti (2018) a hydraulic model needs to be implemented in Plaxis to account for freezing characteristic function in freezing soil. The van Genuchten model (van Genuchten, 1980) expresses the water saturation S as function of the pressure head ϕ_p as:

$$\phi_p = \frac{p_w}{\gamma_w} \tag{18}$$

$$S(\phi_p) = S_{res} + (S_{sat} - S_{res})\left(1 + \left(g_a|\phi_p|\right)^{g_n}\right)^{g_c} \tag{19}$$

Where S_{res} is the residual saturation, which is the fluid that remains in soil pores at high suction, S_{sat} is the saturation in saturated state, and g_a, g_n and g_c are fitting parameters.

Rostami (2017) and Cicchetti (2018) relate the van Genuchten fitting parameters to the NTNU model fitting parameters ρ_r and λ_r for unfrozen water saturation as:

$$g_a = \frac{p_w}{\rho_r} \tag{20}$$

$$g_n = \frac{1}{1 - \lambda_r} \tag{21}$$

$$g_c = -\lambda_r \tag{22}$$

It has been recently observed (Teng et al., 2018; Zhang et al., 2016) that moisture can also accumulate due to vapor transfer in relatively dry freezing soils under impervious cover such as bituminous pavement, where the groundwater table is deep, which is known as the canopy effect. This can even occur in soils considered not frost-susceptible with good liquid water drainage due to desublimation of vapor into ice, leading to significant accumulation of ice. The canopy effect thus can lead to frost damage in pavements. As the model does not consider the effect of vapor transfer, the canopy effect is not taken into account in the modelling.

5.5 Heat transfer

The Fourier law of heat transfer (Fourier, 1878) is used to represent the law of energy conservation of heat in freezing soil, which states that the sum of change in the heat content of soil $\boldsymbol{\Phi}$ and change in the heat flux $\boldsymbol{Q}$ must be zero. According to Thomas et al. (2009) this can be expressed for a unit volume dV as:

$$\frac{\partial(\boldsymbol{\Phi} dV)}{\partial t} + \nabla \boldsymbol{Q} dV = 0 \tag{23}$$

The heat content of soil $\boldsymbol{\Phi}$ represents the capacity of soil particles, ice and water to store heat and additionally the latent heat related to freezing/melting of ice. The heat flux $\boldsymbol{Q}$ represents the thermal conductivity of the soil particles, ice and water along with pore water convection.

5.6 Mechanical model

The mechanical model is a critical state elasto-plastic soil model initially presented in the work of Ghoreishian Amiri et al. (2016b) with two stress state variables: cryogenic suction and solid phase stress.

Mechanical static equilibrium states that the sum of change in total stresses $\boldsymbol{\sigma}$ and body forces $\boldsymbol{b}$ must be zero. This can be represented as:

$$\nabla \cdot \boldsymbol{\sigma} + \boldsymbol{b} = 0 \tag{24}$$

The body forces $\boldsymbol{b}$ represent the external forces distributed throughout the soil body and the total stresses $\boldsymbol{\sigma}$ represent the internal forces that are induced to counteract body forces and externally applied forces.

An extended effective stress termed solid phase stress is proposed by the original developers of the model in their publication (Ghoreishian Amiri et al., 2016b). It is defined as the combined stress in solid soil grains and ice. This extended effective stress formulation is a Bishop single effective stress, where the unfrozen water content is the Bishop's parameter. The unfrozen water content affects the solid phase stress because the effect of pore water pressure is dependent on the contact area between soil grains and pore water (Aukenthaler, 2016). The solid phase stress is thus defined as follows:

$$\boldsymbol{\sigma}^* = \boldsymbol{\sigma} - S_{uw} p_w \boldsymbol{I} \tag{25}$$

Here $\boldsymbol{\sigma}$ is the net stress and $\boldsymbol{I}$ is unit tensor.

By using both solid phase stress and cryogenic suction as stress-state variables, the model is able to take into account the effect of unfrozen water, ice and temperature on the mechanical behavior of frozen soil (Aukenthaler, 2016).

Using these stress-state variables, any strain increment can be divided into elastic and plastic strains due to solid phase stress and cryogenic suction increments as:

$$d\epsilon = d\epsilon^{me} + d\epsilon^{se} + d\epsilon^{mp} + d\epsilon^{sp} \tag{26}$$

Here $d\epsilon^{me}$ and $d\epsilon^{se}$ are the elastic strain increments due to solid phase stress and cryogenic suction variation, and $d\epsilon^{mp}$ and $d\epsilon^{sp}$ are the plastic strain increments.

5.7 Elastic response

The elastic strains due to solid phase stress can be calculated based on the equivalent stress dependent shear modulus and bulk modulus of the soil, which are:

$$K = (1 - S_{ice})\frac{(1+e)p_{y0}^{*}}{\kappa_0} + \frac{S_{ice}E_f}{3(1-2\nu_f)} \tag{27}$$

$$G = (1 - S_{ice})G_0 + \frac{S_{ice}E_f}{2(1+\nu_f)} \tag{28}$$

Here e is the soil void ratio, p_{y0}^{*} is the preconsolidation stress for unfrozen soil, κ_0 is the elastic compressibility coefficient, E_f is the Young's modulus of frozen soil and ν_f is the frozen soil Poisson's ratio. The ice saturation in a fully saturated soil is simply determined as:

$$S_{ice} = 1 - S_{uw} \tag{29}$$

The temperature-dependent behavior of ice is taken into account by increasing stiffness of the soil with decreasing temperature in reference to an arbitrary reference temperature T_{ref}:

$$E_f = E_{f,ref} - E_{f,inc}(T - T_{ref}) \tag{30}$$

The elastic strain increment due to cryogenic suction increment is defined as:

$$d\epsilon^{se} = \frac{\kappa_s}{1+e} \cdot \frac{ds_c}{s_c + p_{at}} \tag{31}$$

where κ_s is the elastic compressibility coefficient for suction variation.

The volumetric and shear components of elastic strain increment are defined as:

$$d\epsilon_v^e = \frac{1}{K}dp^* + \frac{\kappa_s}{1+e}\frac{ds_c}{s_c + p_{at}} \tag{32}$$

$$d\epsilon_q^e = \frac{1}{3G}dq^* \tag{33}$$

Here dp^* and dq^* are the changes in solid phase mean stress p^* and solid phase deviatoric stress q^* respectively.

The solid phase mean stress p^* and the solid phase deviatoric stress q^* are defined according to Ghoreishian Amiri et al. (2016b) as follows:

$$p^* = \frac{\sigma_{11}^* + \sigma_{22}^* + \sigma_{33}^*}{3} \tag{34}$$

$$q^* = \sqrt{\left(0.5\left((\sigma_{11}^* - \sigma_{22}^*)^2 + (\sigma_{11}^* - \sigma_{33}^*)^2 + (\sigma_{33}^* - \sigma_{22}^*)^2 + 3\left({\sigma_{12}^*}^2 + {\sigma_{13}^*}^2 + {\sigma_{23}^*}^2\right)\right)\right)} \tag{35}$$

5.8 Yield conditions

For the frozen state, two cryogenic suction dependent yield functions are implemented to take into account the premelting effects described before. The model borrows these yield functions from BBM by treating frozen soils as analogous to unsaturated soil. The curvature-induced premelting is described by the loading-collapse LC yield surface and the interfacial premelting by the grain segregation GS yield curve.

The curvature-induced premelting binds the soil grains together resulting in compressive elastic deformation due to suction increase (and swelling due to suction decrease). The loading-collapse yield surface thus expands with increasing suction, which is shown in Figure 12. Based on the BBM definition for the LC yield surface to describe this behavior, the yield surface is expressed in terms of solid phase mean stress p^* and solid phase deviatoric stress q^* as:

$$F_1 = (p^* + k_t s_c)\left((p^* + k_t \cdot s_c)(S_{uw})^m - \left(p_y^* + k_t s_c\right)\right) + \frac{(q^*)^2}{M^2} = 0 \tag{36}$$

The key difference in the yield surface between the Unfrozen and Frozen Soil model and the original BBM is that this model is formulated in terms of effective stress and incorporates the unfrozen water saturations, while the BBM is formulated using total stress.

Here k_t is the increase in apparent cohesion with cryogenic suction, m is a parameter controlling the effect of unfrozen water saturation and M the slope of the critical state line. Pseudo preconsolidation stress for frozen conditions p_y^* is calculated with the elastic and elastoplastic compressibility coefficients for frozen soil κ and λ:

$$p_y^* = p_c^* \left(\frac{p_{y0}^*}{p_c^*}\right)^{\frac{\lambda_0 - \kappa}{\lambda - \kappa}} \tag{37}$$

$$\kappa = \frac{1 + e}{K} p_{y0}^* \tag{38}$$

$$\lambda = \lambda_0((1 - r)exp(-\beta s_c) + r) \tag{39}$$

Here λ_0 is the elastoplastic compressibility coefficient for unfrozen soil, r is a constant for maximum stiffness of the soil and β is a parameter for controlling rate of change in soil stiffness with suction.

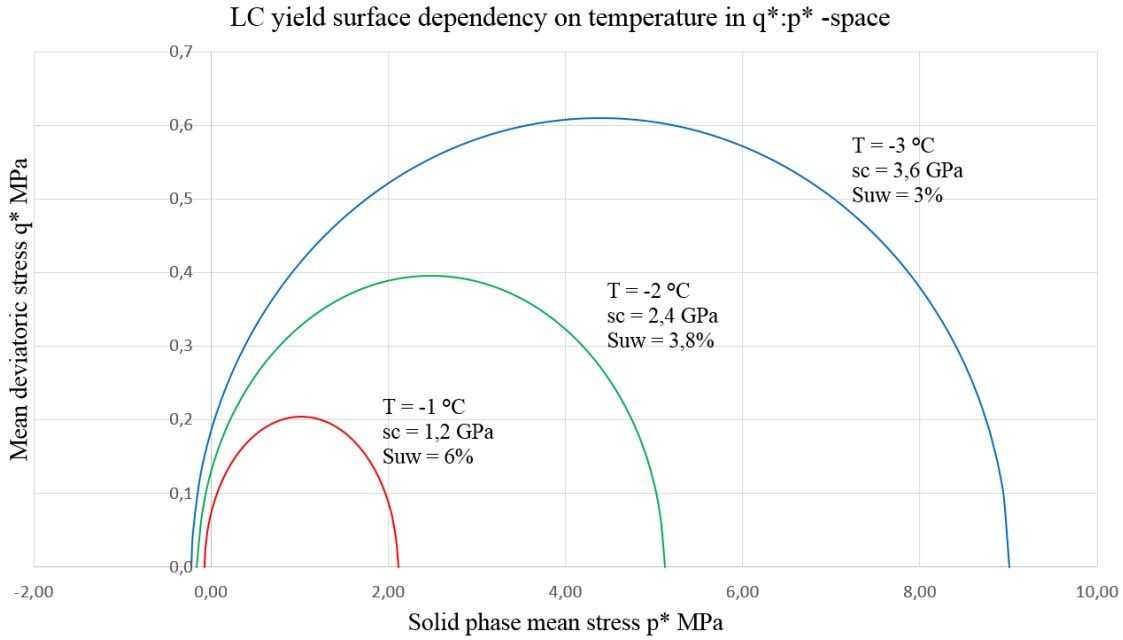

Figure 12 The effect of cryogenic suction on the shape of the LC yield surface.

Frozen-soil yield behavior depends on the amount of remaining unfrozen water. The soil behaves like ice rubble or sand when there is little unfrozen water remaining and it won't yield without shearing. To take this into account, the unfrozen water content affects the yield surface, changing it from Modified Cam-Clay type to Mohr-Coulomb type with decreasing unfrozen water saturation. The fitting parameter m affects how much this behavior is in effect, which is illustrated in Figure 13 (Aukenthaler, 2016).

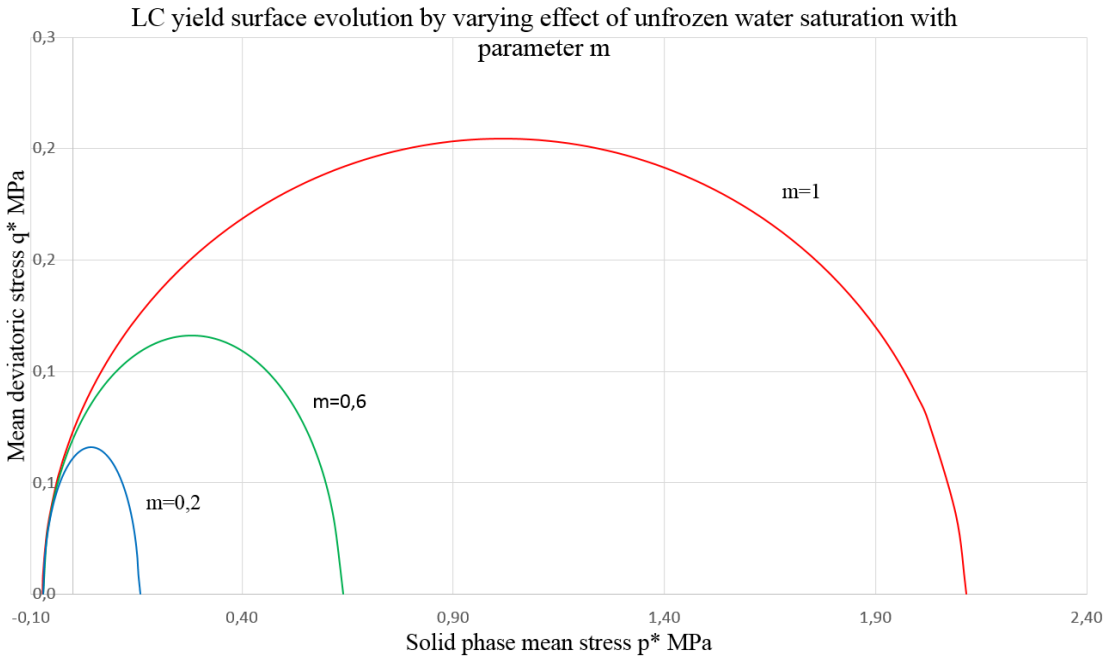

Figure 13 The effect of parameter m on the shape of the LC yield surface.

The interfacial premelting pushes the soil grains and the ice apart when the suction is increased. It causes a dilative plastic deformation due to suction, which manifests as grain segregation and formation of ice lenses in the soil. The GS yield curve due to the interfacial premelting is expressed with the threshold value for initiation of ice segregation $s_{c,seg}$

that describes the transition from elastic soil behavior to virgin loading and grain segregation under suction variation as follows:

$$F_2 = s_c - s_{c,seg} \tag{40}$$

5.9 Hardening rules

The hardening behavior of the LC and GS yield functions is coupled. In plastic compression due to solid phase stress variation the soil becomes stiffer and the LC yield surface expands, while the size of voids in the soil decreases and the ice segregation threshold value is thus decreased, shrinking the GS yield curve. Plastic dilation on the other hand causes expansion of soil voids due to ice segregation and expands the GS yield curve, while the LC yield surface shrinks as the soil stiffness decreases (Aukenthaler, 2016).

The model couples the yield functions by assuming that their position is controlled by the total plastic volumetric deformation. Based on this assumption the hardening rule for the LC yield surface becomes:

$$\frac{dp_{y0}^*}{p_{y0}^*} = \frac{1+e}{\lambda_0 - \kappa}(d\epsilon_v^{mp} + d\epsilon_v^{sp}) \tag{41}$$

To define the hardening rule of the GS yield curve the effect of unfrozen water must be taken into account as the effectivity of interfacial premelting depends on more water being sucked into the gaps between grains and ice. Lowering unfrozen water content reduces frozen soil permeability and limits the availability of water. With a very low unfrozen water saturation little water can flow into the gaps so the increase of cryogenic suction can't increase the soil volume. Frost heave cannot occur if there is no source of water available and thus the GS yield curve can expand without increasing volume at low unfrozen water saturation. The hardening rule for GS yield curve is expressed as:

$$\frac{ds_{c,seg}}{s_{c,seg} + p_{at}} = -\frac{1+e}{S_{uw}(\lambda_s + \kappa_s)} d\epsilon_v^{sp} - \frac{1+e}{\lambda_s + \kappa_s}(1 - \frac{s_c}{s_{c,seg}}) d\epsilon_v^{mp} \tag{42}$$

5.10 Flow rules

To determine the direction of plastic strain increments the LC yield surface is employed with a non-associated flow rule in constant cryogenic suction planes, which is illustrated in Figure 14. The GS yield curve is employed with an associated flow rule. In unfrozen state, associated plasticity is used as in MCC. The flow rules are expressed as follows, where Q_1 is the plastic potential function:

$$d\boldsymbol{\epsilon}^{mp} = d\lambda_1 \frac{\partial Q_1}{\partial \boldsymbol{\sigma}^*} \tag{43}$$

$$d\boldsymbol{\epsilon}^{sp} = -d\lambda_2 \frac{\partial F_2}{\partial s_c} \boldsymbol{I} \tag{44}$$

$$Q_1 = (S_{uw})^{\gamma}\left(p^* - \left(\frac{p_y^* - k_t s_c}{2}\right)\right)^2 + \left(\frac{q^*}{M}\right)^2 \quad (45)$$

The plastic multipliers $d\lambda_1$ and $d\lambda_2$ are obtained with plastic consistency conditions. Unfrozen water content affects the volume change tendency of frozen soil. When there is high amount of unfrozen water free to flow in the pores there is a higher possibility of plastic volume change. At low unfrozen water saturation, there is less water to flow, the frozen soil behaves more like nonporous material, and plastic volume change is less likely. With decreasing unfrozen water content, the plastic potential surface will change from ellipse to straight line as the tendency of volume change decreases. The fitting parameter γ is used to control how much effect the unfrozen water saturation has on volumetric behavior, which is illustrated in Figure 15 (Aukenthaler, 2016).

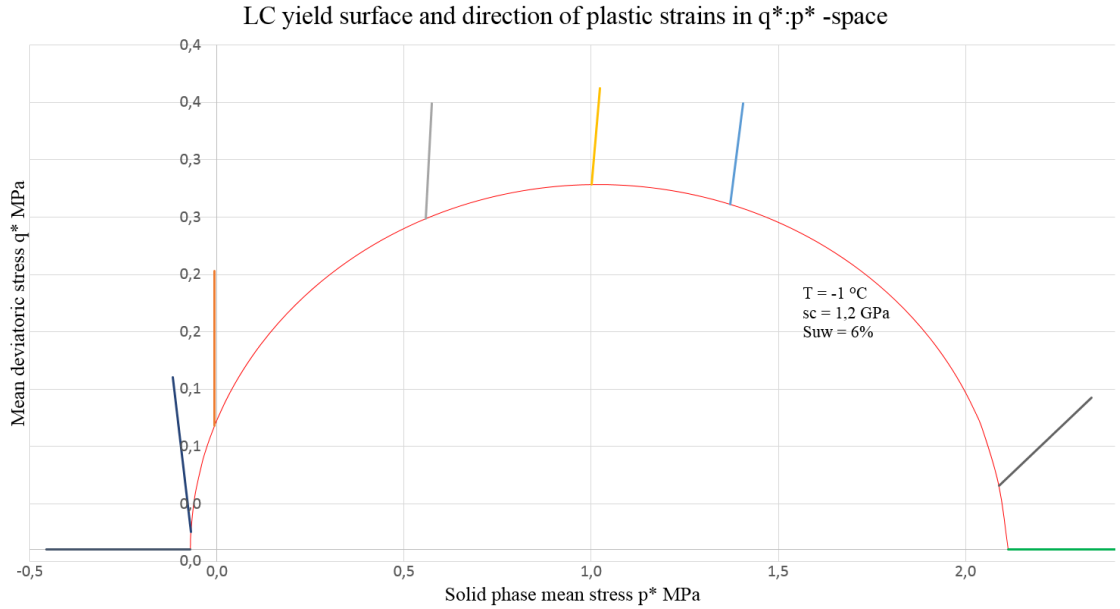

Figure 14 The LC yield surface and the direction of plastic strains.

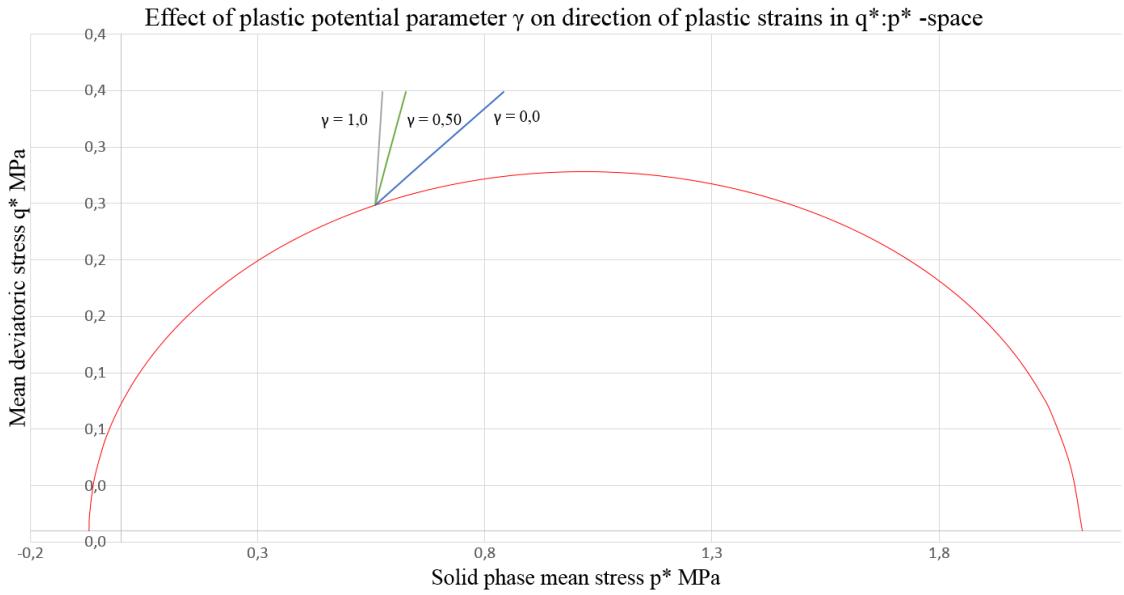

Figure 15 Effect of parameter γ on the direction of plastic strains.

6 Model parameters

Aukenthaler (2016) divides the model parameters into following categories: elastic parameters, strength parameters and parameters controlling virgin loading under isotropic stress state and cryogenic suction variation. He also suggests some tests for the parameter derivation. Additionally ice, water and reference parameters are required model inputs as per Ghoreishian Amiri et al. (2016a). The model parameters are compiled in Table 6 at the end of this chapter.

6.1 Elastic parameters

Parameters of frozen soil describing elastic behavior can further be divided into parameters that describe temperature, pressure and suction dependent elasticity (Aukenthaler, 2016).

Temperature dependence is described by parameters $E_{f,ref}$, $E_{f,inc}$ and ν_f. $E_{f,ref}$ describes the stiffness of fully-frozen soil at reference temperature. It is determined with the unconfined axial compression test at an arbitrary reference temperature in frozen state. $E_{f,inc}$ describes the increase of soil stiffness with decreasing temperature, which is determined with unconfined axial compression test at a different temperature in frozen state. Table 2 presents default values suggested for $E_{f,ref}$ and $E_{f,inc}$ by model developers based on Johnston (1981) and Tsytovich (1975). It is noted they should be used with caution (Aukenthaler, 2016).

Table 2 Frozen soil Young's modulus and its temperature dependency.

Parameter	Frozen Sand	Frozen Silt	Frozen Clay
$E_{f,ref}$ (MPa)	500	400	500
$E_{f,inc}$ (MPa/K)	2100	1400	230

Further parameter ν_f is the Poisson's ratio of fully-frozen soil, which is also determined with unconfined axial compression test at an arbitrary reference temperature in frozen state. The model developers suggest using a value close to the Poisson's ratio of ice 0.31. The Poisson's ratio in the model is assumed to be constant for frozen soil, which is an estimation as it has been observed to decrease along with decreasing temperature as pore water freezes and soil becomes more rigid (Andersland and Ladanyi, 2004; Shibata et al., 1985).

Pressure dependence is handled by parameters G_0 and κ_0. G_0 is the shear modulus of unfrozen soil determined with simple shear test in unfrozen state. κ_0 is the unfrozen soil elastic compressibility coefficient, which is a standard MCC parameter. It is derived from an unfrozen oedometer test.

Suction dependent elasticity is described by the parameter κ_s, which is the elastic compressibility coefficient for suction variation. It is analogous in function to parameter κ_0 as it describes the elastic part of strain with change in suction. It is suggested to be determined with suction-controlled frost heave test.

The parameter $\left(s_{c,seg}\right)_{in}$ is the initial value of grain segregation threshold derived from suction-controlled frost heave test. Aukenthaler describes it as a strength parameter, but as it is related to elastic behavior and strains it is presented here with elastic parameters. As written before, it describes the limit after which both elastic and plastic strains occur

with increasing cryogenic suction. The Table 3 below presents default values suggested by model developers based on Rempel (2007):

Table 3 Suggested default values for initial value of ice segregation threshold.

Parameter	Sand	Silt	Clay
$(s_{c,seg})_{in}$ (MPa)	0.55	1.25	3.50

6.2 Strength parameters

Parameters describing the strength of the frozen soil are M, k_t, m and γ.

M is the slope of the critical state line that describes a state of no volumetric deformation in shear. It is determined using a simple shear test in an unfrozen state. The slope of critical state line for unfrozen soil is assumed to be constant and to also apply for frozen state, while it has been shown in literature that the slope depends on both temperature and pressure at least for silt (Lai et al., 2010).

Parameter k_t is the increase of apparent cohesion with cryogenic suction that is determined by comparing cohesion values in unconfined axial compression tests at different freezing temperatures. The model assumes a linear increase of cohesion, but it has been shown that cohesion does not increase in a linear fashion (Zhou et al., 2015).

Parameters m and γ are fitting parameters for controlling the effect of unfrozen water saturation on the LC yield surface F_1 and plastic potential function Q_1 respectively.

6.3 Parameters controlling virgin loading under isotropic stress state and cryogenic suction variation

The parameters β, λ_0, r, p_c^*, $\left(p_{y0}^*\right)_{in}$ and λ_s that describe soil behavior in virgin loading under isotropic stress are borrowed from the BBM. The parameters β, r and p_c^* are generally considered the hardest parameters to derive as they simultaneously affect multiple aspects of soil behavior under isotropic stresses, requiring fitting methods to adjust model results to experimental curves (Aukenthaler, 2016).

The parameters λ_0 and λ_s are elastoplastic compression coefficients for unfrozen soils and suction variation respectively, which represent the virgin consolidation of soil once it has yielded. Like λ_0, the parameter λ_s is the slope of volume change line. λ_0, which is a standard MCC parameter, is defined from unfrozen oedometer tests and λ_s from suction-controlled frost heave tests. The effect of parameter λ_s is illustrated in Figure 16.

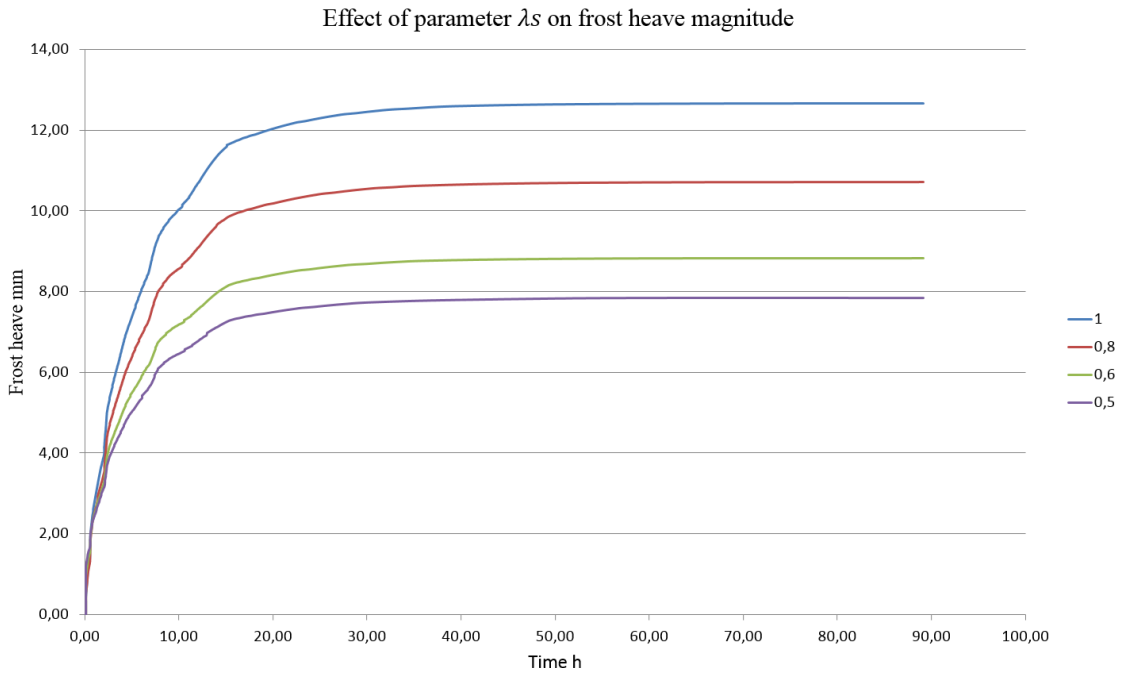

Figure 16 Effect of parameter λ_s on frost heave magnitude.

Finally, $(p^*_{y0})_{in}$ is the initial preconsolidation stress in unfrozen conditions at reference depth Y_{ref} that is suggested to be defined from unfrozen oedometer tests. The effect of this parameter is illustrated in Figure 17. The change of preconsolidation stress with depth is represented by the parameter Δp^*_{y0}.

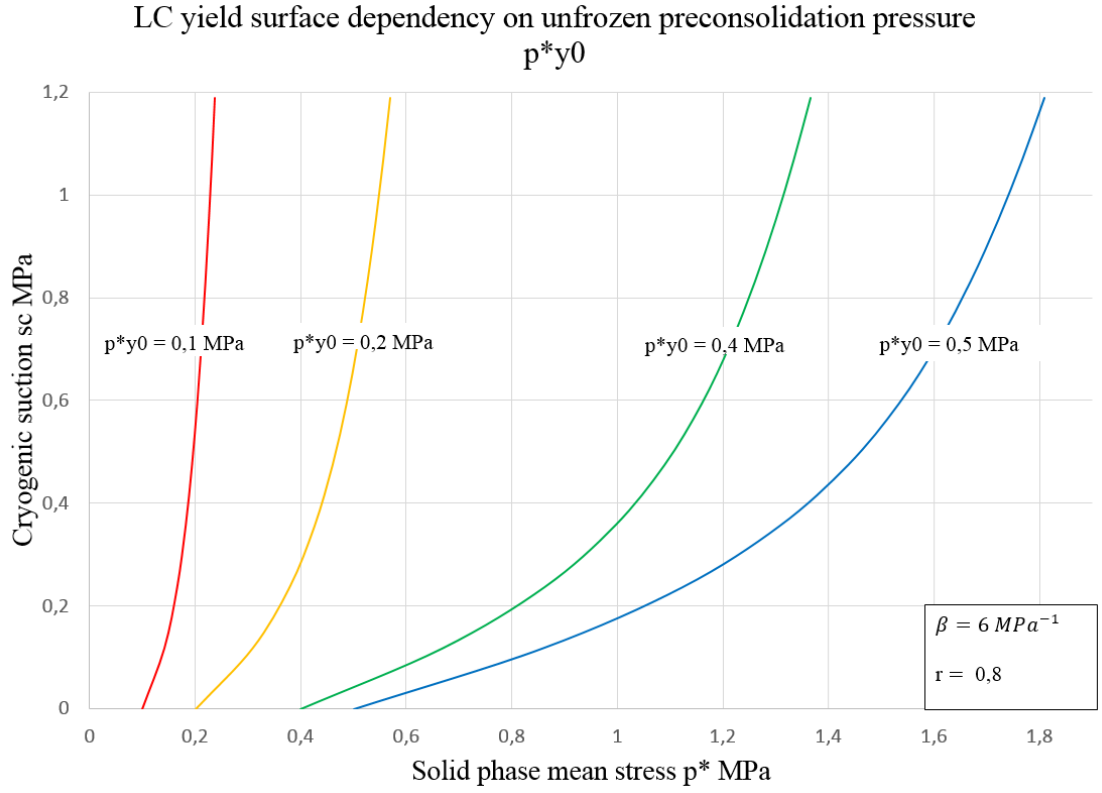

Figure 17 The effect of parameter $(p^*_{y0})_{in}$ on the shape of the LC yield curve (after Alonso et al., 1990).

The parameter β controls the rate of change in soil stiffness with suction variation and can be seen as the parameter that controls the relative spacing of normal compression lines in v^*-ln p space. Its effect on the LC yield surface is represented in Figure 18. Parameter r is a coefficient for maximum soil stiffness, the effect of which is shown in Figure 19. p_c^* is the soil reference stress. These parameters are suggested to be estimated from oedometer tests at different constant positive and negative temperatures (constant suction values) using the calibration process adapted by the model authors from the work of Zhang et al. (2016).

In the work of Zhang et al. (2016b) an explicit formulation for the at-rest coefficient K_0 for unsaturated soils is derived. Based on this formulation, the modified state surface approach (MSSA) to model elasto-plastic behavior of unsaturated soils is combined with quasi-Newton method to calibrate simultaneously the parameters affecting virgin unsaturated soil behavior using suction-controlled oedometer tests. This is done by minimizing the difference between experimental results and the predicted theoretical results using a least-squares method based on objective function (Zhang et al., 2016b). As suction-controlled oedometer tests are unavailable for this thesis, the parameters β, r, and p_c^* are assumed by fitting available measurements.

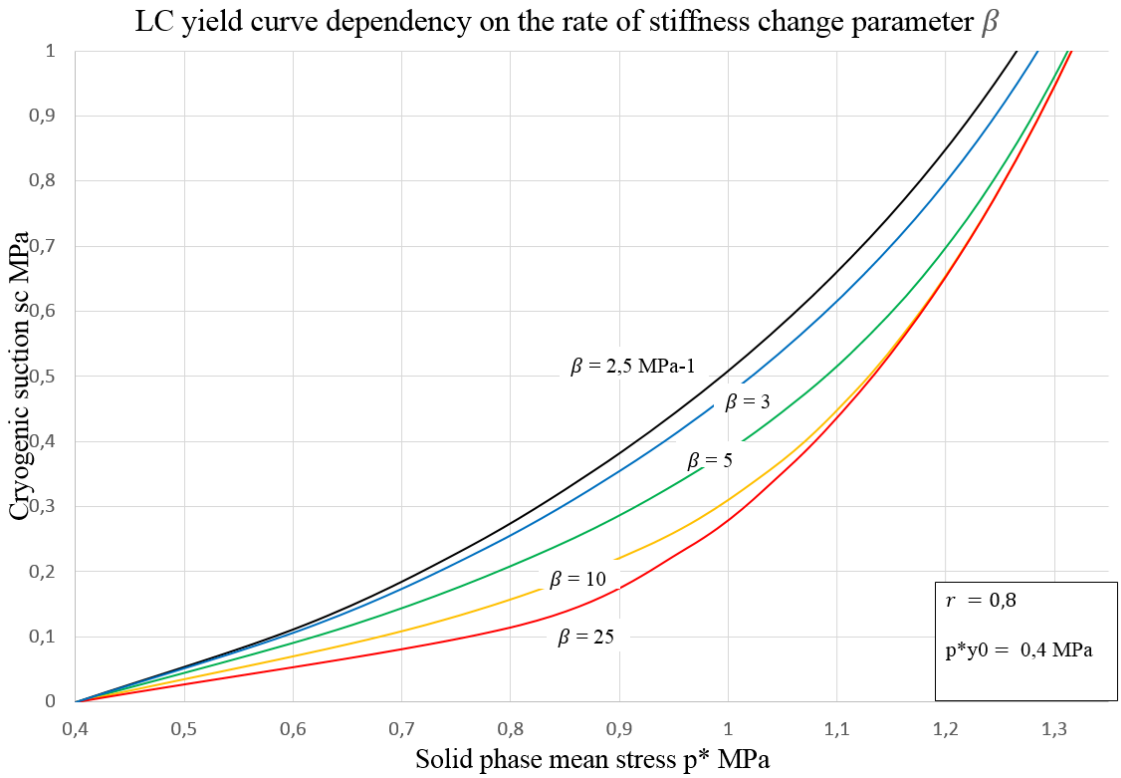

Figure 18 The effect of parameter β on the shape of the LC yield curve (after Alonso et al., 1990).

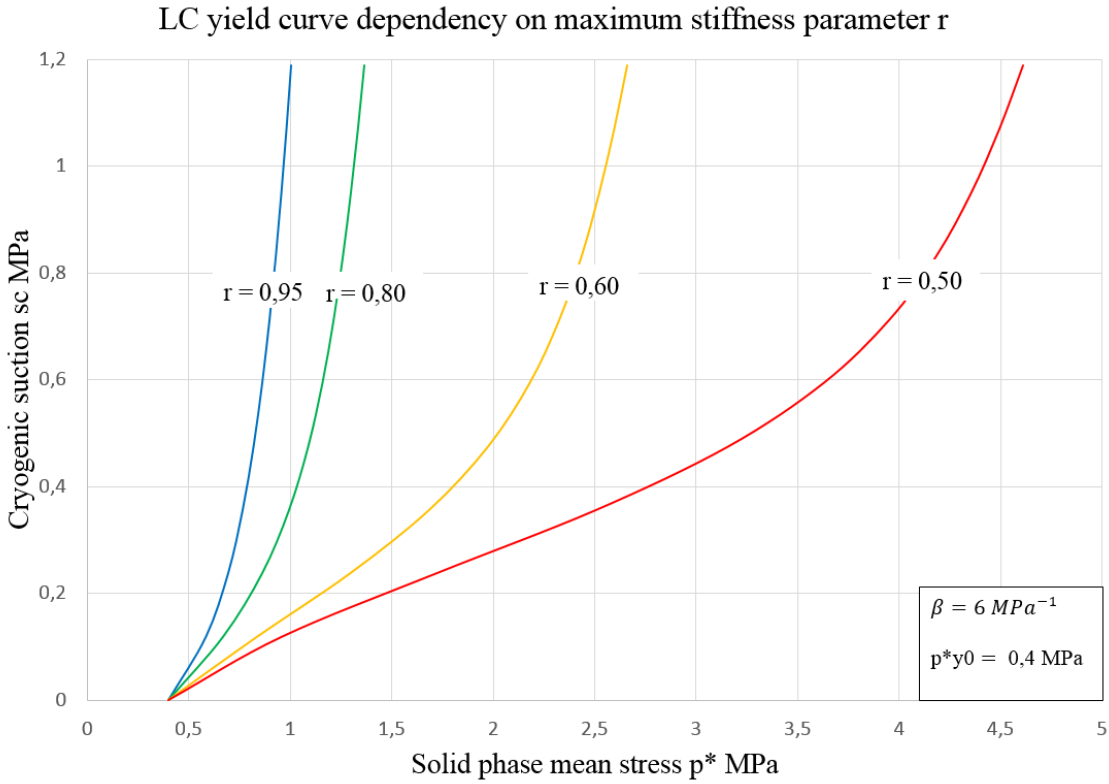

Figure 19 The effect of parameter r on the shape of the LC yield curve (after Alonso et al., 1990).

6.4 Ice, water and reference model parameters

The parameters α, λ_r, ρ_r, T_{ref} and p_{ref} are used for calculating the soil freezing/thawing temperature and fitting the unfrozen water saturation curve. The initial void ratio of soil e_0, bulk modulus of water K_W and atmospheric pressure p_{at} are also required inputs for the model parameters.

6.5 General modelling parameters

The model's implementation in Plaxis requires also other parameters in addition to the actual model parameters. These are the thermal parameters of the soil, water and ice along with general soil parameters such as the soil unit weight in saturated and unsaturated conditions and coefficient of at-rest earth pressure. The initial void ratio needs to also be input in the Plaxis General tab sheet. For groundwater flow the van Genuchten model parameters and the saturated soil permeability can be input as values by the user instead of Plaxis setting them automatically using default soil data sets and calculating the permeability using the Tarnawski and Wagner (1996) method represented in chapter 5.4. The general soil parameters are illustrated in Table 4 and the water and ice thermal parameters in Table 5.

Table 4 General soil parameters

Parameter	Description	Unit
γ_{sat}	Soil saturated unit weight	N/m^3
γ_{unsat}	Soil unsaturated unit weight	N/m^3
e_0	Initial void ratio	-
S_{res}	Residual saturation	-
S_{sat}	Saturation in saturated conditions	-
g_n	Fitting parameter of rate of water extraction	-
g_a	Fitting parameter related to air entry value of soil	1/m
g_l	Fitting parameter for relative soil permeability	-
k_x	Horizontal permeability	m/s
k_y	Vertical permeability	m/s
c_s	Specific heat capacity	J/kg/K
ρ_s	Specific gravity	kg/m^3
λ_s	Thermal conductivity	W/m/K
$\alpha_{x,y,z}$	Thermal expansion coefficient	1/K
K_0	At rest earth pressure coefficient	-

Table 5 Water and ice thermal parameters

Parameter	Description	Unit
T_{ref}	Reference temperature	K
γ_{water}	Water unit weight	N/m^3
c_{water}	Water specific heat capacity	J/kg/K
λ_{water}	Water thermal conductivity	W/m/K
L_{water}	Water latent heat of fusion	J/kg
α_{water}	Water volumetric thermal expansion coefficient	1/K
T_{water}	Water temperature	K
c_{ice}	Ice specific heat capacity	J/kg/K
λ_{ice}	Ice thermal conductivity	W/m/K
α_{ice}	Ice volumetric thermal expansion coefficient	1/K

Table 6 Model parameters

Model parameter	Description	Unit
$E_{f,ref}$	Frozen soil Young's modulus at a reference temperature	N/m^2
$E_{f,inc}$	Increase in Young's modulus with temperature	$N/m^2/K$
ν_f	Frozen soil Poisson's ratio	-
G_0	Unfrozen soil shear modulus	N/m^2
κ_0	Unfrozen soil elastic compressibility coefficient	-
κ_s	Elastic compressibility coefficient for suction variation	-
$(s_{c,seg})_{in}$	Initial segregation threshold	N/m^2
M	Slope of the critical state line	-
k_t	Rate of change in apparent cohesion with suction	-
m	Yield surface fitting parameter	-
γ	Plastic potential surface fitting parameter	-
λ_0	Unfrozen soil elasto-plastic compressibility coefficient	-
λ_s	Elasto-plastic compressibility coefficient for suction variation	-
$(p_{y0}^*)_{in}$	Initial pre-consolidation stress for unfrozen condition	N/m^2
Δp_{y0}^*	Change of preconsolidation stress with depth	N/m2/m
Y_{ref}	Reference depth	m
β	Rate of change in soil stiffness with suction variation	m^2/N
r	Coefficient related to the maximum soil stiffness	-
p_c^*	Reference stress	N/m^2
α	Constant parameter for freezing/thawing temperature	-
λ_r	Unfrozen water saturation fitting parameter	-
ρ_r	Unfrozen water saturation fitting parameter	-
T_{ref}	Reference temperature	K
p_{ref}	Reference pressure	N/m^2
e_0	Initial void ratio	-
K_W	Bulk modulus of water	N/m^2
p_{at}	Atmospheric pressure	N/m^2

7 Calibration of clay parameters for the NTNU model

7.1 Vesilahti site

Valkkistentie, a low-volume road section of connecting road 2983 located in Vesilahti, Finland, was chosen as the subject for the modelling section of the thesis due to availability of frost heave, temperature and groundwater level measurement data. The location of the road in southern Finland is represented in Figure 20. The road section of Valkkistentie was renovated and instrumented in the Management of Pavement Service Life by Using New Technology -project conducted by the Tampere University of Technology (TUT) between the years 2006 and 2008 (Luomala et al., 2008).

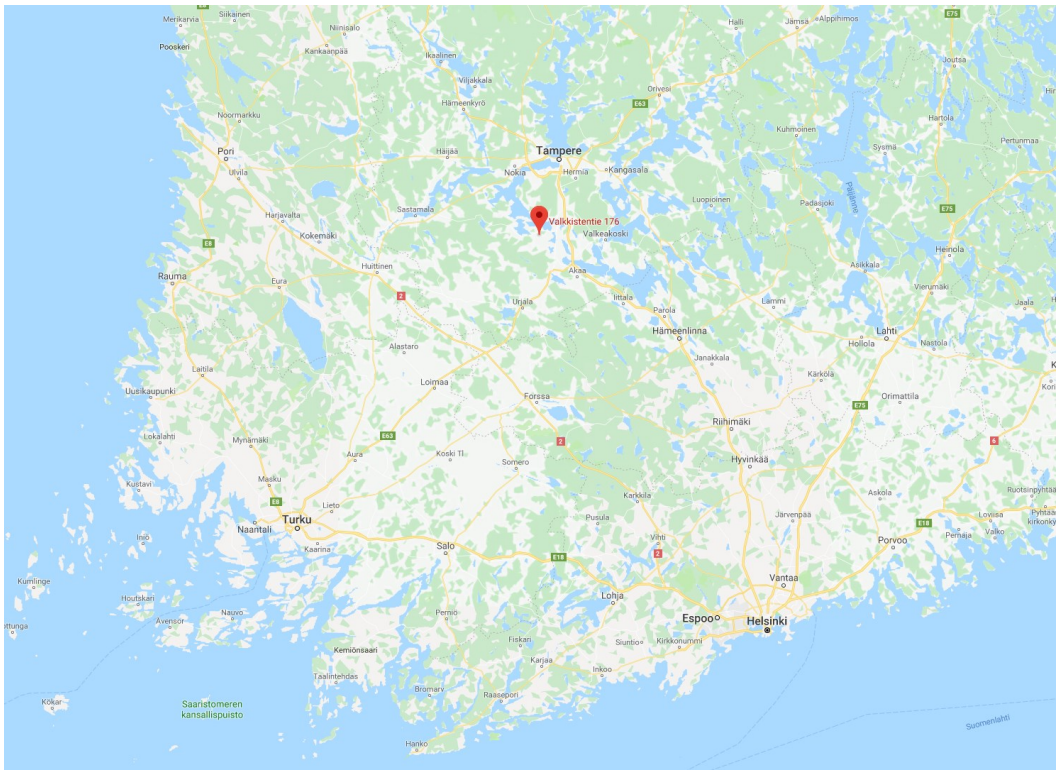

Figure 20 Location of Vesilahti site in South-Western Finland.

The road structure was renovated in the summer of 2006. The pavement structure after renovation consists of a 40 mm layer of soft asphalt pavement PAB-V, 100 mm layer of crushed rock, 150 mm layer of mixed old asphalt and crushed rock and 200 mm layer of crushed gravel. The pavement in the location was thin and the bearing capacity of the pavement was noted to be weak even after the renovation: the structural capacity measured with falling weight deflectometer was between 80-100 MPa (Luomala et al., 2008). According to Luomala et al. (2008) the pavement subgrade consisted of a 1 m layer of dry crust clay, a 1 m thick soft silty layer and till in the depth of circa 2 m, but during the sampling for this thesis the dry crust clay layer was found to extend from the ground surface up to the till layer at circa 2.5 m depth with no notable silty layers.

The monitoring began in October 2006. Three measurements of the road surface frost heave were conducted during the winter at three cross sections of the road each time by levelling with laser: initial measurement in October 2006 before the winter, the high frost heave measurement in March 2007 and measurement after thawing of the road in May 2007, when the road had settled back to its initial level. The temperature and groundwater level monitoring began in November 2006 and continued until the year 2014 (Luomala

et al., 2008). Unfortunately, the temperature and groundwater level data are missing from mid-January to end of January 2007 probably due to a power cut. Before the measurement started the road froze slightly in October due to a short cold time period, which was chosen to be ignored in the modelling due to unavailability of data.

7.2 Sampling at Vesilahti

To derive the soil parameters sampling was conducted at the site on 31st of October in 2018. The sampling point was in a field next to the instrumented road section on the opposite side of the instrumentation measurement station. The layout of sampling site is shown in Figure 21 and Figure 22. The road surface was observed to be level and there was no notable rutting, but the pavement was cracked in places and some of the instrumentation was visible through the cracks. Pavement had been repaired locally along the wheel paths presumably due to rutting. The site is shown in Figure 23. No visual observation of groundwater level was made during digging, which was assumed to be due to dry summer and autumn in the area. The subgrade was observed to be stiff dry crust clay and a hard till layer was hit at around 2.5 m depth. The clay was notably stiff, dry and cracked up to around 1.5 m depth, below which it was more uniform moist clay.

Figure 21 Aerial photo of the Vesilahti site. Sampling point marked with red circle.

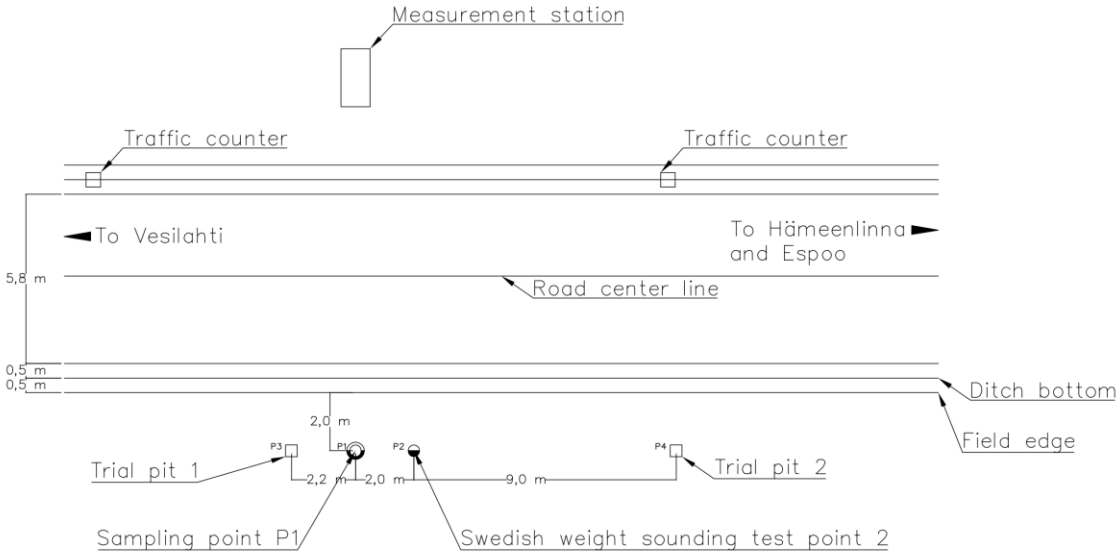

Figure 22 Map of the sampling site and test points.

Figure 23 Site conditions at Vesilahti in October 2018 showing the cracked asphalt surface and local repairs.

The following site tests and measurements summarized in Table 7 were performed at Vesilahti. Two trial pits were dug by an excavator: first to 2.2 m depth and second to 2.5 m depth. 11 thin sampling tubes (15 cm long and 5 cm wide) were taken from 0.3 m depth to 1.95 m depth at sampling point 1 and three wide sampling tubes (10 cm long and 10 cm wide) were taken from 0.6 m depth at the trial pit 2. Disturbed samples were taken from the excavator claw from the first trial pit at 1.6 m depth and from the second at 2.5 m depth. Swedish weight sounding test was performed by hand at point 2 and finally the

site was levelled to measure surface geometry of the road and the surrounding site. The standard sampling tubes used in Finland, types St II and NGI 54, were deemed unfeasible for the very stiff dry crust clay, so the shorter 15 cm long and 5 cm wide cylindrical sampling tubes were manufactured at Aalto University for this sampling.

Table 7 Vesilahti site measurements

Site measurement type	Notes
Trial pit 1	End depth 2.2 m. Disturbed sample taken from the excavator claw at 1.6 m depth.
Trial pit 2	End depth 2.5 m. Disturbed sample taken from the excavator claw at 2.5 m depth.
Sampling at point P1	Eleven sampling tubes taken at 15 cm intervals from 0.3 m depth to 1.95 m depth. Tube type: thin, 15 cm long and 5 cm wide.
Sampling from trial pit 2	Three sample tubes taken from 0.6 m depth. Tube type: wide, 10 cm long and 10 cm wide.
Swedish weight sounding test at point P2	The full 1 kN load and rotation applied during the whole process. Sounding terminated at 2.7 m depth when hard rocky layer or boulder was hit.
Levelling of the site	Traffic counter base plate used as reference height for the levelling.

7.3 Experiments for clay parameters

To derive the dry crust clay parameters required for the modelling the following tests were performed in November and December of 2018 at Aalto University Mineral Based Materials and Mechanics research laboratory:

- tests for classification properties of the clay
- 10 oedometer tests on unfrozen samples
- two water permeability oedometers on unfrozen samples
- two shear box tests on unfrozen samples
- two unconfined axial compression tests on unfrozen samples
- frost heave test

All tests were performed using the samples from the 15 cm long and 5 cm wide thin sampling tubes, except the frost heave test for which a wide sample was used. As temperature- and suction-controlled equipment were unavailable for the oedometer, the unconfined axial compression tests and the frost heave test, it was decided to calibrate the model parameters determined with these tests during the modelling and determine the more usual unfrozen clay properties using the standard laboratory equipment.

Classification tests were used to determine clay grain size distribution, specific weight, specific gravity, bulk density, organic content and void ratio. Oedometer tests were used

to determine deformation parameters κ_0 and λ_0, vertical permeability and the initial clay preconsolidation stress, which was estimated using the Casagrande method. Shear box tests were used to determine clay cohesion and the angle of shearing resistance. Unconfined axial compression tests were used to determine the Young's modulus of unfrozen soil. The frost heave test was used to evaluate freezing of the dry crust clay. Laboratory tests are summarized in Table 8.

Table 8 Laboratory tests

Laboratory test type	Determined property and purpose
Classification tests	Grain size distribution, specific weight, specific gravity, bulk density, organic content, void ratio.
Oedometers tests	Deformation parameters κ_0 and λ_0, vertical permeability estimate, initial preconsolidation stress.
Water permeability oedometer tests	Vertical permeability estimate.
Shear box tests	Cohesion and angle of shearing resistance.
Unconfined axial compression tests	Young's modulus.
Frost heave test	Freezing characteristics of the clay.

The grain size distribution of samples is represented in Figure 24. This also illustrates the frost susceptibility criterion based on grain size by ISSMFE-TC8 (1989), which indicates the clay is slightly frost-susceptible. Grain size distribution located in areas 2, 3 and 4 is non-frost-susceptible, distribution in area 1 is frost-susceptible and in area 1L slightly frost-susceptible. If the distribution intersects two areas, it is also frost-susceptible.

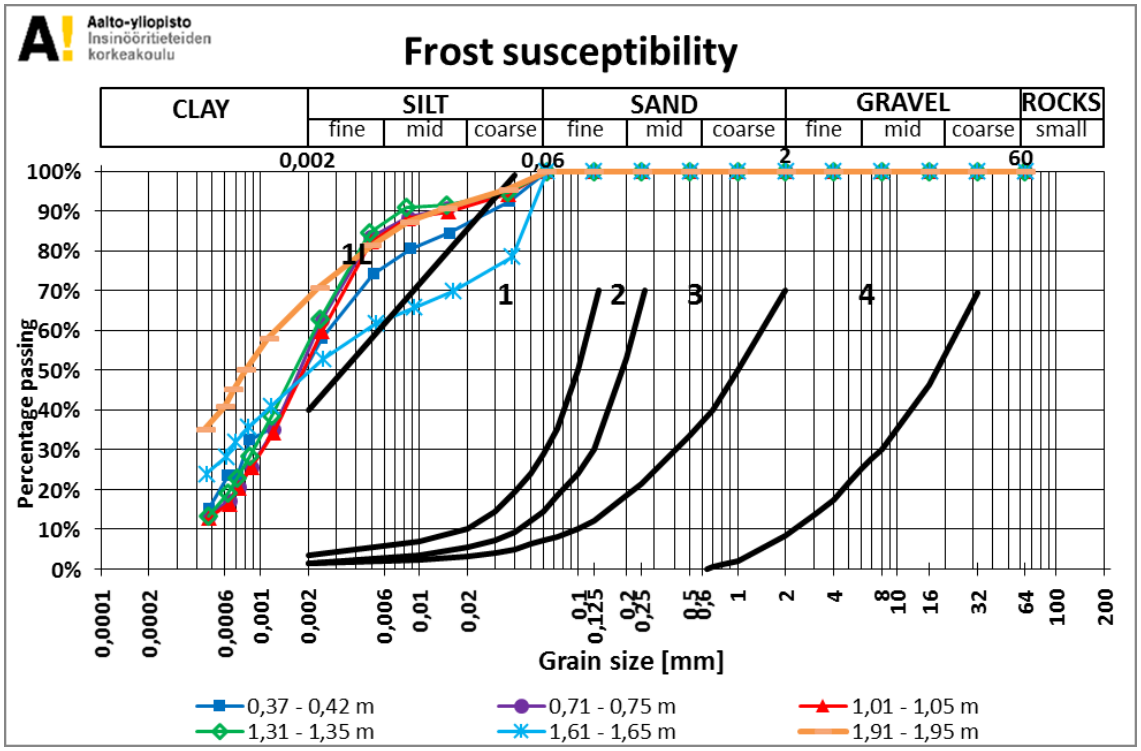

Figure 24 Grain size distribution of clay samples with frost susceptibility limits.

The classification properties of the clay are shown in following Table 9 and Table 10.

Table 9 Clay content, organic content, specific gravity and bulk density of the samples.

Depth m	Clay content %	Organic content %	Specific gravity g/cm^3	Bulk density g/cm^3
0.37-0.42	55.4	1.20	2.84	1.85
0.71-0.75	52.9	0.34	2.80	1.87
1.01-1.05	50.6	0.66	2.81	1.84
1.31-1.35	54.8	0.76	2.84	1.76
1.61-1.65	48.5	1.78	2.86	1.66
1.91-1.95	67.1	1.08	2.79	1.65

Table 10 Unit weight from fall cone test samples and unit weight and void ratio from oedometer test samples.

Depth m	Unit weight (fall cone samples) kN/m^3	Unit weight (oedometer samples) kN/m^3	Void ratio (oedometer samples) -
0.37-0.42	18.1	18.8	0.93
0.71-0.75	18.3	18.5	1.01
1.01-1.05	18.0	18.0	0.98
1.31-1.35	17.3	17.3	1.25
1.61-1.65	16.3	16.9	1.44
1.91-1.95	16.2	16.2	1.54

The deformation parameters along with estimated preconsolidation stress and vertical permeability from oedometer tests are shown in Table 11.

Table 11 Deformation parameters, preconsolidation stress and vertical permeability estimates from oedometer tests.

Depth (m)	λ	κ	Preconsolidation stress (kPa)	Permeability (m/s) Taylor	Permeability (m/s) Casagrande
0.30-0.43	0.075	0.030	115.6	$3.31\cdot10^{-10}$	$3.90\cdot10^{-10}$
0.69-0.71	0.079	0.029	148.4	$11.9\cdot10^{-10}$	$6.42\cdot10^{-10}$
0.95-0.97	0.062	0.022	190.6	$3.04\cdot10^{-10}$	$3.44\cdot10^{-10}$
0.97-0.99	0.068	0.023	165.7	$4.80\cdot10^{-10}$	$3.32\cdot10^{-10}$
0.99-1.01	0.073	0.024	164.0	$4.92\cdot10^{-10}$	$3.85\cdot10^{-10}$
1.28-1.30	0.078	0.028	188.7	$3.03\cdot10^{-10}$	$3.56\cdot10^{-10}$
1.58-1.60	0.145	0.045	270.4	$3.08\cdot10^{-10}$	$2.99\cdot10^{-10}$
1.84-1.86	0.211	0.063	399.4	$1.55\cdot10^{-10}$	$1.52\cdot10^{-10}$
1.86-1.88	0.205	0.061	403.4	$1.34\cdot10^{-10}$	$1.85\cdot10^{-10}$
1.88-1.90	0.213	0.058	403.4	$2.93\cdot10^{-10}$	$2.48\cdot10^{-10}$

The measured vertical permeabilities in the water permeability oedometer tests were $3.80\cdot10^{-9}$ m/s and $1.98\cdot10^{-10}$ m/s. The clay cohesion from shear box tests was 33.3 kPa and

angle of shearing resistance 39 °. Young's modulus from unconfined axial compression tests was 28.15 MPa.

7.4 Clay parameters used in modelling

Based on the laboratory tests and calibration of the model during calculations for best fit to measurements, the parameters in Table 12 and Table 13 were chosen for the Vesilahti clay to model the road frost heave. As the clay parameters from laboratory tests varied a bit with depth, it was chosen to divide the clay into two layers at 1.3 m depth to take this into account. The clay material was set as drained in Plaxis, which allows for calculation and dissipation of pore pressures. The thermal conductivity and specific heat capacity of clay were determined based on literature values from Sundberg (1988) and the thermal expansion coefficient was calculated based on formula for volumetric thermal expansion coefficient in work of Jobmann et al. (2007).

Model parameters that were not determined or calculated from the laboratory test results were approximated initially and then calibrated during the modelling process as necessary. As experimental results were unavailable, the parameters λ_r and ρ_r to determine soil unfrozen water content by Nishimura et al. (2009) were calculated by first using the grain size distribution method by Anderson and Tice (1972) to estimate the unfrozen water saturation of clay and then fitting the curves shown in Figure 25 andFigure 26. The calculated unfrozen water saturations were then input as a table for each clay layer into Plaxis program.

Using the NTNU model fitting parameters, the van Genuchten model parameters were calculated based on relations described in chapter 5.4, the parameter g_l was assumed based on previous work with the model by Rostami (2017). The parameters $E_{f,inc}$, ν_f and p_c^* were assumed based on model manual by Ghoreishian Amiri et al. (2016a), and the parameters κ_s, $(s_{c,seg})_{in}$, k_t, λ_s, β and r were initially estimated based on the manual and thesis of Aukenthaler (2016) and then calibrated during the calculation process. It should be noted that the clay layer 1 value of the segregation threshold $(s_{c,seg})_{in}$ of 1.4 MPa is lower than what should be expected for a clay that has experienced multiple freeze-thaw cycles already, but is similar in magnitude to the low value of 250 kPa utilized by Rostami in his thesis (2017), where frost heave of silt was investigated. The at-rest coefficient of earth pressure K_0 was calculated automatically by Plaxis.

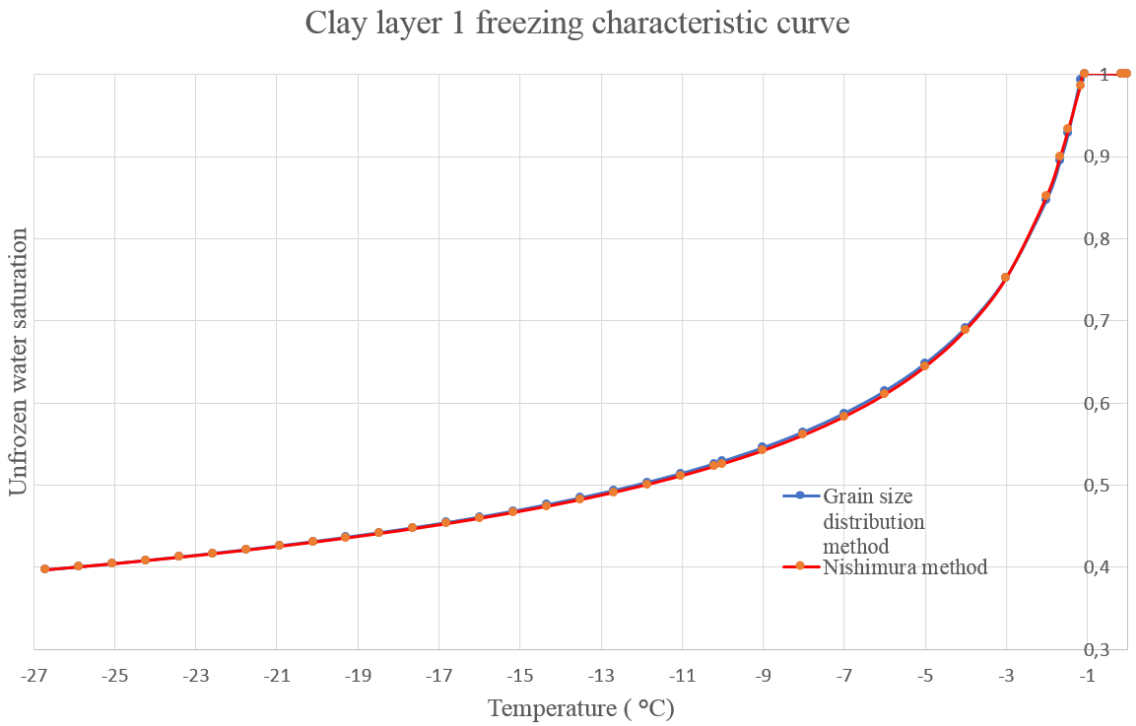

Figure 25 Clay layer 1 freezing characteristic curve fitting.

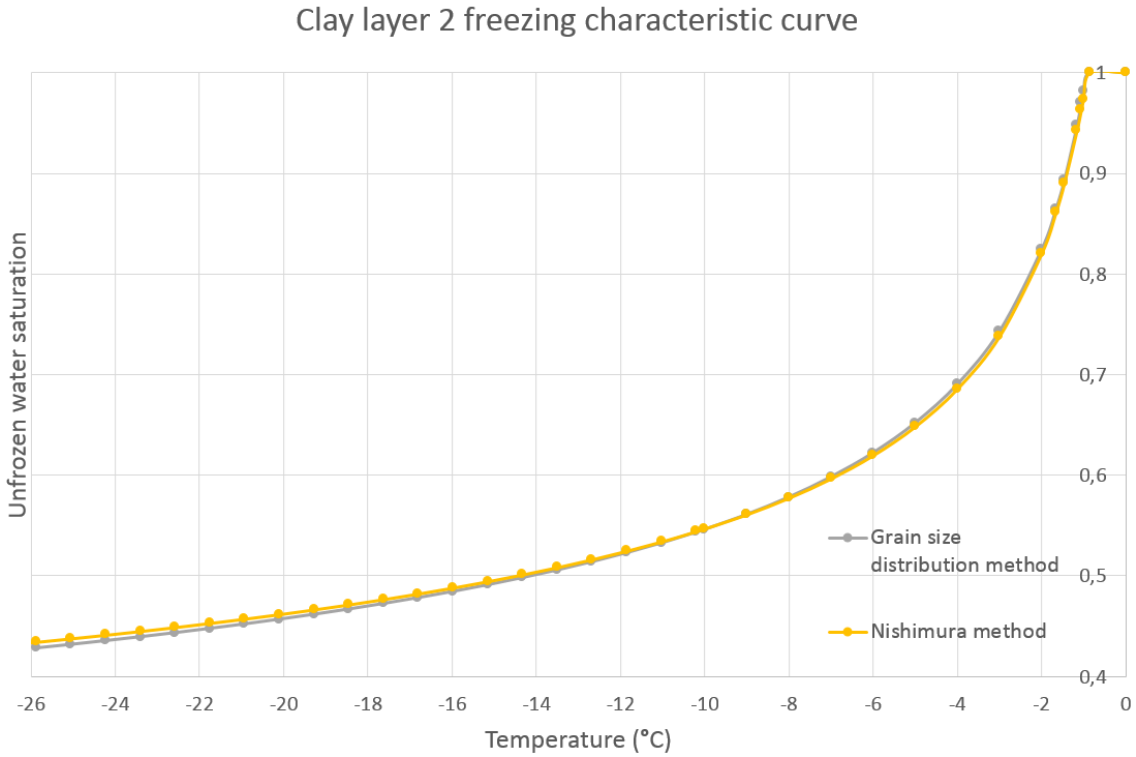

Figure 26 Clay layer 2 freezing characteristic curve fitting.

Table 12 General parameters of clay used in the road modelling.

Parameter	Clay layer 1	Clay layer 2	Unit
γ_{sat}	18.3	16.7	kN/m^3
γ_{unsat}	18.3	16.7	kN/m^3
e_0	1	1.4	-
S_{res}	0.39	0.40	-
S_{sat}	1	1	-
g_n	1.27	1.23	-
g_a	0.01	0.01	1/m
g_l	0.5	0.5	.
k_x	$3.8 \cdot 10^{-9}$	$0.3 \cdot 10^{-9}$	m/s
k_y	$3.8 \cdot 10^{-9}$	$0.3 \cdot 10^{-9}$	m/s
c_s	990	990	J/kg/K
ρ_s	2820	2830	kg/m^3
λ_s	1.1	1.4	W/m/K
$\alpha_{x,y,z}$	$1.8 \cdot 10^{-4}$	$2.7 \cdot 10^{-4}$	1/K
K_0	0.5	0.5	-

Table 13 Model parameters of clay used in the road modelling.

Model parameter	Clay layer 1	Clay layer 2	Unit
$E_{f,ref}$	28.15	28.15	MPa
$E_{f,inc}$	10	10	MPa/K
ν_f	0.35	0.35	-
G_0	10.43	10.43	MPa
κ_0	0.026	0.057	-
κ_s	$0.1 \cdot 10^{-3}$	$0.1 \cdot 10^{-3}$	-
$(s_{c,seg})_{in}$	1.4	1	MPa
M	1.6	1.6	-
k_t	0.15	0.07	-
m	1	1	-
γ	1	1	-
λ_0	0.073	0.194	-
λ_s	0.9	0.6	-
$(p_{y0}^*)_{in}$	-120	-120	kPa
Δp_{y0}^*	-110	-110	kPa/m
Y_{ref}	-0.3	-0.3	m
β	$0.8 \cdot 10^{-6}$	$0.8 \cdot 10^{-6}$	m^2/N
r	0.6	0.6	-
p_c^*	-50	-50	kPa
α	9	9	-
λ_r	0.21	0.19	-
ρ_r	$1 \cdot 10^6$	$800 \cdot 10^3$	-
T_{ref}	273.16	273.16	K
p_{ref}	-395	-395	MPa
e_0	1	1.4	-
K_W	1	1	GPa
p_{at}	-100	-100	kPa

7.5 Suggestions for future model parameter development

In this thesis the laboratory tests were used to determine the more general clay parameters, and the model specific parameters especially affecting frozen behavior were estimated to fit the desired final values.

The model parameters important for the freezing and thawing behavior of soil $E_{f,inc}$, ν_f, p_c^*, κ_s, $(s_{c,seg})_{in}$, k_t, λ_s, β and r were initially approximated based on values used in previous works with the NTNU model (Ghoreishian Amiri et al., 2016a, Aukenthaler, 2016) and then adjusted as necessary to fit the site measurement results. The suggested calibration method of the virgin soil state parameters by Zhang et al. (2016b) was omitted due to unavailability of required suction-controlled oedometer tests. The utilized parameter values are well in the range of values observed in previous works with the NTNU model.

To better validate the calculation and the results, the suggested laboratory tests with temperature and suction control should be used in the parameter definition. While the currently obtained results are qualitatively correct, this approach omits evaluating the actual performance and results of the model with verified laboratory tested parameters. Modelling with laboratory derived parameters could provide key insights into differences between reality and behavior estimated by the model.

In this thesis the goal is to replicate the observed behavior, but parameters derived from laboratory analysis would allow comparison of results with the "true" soil parameters and whether adjusting them to fit observed real behavior would be necessary. Actual laboratory test data used to determine the parameters would thus provide better ground for the parameter choice in the reality, enable more in-depth analysis of the model capabilities and limits in replicating actual frozen soil behavior, and divine whether issues in the calculation are possibly more related to the constitutive model implementation than parameter choice.

The thermal parameters of the clay were determined from literature and the used average values might not accurately represent the properties of the Vesilahti dry crust clay. The unfrozen water saturation of the clay was estimated with an empirical equation and fitted with the model parameters. Determining these important properties of a freezing soil with laboratory experiments would improve the accuracy of the calculation and remove additional degrees of freedom from the calibration of results.

Many properties of the model are influenced by multiple parameters simultaneously, and some of the parameters also affect multiple physical properties. The effect of variation of a single parameter is thus not unequivocal and can lead to unexpected results. Parameter variation process to obtain the desired results has been time-consuming and, due to the aforementioned nature of the model parameters and processes, other parameter combinations could provide similar results. This accentuates the importance of precise, laboratory test proven parameters to back up the choice of model parameters and validate the result of calculations beyond qualitative similarity. As suggested before, future research on this subject could improve on this work by determining the Vesilahti clay thermal properties by laboratory testing and also implement the suggested suction and temperature dependent laboratory tests for the model parameter determination.

8 Numerically modelling Vesilahti case study on pavement deformation

8.1 Measurement data on freezing

As stated before, the obtained measurement data from Vesilahti contained continuous temperature and groundwater depth data from winter 2006-2007 except for a short break in January. The temperature data is illustrated in Figure 27 and groundwater level data in Figure 28. The temperature was measured in the asphalt layer and at 0.26 m, 0.39 m, 0.52 m, 0.72 m, 1.02 m, 1.32 m and 1.62 m depths at the edge of the road. The groundwater level pipe was at the side of the road. Frost depth in the middle of the road and road edge was estimated from temperature measurements, which indicates that the center section was fully thawed in by 24.4.2007 and the edge around a week earlier. The frost depth estimates are shown in Figure 29.

The frost heave of the road was measured at three cross sections three times: in October 2006, March 2007 and May 2007. The October measurement was the initial, March the high frost heave and May the after thawing final measurement. The heave of the surface was levelled at 11 points at circa 0.5 m intervals. Based on this available data the goal of the modelling was chosen to be replicating the road frost heave in the May and March states to match the freezing and thaw deformation behavior of the pavement. As there was no continuous data on the frost heave, the analysis of deformation behavior with time was considered a secondary priority for qualitative consideration.

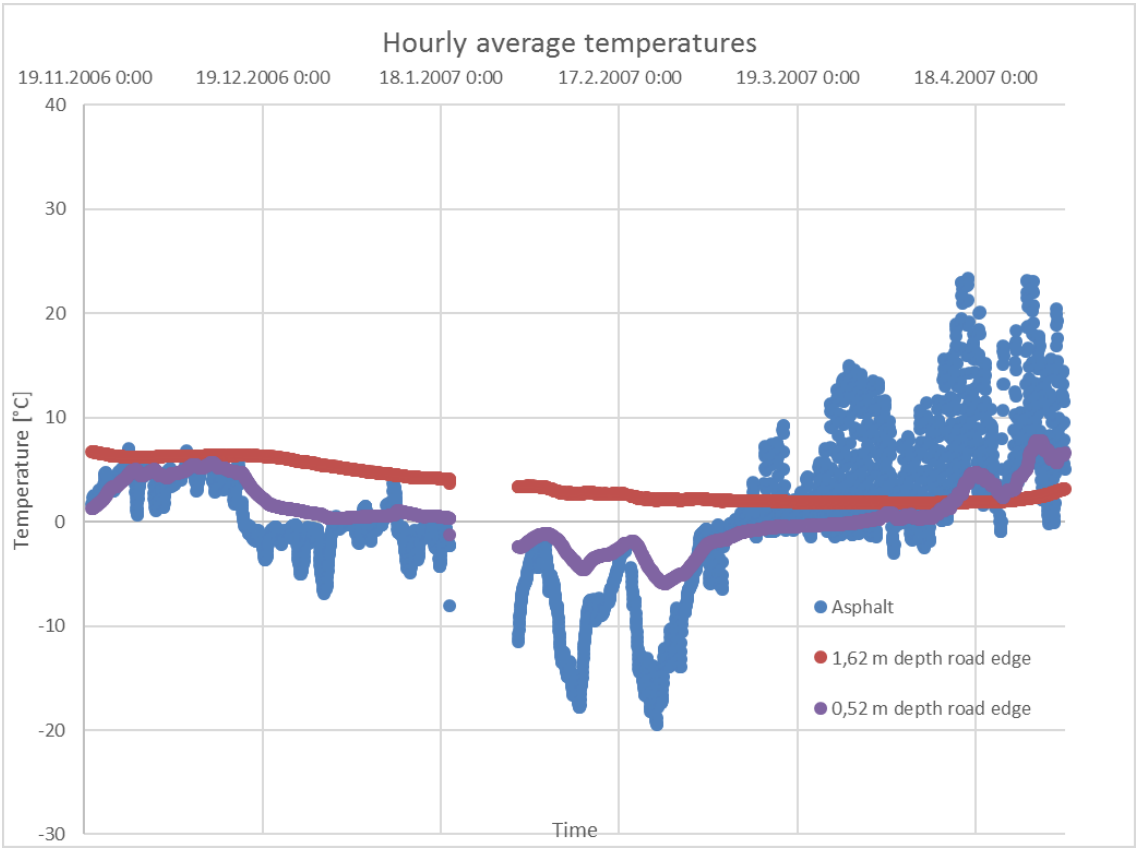

Figure 27 Vesilahti temperature measurement data of asphalt surface and two depths for illustration. The gap in measurements in the end of January was probably due to power cut.

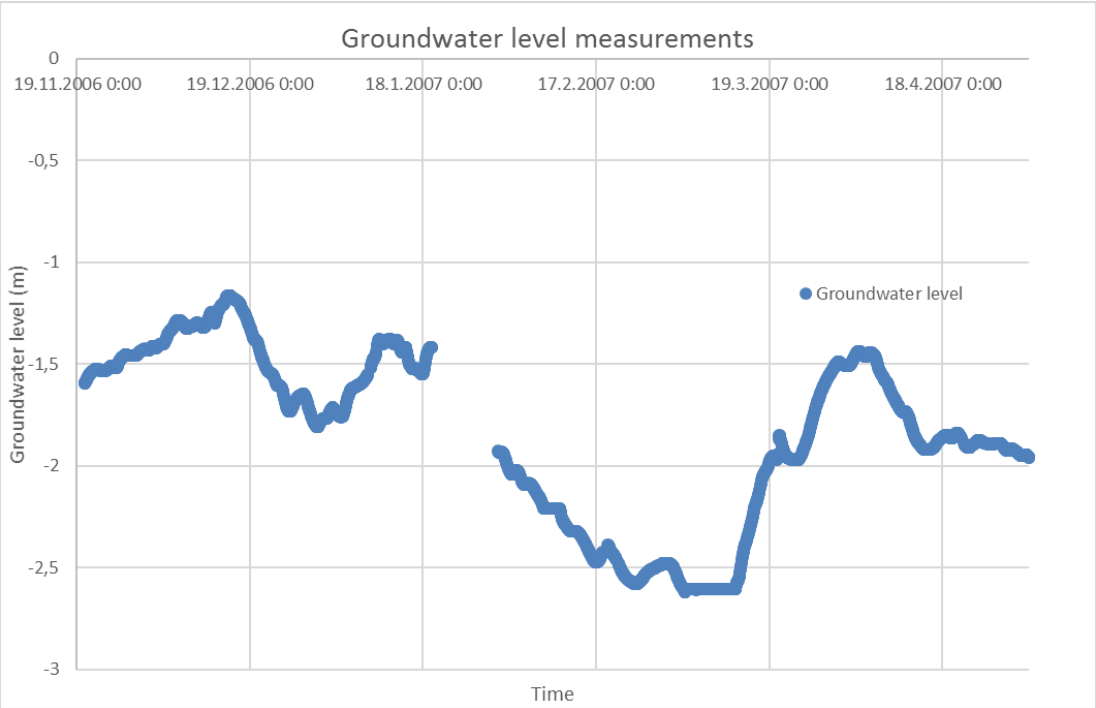

Figure 28 Vesilahti groundwater level measurement data.

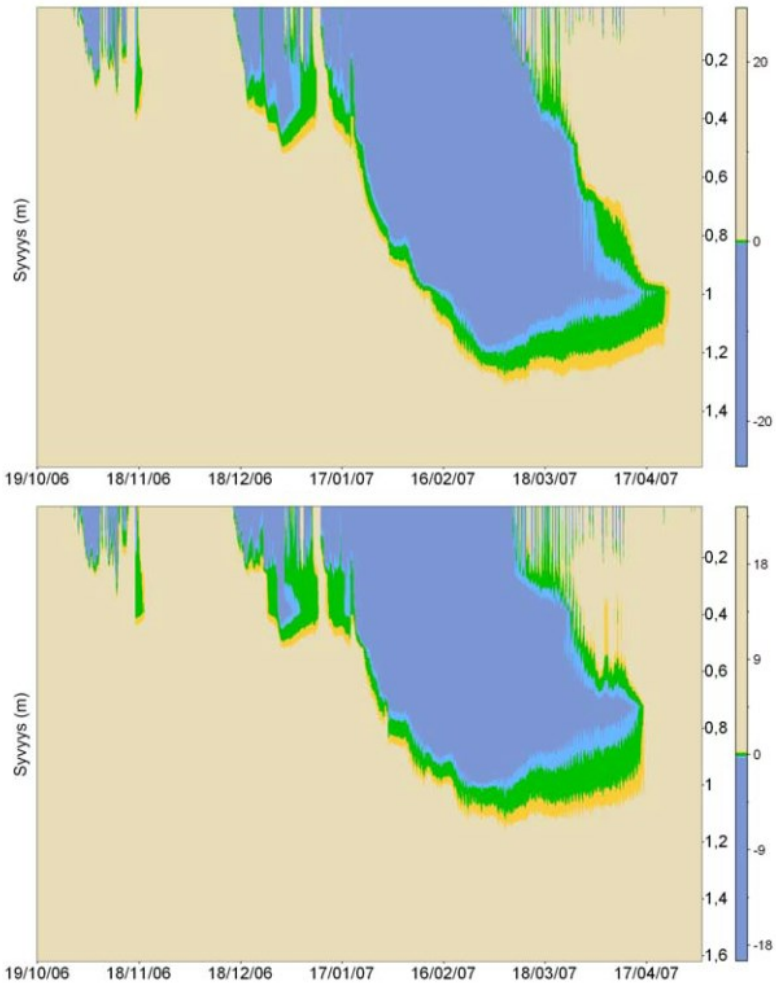

Figure 29 Frost depth in the middle of the road (top) and the edge of the road (bottom) (Luomala et al., 2008).

There was no measurement data on the snow cover at Vesilahti during the winter of 2007 so archive data from Finnish environmental administration for municipality of Pälkäne, which is circa 40 km east of Vesilahti, was chosen to estimate snow cover in the modelling. The snow cover and frost depth data at Pälkäne is illustrated in Figure 30.

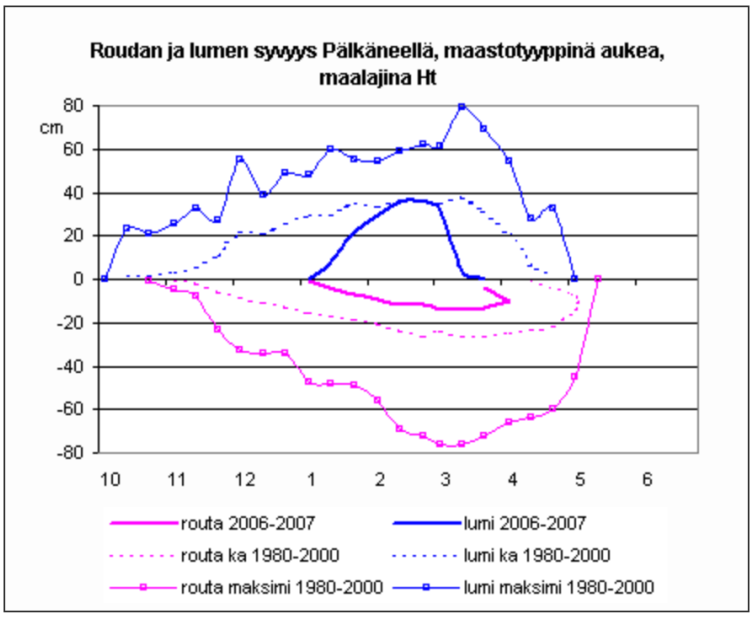

Figure 30 Snow cover and frost depth data from Pälkäne in winter 2006-2007.

8.2 Modelling the road frost heave

For the modelling, only half of the road structure was considered due to symmetry. The calculation was performed with the Plaxis 2D version 2018.01. The modelling was performed as a plane-strain problem and the used elements were 6-noded triangles. The calculation geometry and mesh are visible below in Figure 31, which also illustrates the applied traffic load, pavement layers, snow cover and the two clay layers.

The used mesh was 272-element coarse mesh, which was considered to be an adequate balance between decent calculation times and accuracy of results. Mesh was refined on the road surface for more accurate heave results and around the ditch as numerical issues with the steep slope arose during calculations.

Width of the geometry was set at 6 m so that the right boundary would not affect the ditch. The depth of geometry was set to 2.5 m at the approximate boundary of the hard till layer. A 10 kPa line load was applied on the pavement surface as reportedly there was heavy vehicle traffic at the road during the measurement time (Luomala et al., 2008).

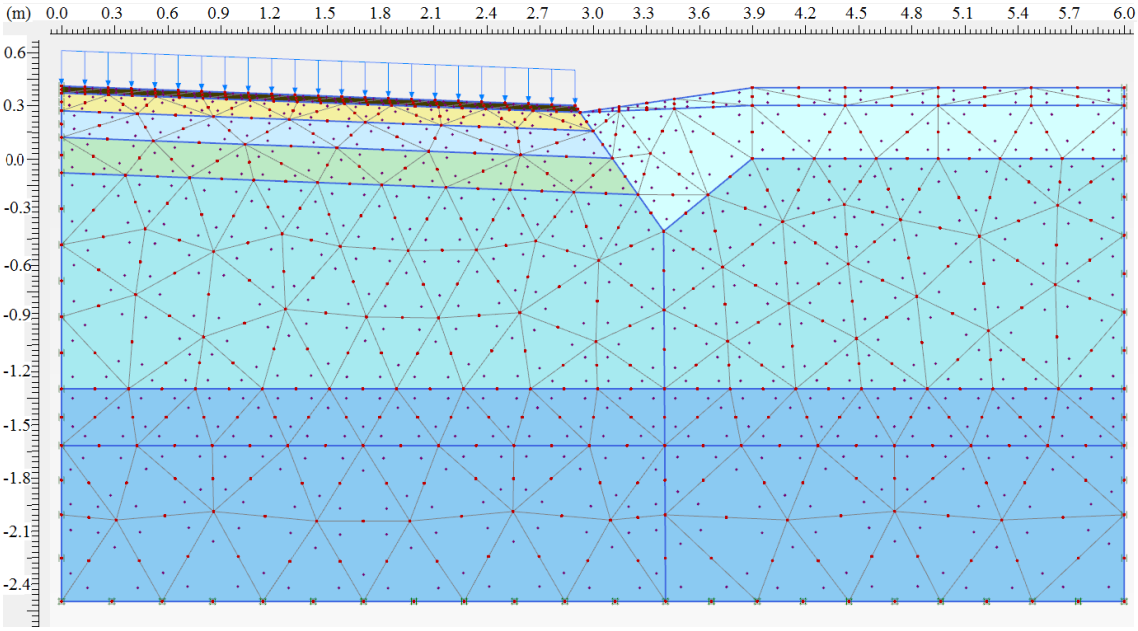

Figure 31 Road calculation geometry and mesh.

The calculation phases were chosen to replicate the available temperature and groundwater level data. The temperatures were implemented as temperature boundary conditions on the model top surface and on a line in 1.62 m depth as this was the deepest measurement available. The groundwater level in each calculation phase was either kept constant or assigned a function to match the measured change in the level.

The initial state of the soil was calculated as K_0 procedure and all other phases were fully coupled flow deformation as required by the user-defined soil model. Based on suggestions by Ghoreishian Amiri et al. (2016a) the maximum calculation steps were increased to 10000 and the over-relaxation factor was set to 0.8 for all phases incorporating freezing and thawing effects. The maximum load increment was set to 0.01 for these phases. For the thaw phases the maximum number of iterations was increased to 200 as the calculation struggled to converge in the default 60 iterations. The calculation phase information is described in Table 14 and Table 15.

The model left-symmetry boundary is normally supported and closed for water and heat flow. The right boundary is normally supported, closed for heat flow and open for water flow. On the top surface boundary, the top temperature boundary condition is applied, and it is set to seepage for water flow. When the snow layer was applied, the temperature condition was applied on top of it. The bottom boundary is fully supported, and no other conditions are imposed on it.

Table 14 Calculation phase types, time intervals and maximum number of steps.

Phase	Calculation type	Time interval	Max steps
Initial phase	K_0 procedure	-	1000
Constant temperature +3 °C	Fully coupled flow deformation	30 days	1000
First freezing phase -2 °C	Fully coupled flow deformation	30 days	10000
Primary freezing phase with varying temperature	Fully coupled flow deformation	45 days	10000
Temperature increase to -2 °C	Fully coupled flow deformation	7 days	10000
Thaw temperature increase 1	Fully coupled flow deformation	30 days	10000
Thaw temperature increase 2	Fully coupled flow deformation	30 days	10000

Table 15 Tolerated error, over-relaxation factor and maximum number of iterations.

Phase	Tolerated numerical error	Tolerated flow error	Over-relaxation factor	Max number of iterations
Initial phase	0.01	-	1.2	60
Constant temperature +3 °C	0.01	0.005	1.2	60
First freezing phase -2 °C	0.03	0.005	0.8	60
Primary freezing phase with varying temperature	0.03	0.005	0.8	60
Temperature increase to -2 °C	0.03	0.005	0.8	60
Thaw temperature increase 1	0.03	0.005	0.8	200
Thaw temperature increase 2	0.03	0.005	0.8	200

The temperature and groundwater level conditions imposed in each phase are described in Table 16. The first calculation phase represents the one-month time interval from mid-November to mid-December. The surface temperature is set as constant +3 °C and the bottom to +6 °C. The groundwater level is set to linearly rise during the phase from 1.6 m depth to 1.2 m depth.

The second phase also lasts one month from the end of previous phase to mid-January. The measured surface temperature slightly varied during the time of the second phase and -2 °C was chosen as the average value for the phase. The bottom temperature is set to +2 °C, which is kept also for the following two freezing phases and the first thaw phase. In the second phase the groundwater level decreases to 1.8 m depth and rises again to 1.4 m depth according to a harmonic function emulating the measured level.

Third phase lasts one and half months to beginning of March, during which surface temperature varies between -2.5 °C and -17.5 °C according to a harmonic function to emulate the high variation of temperature in measurements. The water level decreases to 2.5 m depth.

Fourth phase is one week long, during which the surface temperature linearly increases to -2 °C. The end of this phase corresponds with the measurement time of high frost heave at the end of first week of March. The water level is kept at constant 2.6 m depth.

During the two thaw phases, each one month long, the surface temperature increases linearly to +10 °C, which was an approximated value from the highly varying surface temperature data during the spring time. In the second thaw phase the bottom temperature increases to +3.8 °C. During the first thaw phase the water level rises to 1.4 m depth and in the second thaw phase it decreases to 2 m depth.

Table 16 Surface and bottom temperature and groundwater depth variation in the calculation phases.

Phase	Surface temperature (°C)	Bottom temperature (°C)	Groundwater depth (m)
Initial phase	+3	+6	1.6
Constant temperature +3 °C	+3	+6	Linear increase to 1.2
First freezing phase -2 °C	-2	+2	Harmonic between 1.8 to 1.4
Primary freezing phase with varying temperature	Harmonic between -2.5 to -17.5	+2	Linear decrease to 2.5
Temperature increase to -2 °C	Linear increase to -2	+2	2.6
Thaw temperature increase 1	Linear increase to +10	+2	Linear increase to 1.4
Thaw temperature increase 2	Linear increase to +10	Linear increase to +3.8	Linear decrease to 2

As the early winter of 2006-2007 was unusually snowless, the snow layer is added in the primary freezing phase representing time from mid-January and the temperature increase phase in March following it. The snow thickness is approximated as 30 cm in the primary phase and 40 cm in the temperature increase phase based on the Pälkäne measurements. As the snow melted very quickly after beginning of March, the layer was removed in the thaw phases.

8.3 Other parameters in the road modelling

Beside the Vesilahti clay parameters described in Table 12 and Table 13, the pavement materials and snow were also required for the calculation in addition to the water and ice

thermal parameters shown in Table 17. For the sake of simplicity, the pavement materials and snow were chosen to be modelled with the linear elastic material model as structural failure was not investigated in this study. The asphalt was set as non-porous and the other materials as drained. The parameters of the pavement structure and snow are compiled in Table 18.

Table 17 Water and ice thermal parameters in calculation.

Parameter	Value	Unit
T_{ref}	274.16	K
γ_{water}	10	kN/m^3
c_{water}	4181	J/kg/K
λ_{water}	0.6	W/m/K
L_{water}	$334 \cdot 10^3$	J/kg
α_{water}	$2.1 \cdot 10^{-4}$	1/K
T_{water}	274.16	K
c_{ice}	2108	J/kg/K
λ_{ice}	2.22	W/m/K
α_{ice}	$5 \cdot 10^{-5}$	1/K

There was very little data available on the Vesilahti pavement materials beside their density and unit weight, so the parameters were mostly estimated from literature values.

The mixed layer of old asphalt and crushed rock was estimated to be roughly similar to pure crushed rock. The void ratios of granular materials were estimated from Yang (2013) and the void ratio of asphalt was assumed as there was no data on that.

The Young's modulus was estimated for asphalt from the work of Taha et al. (2013) and for the granular materials from Obrzud and Truty (2018). The values of Poisson's ratio were taken from Maher and Bennert (2008). The permeability of crushed rock was estimated from Zohrabi and Temporal (2001) and of the other granular materials from Heindel and Noyes (1997).

The thermal conductivity of asphalt was estimated from Chen et al. (2015), specific heat capacity from Ma et al. (2016) and thermal expansion coefficient from Petersen et al. (2005). Thermal parameters of the granular materials were estimated from Sundberg (1988) except for thermal expansion coefficients, which were estimated from Huotari and Kukkonen (2004) for granite based rocks.

To estimate unfrozen water saturation in the pavement materials the automatic calculation option of unfrozen water, based on the default USDA dataset sand, was chosen.

The snow parameters were also estimated using average values from literature. The snow thermal parameters and density were estimated from RIL 218-2001 guidebook (2001) assuming the snow is slightly packed. The thermal expansion coefficient of snow was assumed to be less than that of ice. The Young's modulus of snow was estimated from Gerling et al. (2017) and void ratio from Sidler (2014) based on the assumed density. The Poisson's ratio of snow was assumed to be close to that of ice. The permeability of snow was estimated from work of Kuroiwa (1968).

Table 18 Pavement material and snow parameters.

Parameter	Asphalt	Crushed rock	Old mixture	Crushed gravel	Snow	Unit
γ_{sat}	24	22	21	21	3.9	kN/m^3
γ_{unsat}	24	22	21	21	3.9	kN/m^3
e_0	0.05	0.5	0.5	0.5	1.5	-
E	$14 \cdot 10^3$	150	150	150	300	MPa
ν	0.35	0.35	0.35	0.35	0.3	-
k_x	-	$5 \cdot 10^{-4}$	$1 \cdot 10^{-4}$	$8 \cdot 10^{-5}$	0.02	m/s
k_y	-	$5 \cdot 10^{-4}$	$1 \cdot 10^{-4}$	$8 \cdot 10^{-5}$	0.02	m/s
c_s	950	800	600	560	2100	J/kg/K
ρ_s	1900	2150	2200	2140	400	kg/m^3
λ_s	2	2.9	2.9	0.9	0.4	W/m/K
$\alpha_{x,y,z}$	$2 \cdot 10^{-5}$	$2 \cdot 10^{-5}$	$2 \cdot 10^{-5}$	$2 \cdot 10^{-5}$	$5 \cdot 10^{-5}$	1/K

8.4 Modelling results

The vertical deformations of the model were inspected at six points corresponding to the measurement points from the middle to the edge of the road. The vertical deformation with time is visible in

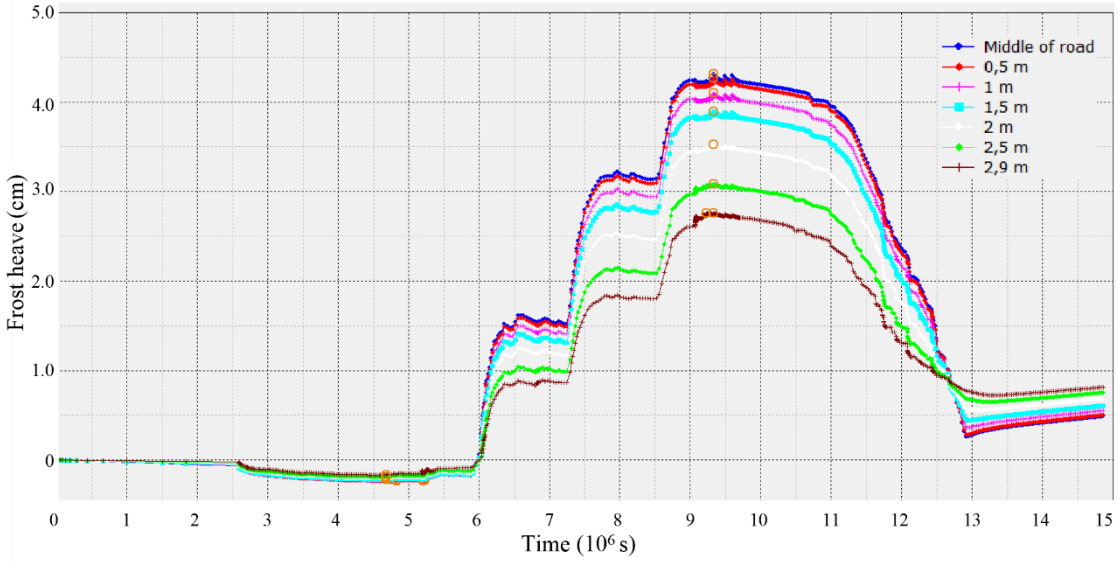

Figure 32.

It can be observed that the road settles very slightly under its own weight and the traffic load during the initial warm phase. The structure then settles more during the first mild freezing phase due to the effect of the parameter κ_s that causes decrease of volume in the freezing soil when the cryogenic suction has not yet increased above the initial segregation threshold.

When the cyclic temperature variance is applied in the primary freezing phase the effect of the varying temperature and the much higher magnitude of cryogenic suction can be observed on the increase of heave. When the temperature decreases toward -17.5 °C and the cryogenic suction is at its highest, the frost heave increases fast, and conversely when

the temperature rises toward -2.5 °C and the cryogenic suction decreases, the accumulation of heave stops. The elastoplastic compression coefficient λ_s controlling the dependence of volume change on cryogenic suction variation and the initial segregation threshold $(s_{c,seg})_{in}$ controlling the limit of frost heave initiation affect the magnitude of frost heave significantly and fitting these two parameters for the best match to measurements was one key issue to address in the simulations.

The high frost heave is measured during the fourth phase when the temperature increases back to -2 °C after the cyclic variation and the frost heave can be seen to remain almost constant during that time.

During the first thaw phase the heave decreases initially slowly as the subgrade clay causing the heave thaws first only from below as the temperature slowly increases at depth when the cooling from surface stops, while the top of the clay layer remains still frozen as the pavement layers thaw. Then the heave can be seen decreasing much more steeply as the clay starts to thaw from the top down too as the pavement structural layers have thawed first. The decreased hydraulic conductivity of the frozen soil and pavement layers hinders the flow of water in the soil during thaw, but as the thawing begins to occur on both the bottom and the top of the frozen clay layer the rate of settlement increases with excess water flowing through the more permeable unfrozen granular structural layers. During the second thaw phase the road geometry thaws completely and the after-thaw measurement corresponds to the end of the phase. However, after thawing fully the pavement surface starts to slightly heave again, while the measurements show that the road settled back to its initial state. The reason behind this seems to be thermal expansion of the clay as running the calculation with unrealistically small or even zero values of clay thermal expansion coefficient yielded results with no surface heave after thawing.

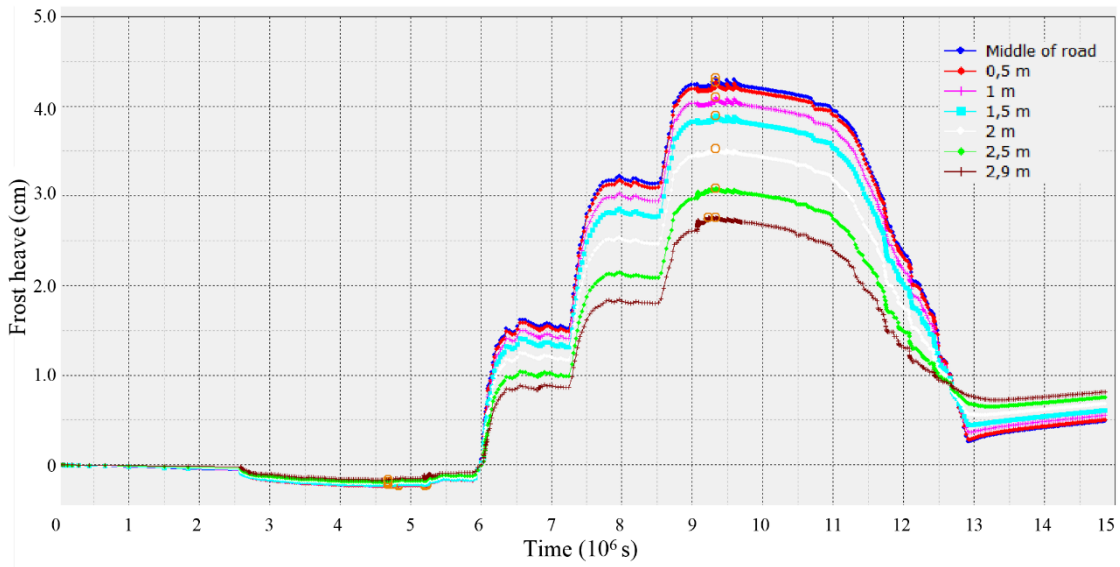

Figure 32 Calculated pavement surface heave across the road cross section.

Comparing the simulated deformation of the road cross section to the three cross section measurement lines 1, 2 and 3 after the fourth calculation phase corresponding to the high frost heave measurement in the beginning of March in Figure 33, it can be seen that the high frost heave simulation corresponds qualitatively well to the measured values. The measurement lines were located at c. 10m intervals from each other with line 3 in the middle of lines 1 and 2. The measurement at line 2 shows quite a bit higher frost heave than at lines 1 and 3, which could indicate local variation of road structure and subsoil

conditions affecting the frost heave. On the measurement site steel bars struck in to the ground in the side of the road were used as reference points for the in-situ frost heave levelling measurements and they were assumed to maintain their vertical position as constant through the measurement time from winter to spring, but a possible source of error could be the movement of the bars along with the ground frost heave.

The calculation however indicates that the heave continuously decreases towards the road edge, while the measured heave is uniform across the whole surface except for the very edge. This seems to be due to the effect of the simulated snow layer that hinders penetration of frost around the ditch and edge of the road. Decreasing the insulating effect and the thickness of the snow layer increased frost penetration, which was already higher in the calculation than the measurements indicated. It also increased frost heave in the middle of the road further so the current result was considered an acceptable compromise.

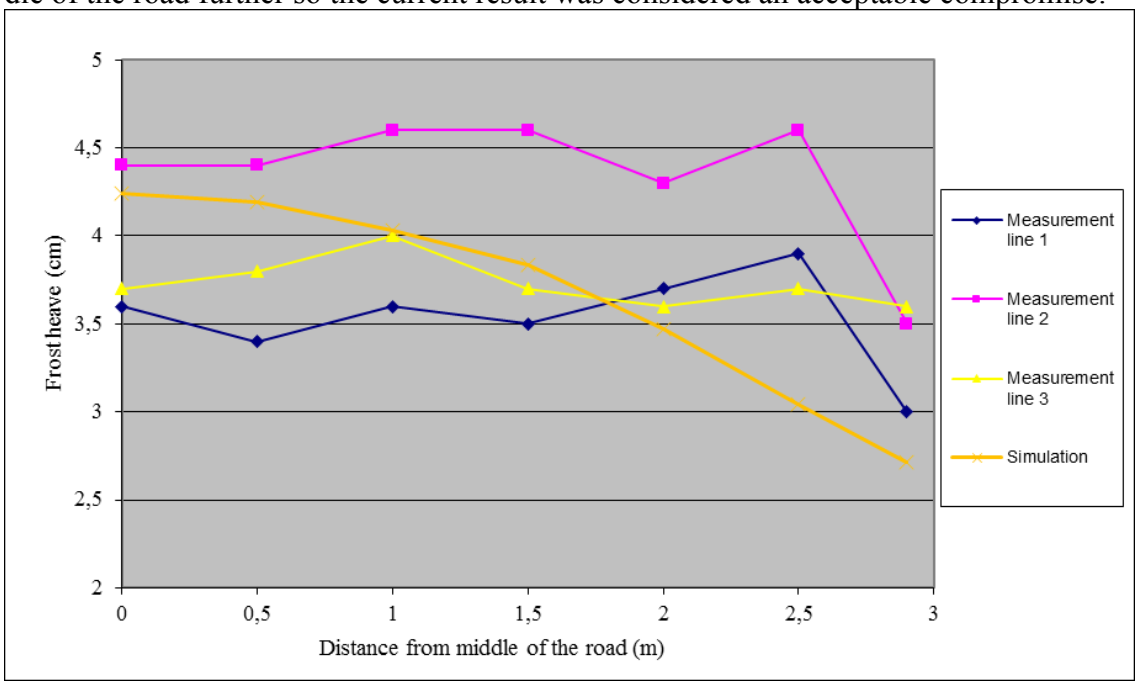

Figure 33 Calculated frost heave in comparison to the three cross section measurements of the high frost heave.

The pavement surface profile in comparison with the three cross section measurement lines after thaw in May is visible in Figure 34. As noted, the calculation indicates slowly increasing vertical deformation after thaw when employing a realistic value of thermal expansion coefficient.

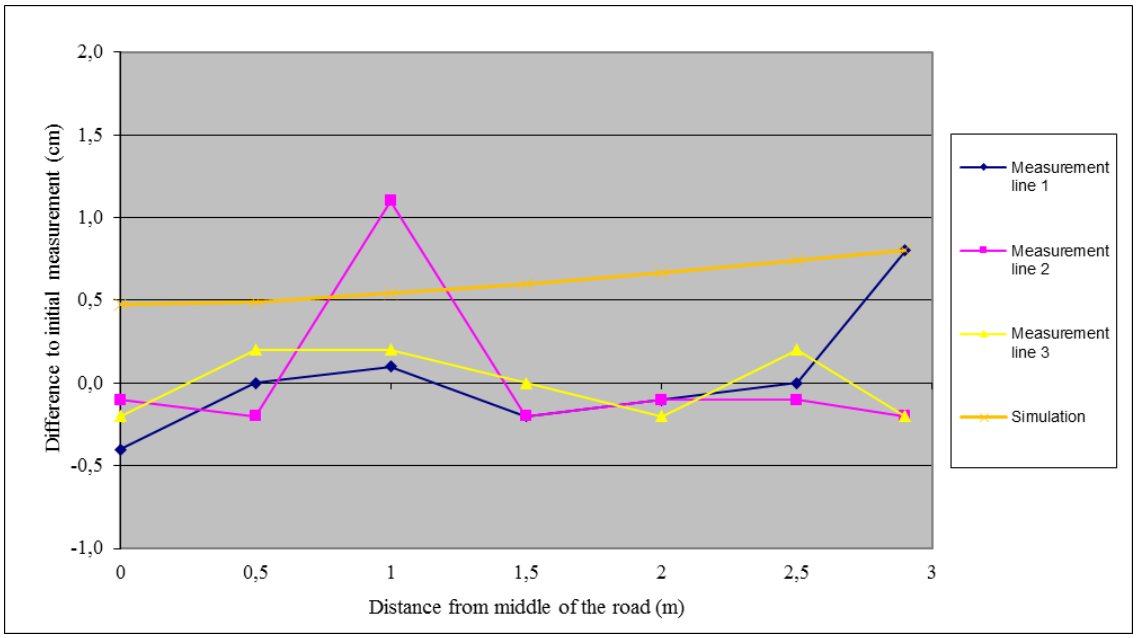

Figure 34 Calculated pavement surface after thaw in comparison to the three cross section measurements after thawing.

The frost depth reached its deepest extent after the freezing phases which is illustrated in Figure 35. Comparing the simulated frost depth to the measured values shows that under the middle of the road the frost depth is at its deepest circa 1.7 m compared to 1.2 m. At the edge of the road the frost depth is close 1 m, which was also the measured value.

The thawing of the road with time agrees well with the measurement data as the calculation indicates the middle of the road is thawed at the end of April and the edge around a week earlier.

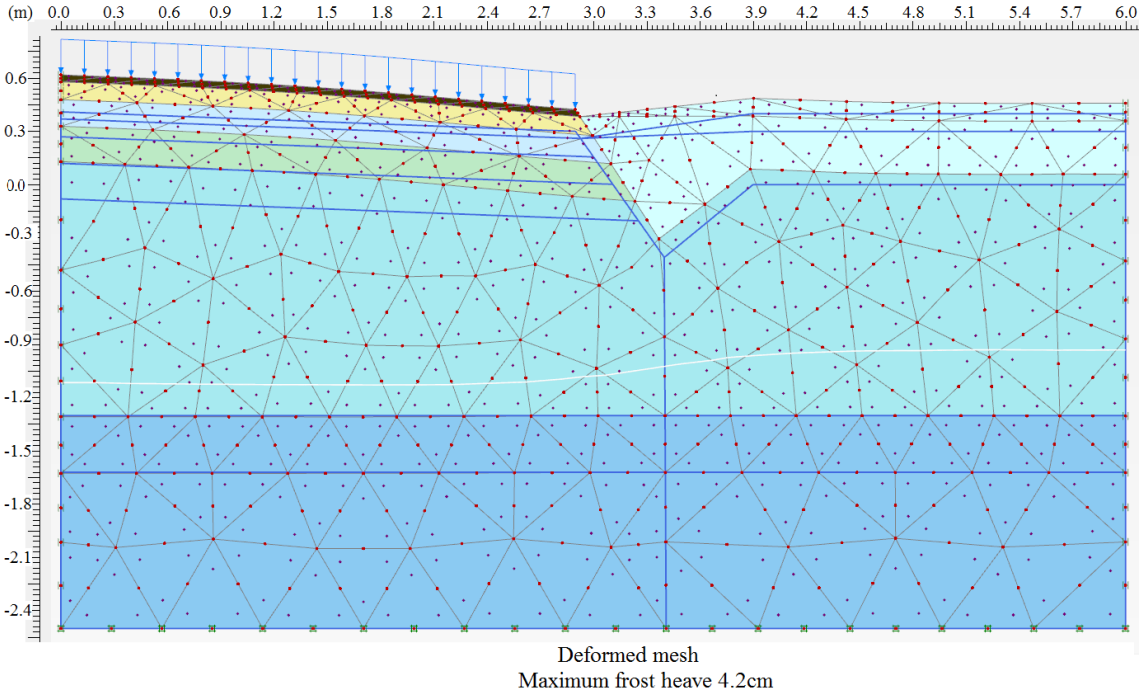

Figure 35 Frost depth at its deepest and frost heave after the freezing phases. Frost depth indicated by the white line.

The temperature profile of the soil after the primary freezing phase and thaw phases is illustrated in Figure 36 and Figure 37. It can be seen that after the varying temperature phase the surface is warmer than the subgrade under the road, as expected, and in the long term the temperature differences in the ground at depth diminish to a steady state.

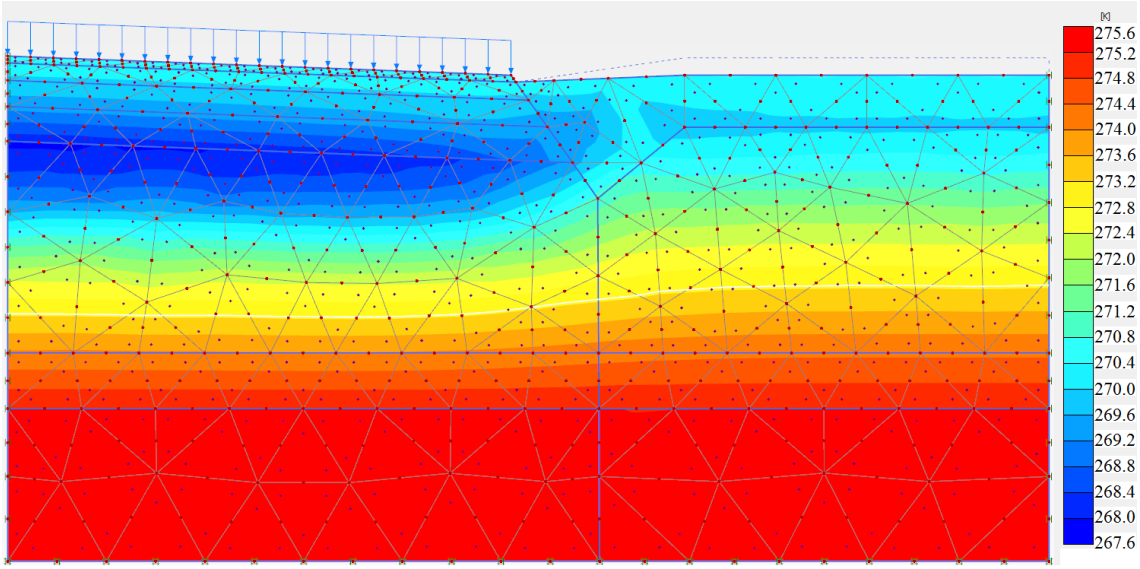

Figure 36 Temperature profile after primary freezing phase.

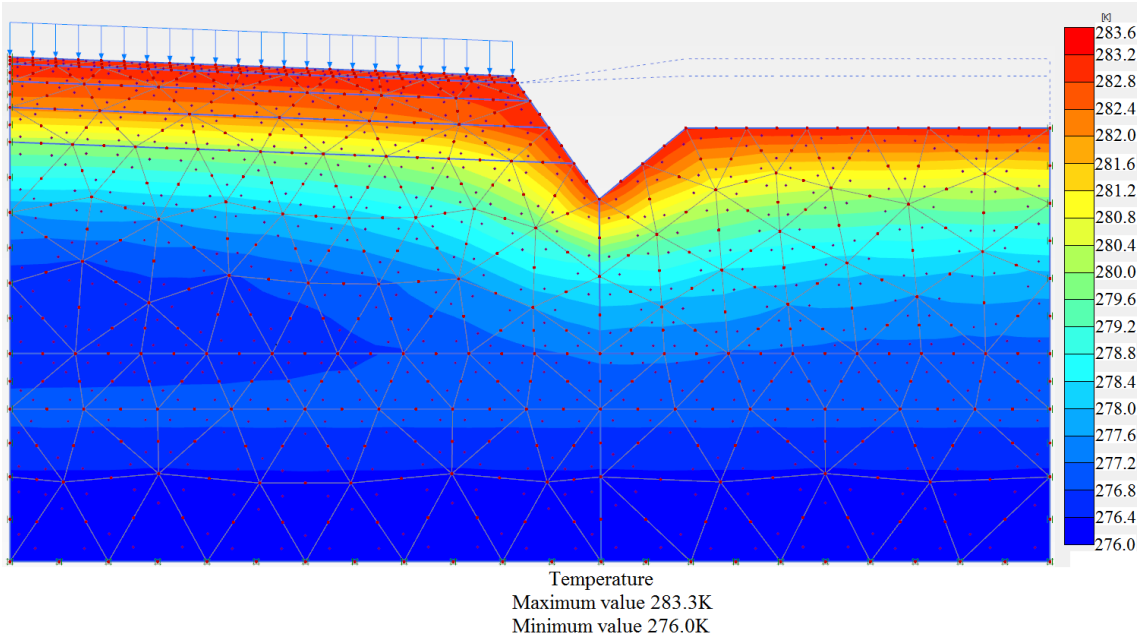

Figure 37 Temperature profile after the second thawing phase.

The ice saturation at its largest extent after the primary freezing phase is shown below in Figure 38. The coarse-grained road structure is frozen through and the fine-grained clay is freezing more gradually due to the premelting effects described in chapter 5.3. The snow packed in the ditch and on the clay in the field side hinders freezing of the clay beneath it.

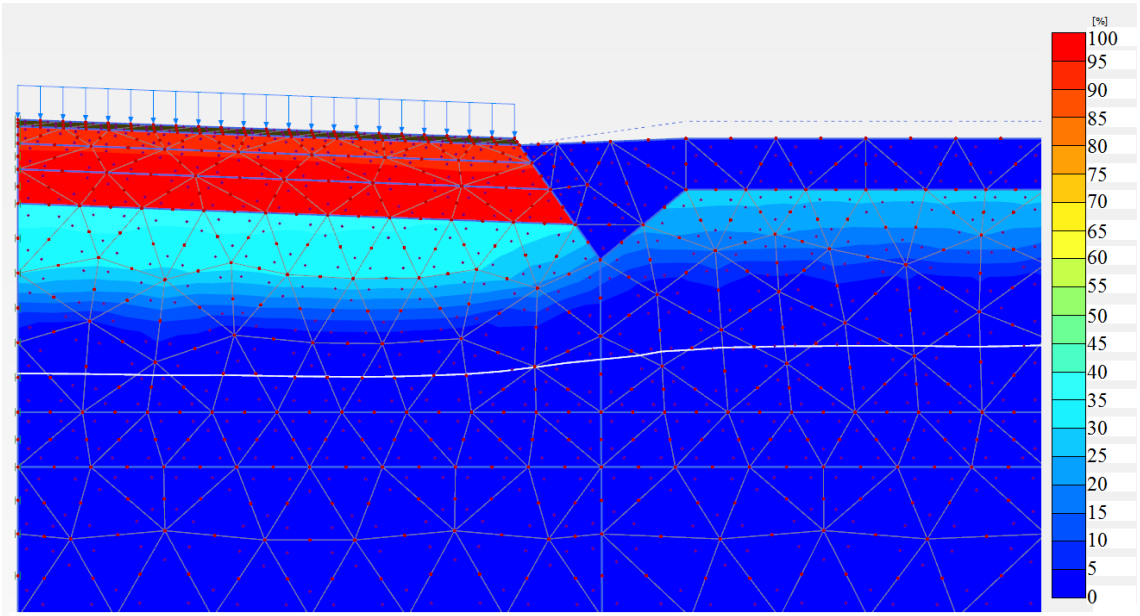

Figure 38 Ice saturation after the primary freezing phase.

The unfrozen state preconsolidation stress decreases in the calculation as the grain segregation yield curve is hit. This is in accordance to the model framework, but there seems to be some errors in the calculation in this regard as the results indicate that during the freezing the stress decreases even below zero but recovers during thawing as should happen. This is visible in Figure 39, Figure 40 and Figure 41 (sign of the stress is opposite in the figures according to Plaxis sign convention).

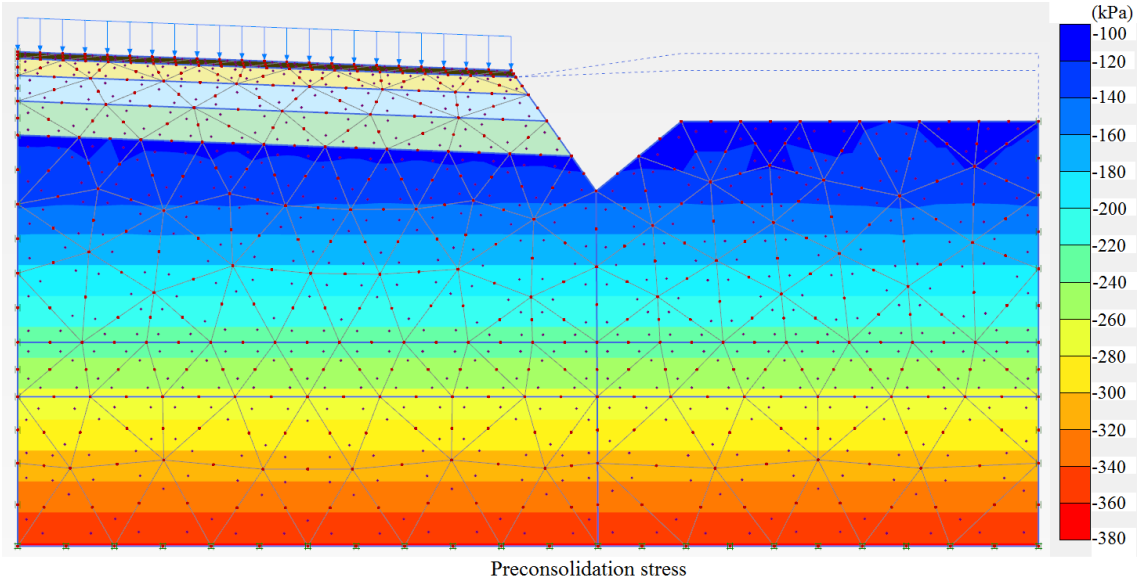

Figure 39 Initial unfrozen state preconsolidation stress distribution.

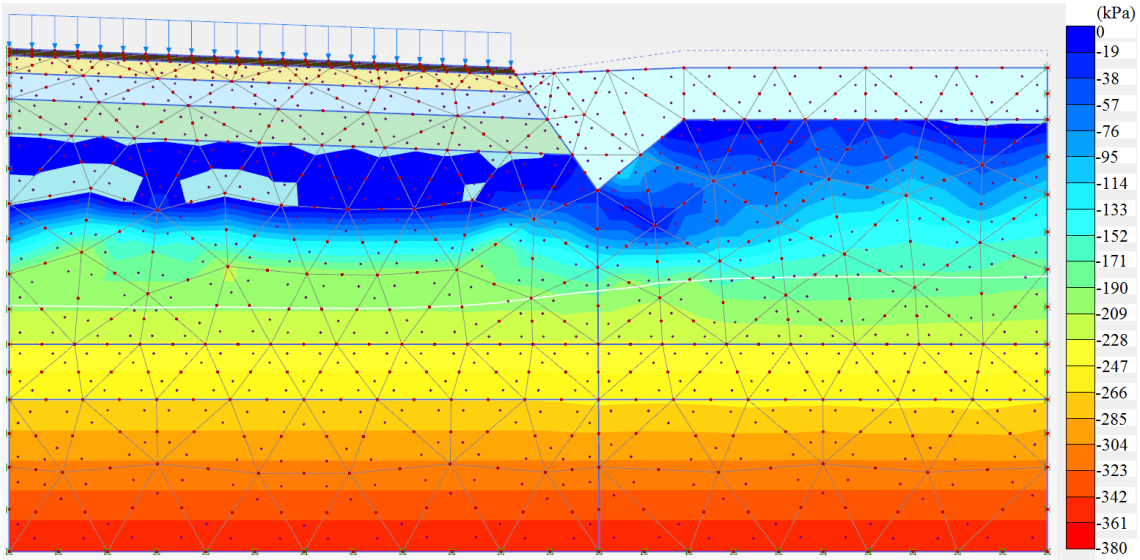

Figure 40 Preconsolidation stress after freezing. Small sections can be seen under the surface where the preconsolidation stress has decreased below zero.

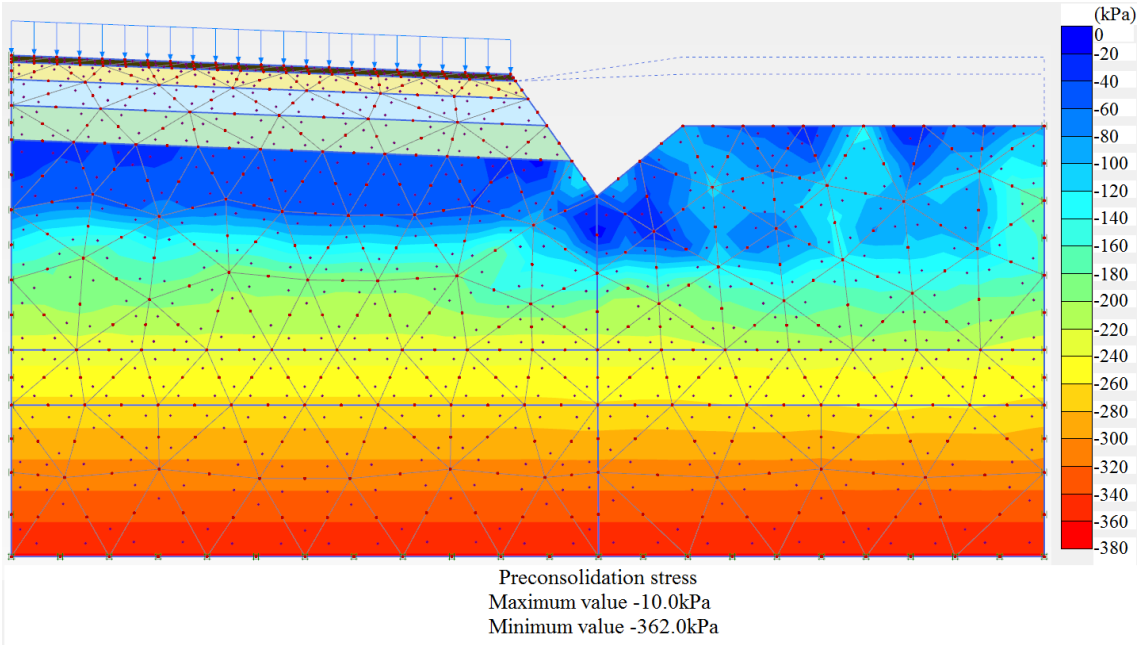

Figure 41 Preconsolidation stress after thawing.

The ice segregation threshold increases with the cryogenic suction during the freezing phases as expected. This is visible in the following Figure 42 and Figure 43 comparing states during early freezing when the cryogenic suction has not increased above segregation threshold and after primary freezing when the cryogenic suction has reached its highest magnitude. The initial value of segregation threshold has a major effect on the maximum magnitude of the calculated frost heave, a less than 10 % decrease in the value of the segregation threshold could increase the maximum heave by over one third from 30 mm to over 40 mm.

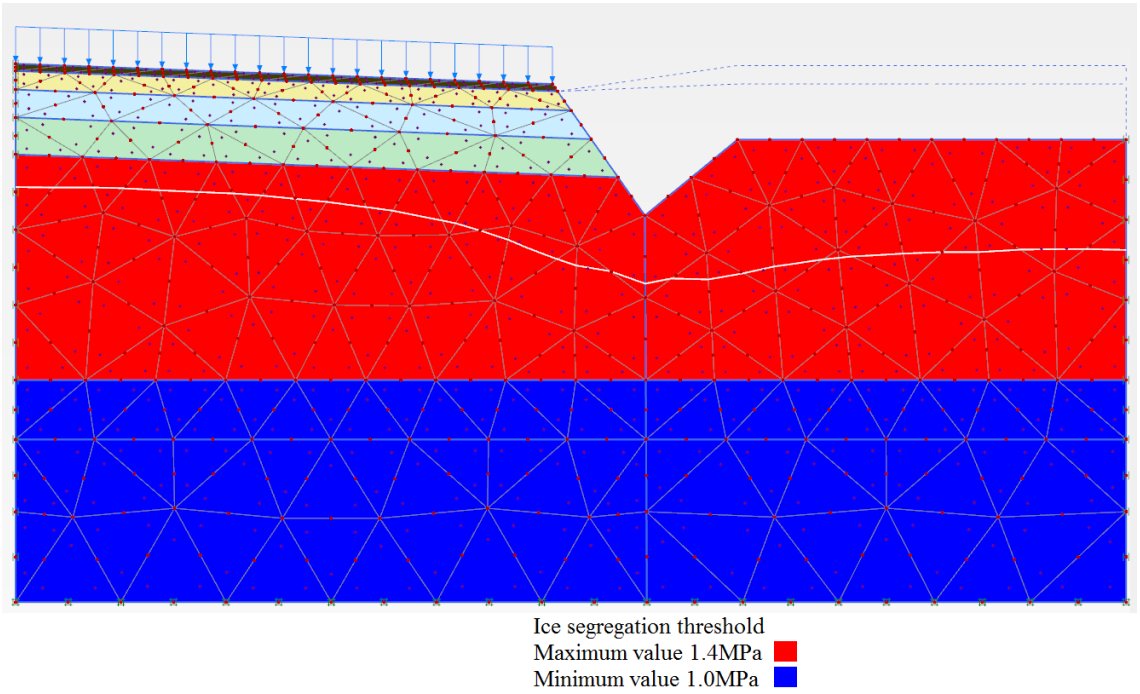

Figure 42 Initial segregation threshold before primary freezing phase.

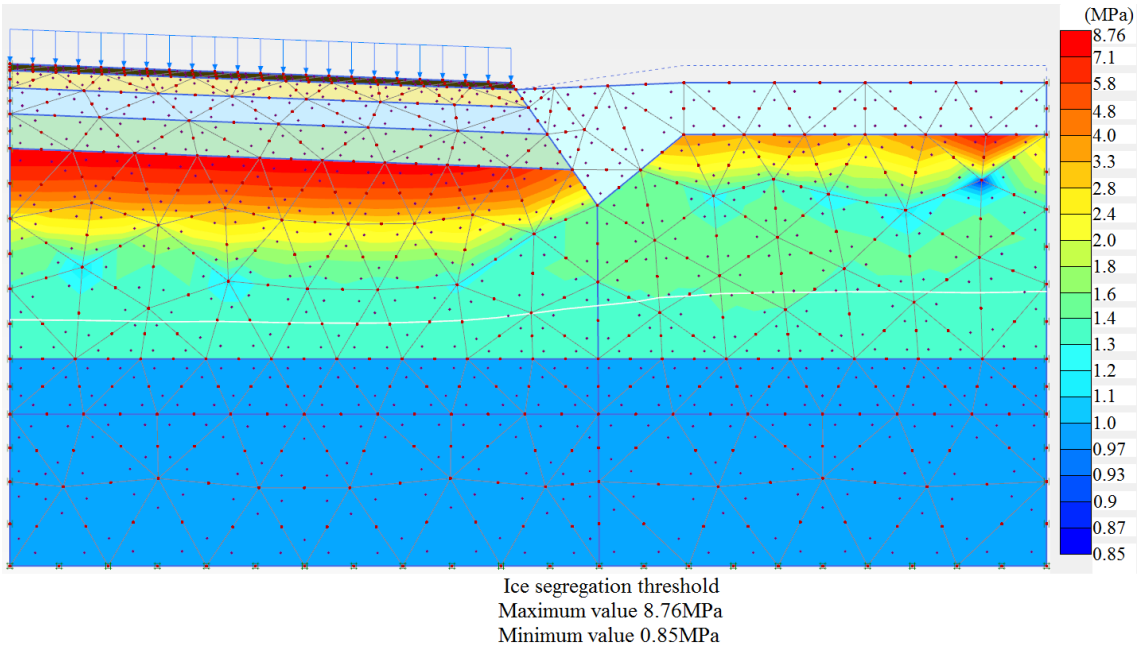

Figure 43 Segregation threshold after the primary freezing.

It seems that there are errors in the calculation with the groundwater flow during freezing and thawing. During freezing it would be expected that the water flows into the freezing soil and conversely during thawing out of it. The results indicate that the opposite is happening as visible in Figure 44 and Figure 45. As expected, the decrease of hydraulic conductivity in the frozen clay limits the water flow during freezing in comparison to thaw, while the water flows more readily through the higher hydraulic conductivity structural layers during thaw, but the flow still seems to be at least partially into the frozen layer rather than out of it during the thaw.

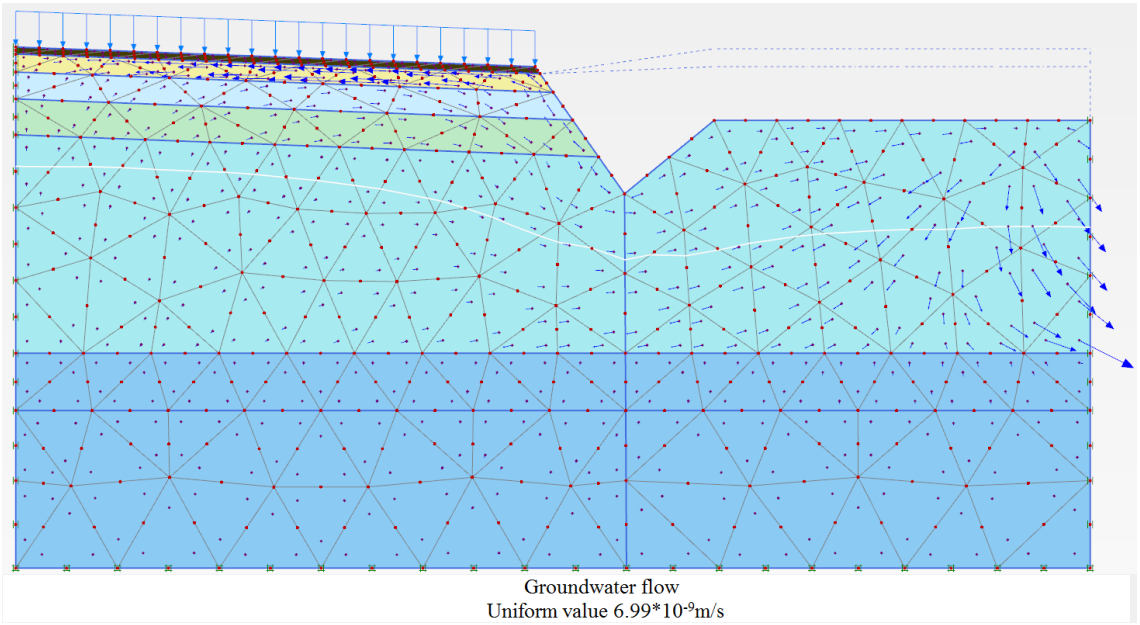

Figure 44 Groundwater flow during freezing.

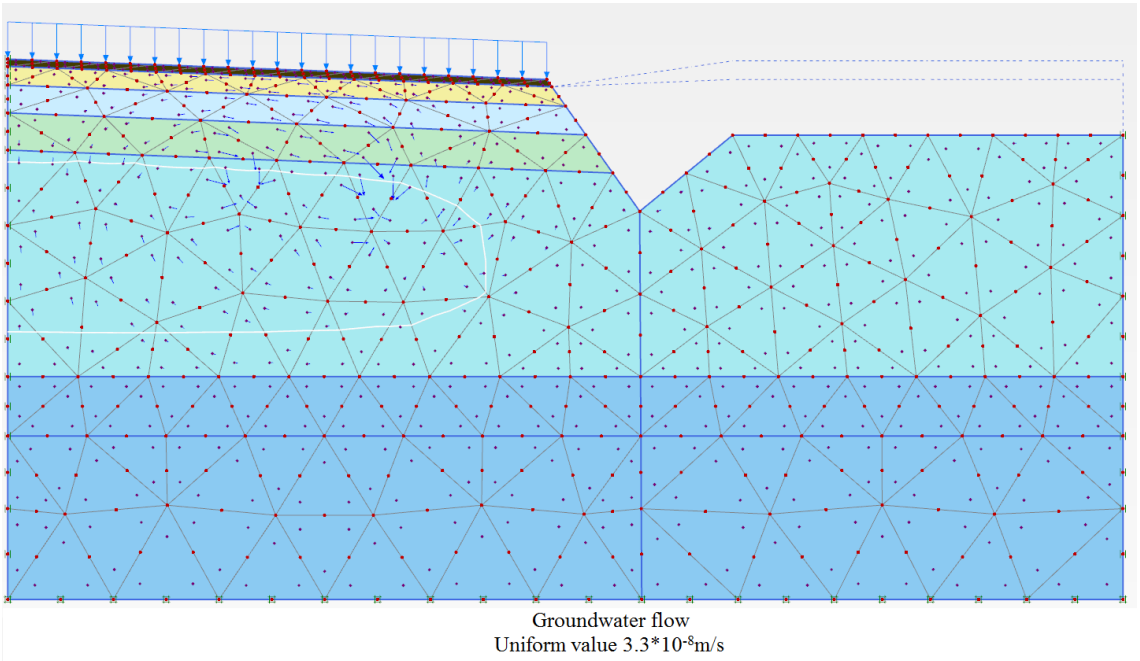

Figure 45 Water flow during thawing.

The thawing of the road proved to be the most troublesome part of the calculation as Plaxis struggled with calculating the thawing at all due to unknown errors related to the user-defined soil model or indicated that the road embankment slope was failing during thaw as the preconsolidating stress increased again as the ice melted. The mesh was refined to improve the iteration process, maximum iteration number in the thaw phases was increased from 60 to 200 and the parameter k_t affecting soil cohesion increase with cryogenic suction was increased to prevent slope failure during thaw.

The achieved frost heave results are in good qualitative accordance with the measurements as shown in Figure 33 and Figure 34. The calculation process was time consuming and there were unknown errors at many points when Plaxis indicated the calculation failed

due to unelaborated user-defined soil model related errors. No complete step-by-step examples of simulations with the model are provided by the developers, limiting the ability of a user to study the model on their own. Including these in the model material would be a great help in using the model on a case study. One prospect of future work on improving the user-defined soil model would be to implement actual error messages so the user could have a deeper understanding of what was awry in a calculation and could improve their simulation more concisely instead of resorting to best estimates in face of unknown. In the current state of the model, the error messages did not give any information on the nature of the problem encountered, limiting the insight the user could gain on the viability of the model constitutive framework implementation in Plaxis and making the calculation process uncertain at times as seemingly reasonable parameter combinations would yield no results at all. It should be noted that simpler methods for analyzing frost effects such as frost heave in pavements exist, for example the SSR method by Saarelainen (1992) has been proven adequate for the task of estimating frost heave of pavements in Finland.

Based on the clay laboratory test data and Vesilahti temperature and groundwater measurements, the boundary conditions and geometry of the model were implemented along with basic clay parameters. The thermal parameters of the clay were estimated from literature for best fit to measurements. The clay model parameters were then calibrated during the calculations to fit the heave results at given times. As mentioned previously, one improvement on this work could be to analyze these properties with appropriate laboratory measurements to reduce degrees of freedom in the simulation.

As very little was known of the pavement structure material properties and snow during the winter, parameters of these materials were also mostly estimated using literature values. The model yielded results in harmony with the expected behavior for most parts, but the process was at times arduous and took time. The modelled frost depth was deeper than measured, but in balancing the heave and frost penetration, the desired heave was the priority. With realistic values of clay thermal expansion coefficient, the calculation results indicate that the road surface rises after thawing, but this can be solved by using negligible or zero values of the coefficient. There are some issues with the decrease of preconsolidation stress and groundwater flow in the calculation, but the root cause of these remained unclear.

In this case study the available measurement data was three level measurements at different time intervals instead of continuous frost heave data. For the purpose of future numerical simulations with this model it would be useful to obtain continuous measurement data to better utilize the capabilities of the model and observe the development of frost heave instead of concentrating on a few select times. The simulated winter was rather mild in this case, but an interesting research path could be to model a colder winter and estimate the development of frost heave in the road and compare it with continuous measurement of frost heave. In the scope of this thesis the focus was on replicating the magnitude of frost heave at the measurement times due to the nature of the source data, but more information on the pavement structure behavior during freezing could be gained by investigating the rate of heave and the cumulative result of continued freezing and thawing.

9 Conclusions and suggestions for future research

In this thesis the frost heave of a road in Vesilahti was studied using the Frozen and Unfrozen Soil model in Plaxis 2D finite element software. For this purpose, a literature review on frozen soil, pavement behavior during freezing and the constitutive model was conducted, and sampling and laboratory analyses on the dry crust clay subgrade from Vesilahti were performed.

Pavement structures undergoing freezing and thawing are subjected to a great variation of environmental conditions inducing various loadings and stresses. Factors affecting the pavement performance under these varying conditions are the quality and properties of the pavement structure itself, subgrade soil, drainage conditions and rate of freezing and thawing. During freezing, uneven frost heave can cause deterioration of pavement service performance due to surface roughness and thermal cracking of the bituminous surface caused by stresses induced in the pavement by varying frost heave. During thawing the pavement can weaken significantly due to accumulation of meltwater in the structure or the subgrade, and combined with heavy traffic loading, this can cause heavy damage to the pavement surface and the granular layers leading to cracking and rutting.

The Frozen and Unfrozen Soil model has been proven to be able to model complex multiphysical phenomena in both freezing and thawing soil. The model is, however, rather complex, precisely due to the complexity of modelling those phenomena, and especially the choice of the many model parameters presents a challenge to bringing the model into design practice even though the model is available in the common geotechnical finite element software Plaxis 2D. The implementation of the model and its constitutive equations in Plaxis is non-transparent to the end user so the causes behind the modelled behavior and especially calculation issues can be difficult to analyze. The source material of the model is not abundant with advice for the user, nor are there any in-depth, complete calculation examples where a model simulation is explained step by step. Sources of errors in the simulations often remained a mystery as the calculation failed due to unexplained reasons. Concluding, in its current state the model implementation in Plaxis is not deemed to be very user-friendly. Improvements could include, for example: (i) provision of full step-by-step examples of model simulations for the user to familiarize themselves with the model, and (ii) implementation of the actual user-defined soil model specific error messages in Plaxis in order to improve the information the user has on their calculation results and failures in calculation and enabling them to solve possible problems in a more effective manner.

In addition to the general soil parameters the model incorporates 28 model parameters, many of which are not standardly used in the engineering practice and deriving them can be quite challenging. In this thesis these parameters were derived for Vesilahti clay based on previous work with the Frozen and Unfrozen Soil model and with a time-consuming trial and error process to fit the calculation results to measurements. Using the proposed temperature- and suction-controlled laboratory tests for obtaining these parameters would reduce the degrees of freedom in the calculation and calibration process and help to better validate the results beyond qualitative fitting of experimental measurements. Additional experimental tests for the thermal properties and unfrozen water saturation of the clay would also limit the uncertainty of these parameters and the need to calibrate the thermal parameters. However, suction-controlled frost heave tests are not performed in Finland at the moment of writing. Implementing these tests could provide interesting opportunities for testing model and its predicted behavior, while comparing experimental parameters to the fitted ones. Additionally, utilizing continuous road frost heave measurement for the

simulations in future could be very beneficial as some of the predictive capabilities of the model are neglected by simply focusing on a few time intervals.

The model replicated the Vesilahti frost heave measurements qualitatively well. The freezing performance of the soil matched expected behavior and the calculated heave at the high frost heave and the thaw time increments was very close to measured values. The heave in time corresponded with expected behavior due to variation of temperature conditions and cryogenic suction. The major effect on the development and magnitude of frost heave was by the temperature variation between extremes in the primary freezing phase, the clay initial value of ice segregation threshold and the elastoplastic compression coefficient of cryogenic suction variation, which affected the development of cryogenic suction in the clay and the deformation dependency on it. The pavement structure settled in the initial phases of positive and small negative temperatures, in the latter as expected under the effect of the elastic compressibility coefficient for suction variation when the cryogenic suction had not exceeded the segregation threshold. In the following freezing phases, the heave increased quickly during the temperature decrease periods and stayed almost constant during the increase to a higher (but still below the freezing point of water) temperature. The insulating effect of the assumed snow layer was noticeable on the frost heave across the road cross section in the calculations as the heave clearly decreased toward the edge of the road where the snow insulated the embankment ditch and slope while the measured heave was in reality very uniform.

During the thawing phases the decreased hydraulic conductivity of the soil and pavement layers and the gradual temperature increase in the clay at depth initially dictated the slow decrease of the heave as the pavement layers not contributing to the frost heave first thawed from the surface and the frozen clay thawed only from below. The heave then decreased more quickly when the road structure had completely thawed and the clay was able to thaw from both sides with water able to flow through the higher hydraulic conductivity unfrozen pavement layers on top. The early calculations indicated failure of the road slope during thawing as the preconsolidation stress increased after the melting of the ice which was prevented by increasing the value of the parameter k_t controlling the increase of clay cohesion with cryogenic suction, making the clay stronger due to the freezing. The calculation predicted slight heave of pavement surface after thawing due to thermal expansion of the clay under increasing temperature, with very low values of thermal expansion coefficient this did not occur. There were inconsistencies with the predicted change of the preconsolidation pressure and the groundwater flow in the simulation, but whether these are due to parameter choice or numerical issues in the fully coupled flow deformation calculation with the model is unclear.

Based on the simulations performed in this research, the Vesilahti road deformations were reproduced successfully and it can be concluded that the Frozen and Unfrozen Soil model is a valid approach to assessing deformation of a road structure on frost-susceptible subgrade during freezing and thawing. However, it is not a pavement permanent deformation model and should not be treated as such. As illustrated in the thesis, the model can capture effects of freezing and thawing on pavement structure deformations caused by the subgrade soil, but it is not made to represent pavement specific issues such as deterioration by fatigue or cracking. Work with the model can be very time consuming and demanding due to the complexity of the parameter determination and the multiple interlinked physical phenomena handled along with the black box model implementation nature for a user. Issues in the simulations might stem from many different combinations of parameters which makes special care in parameter definition and testing in calculations very much

necessary. In its current state the model is not suitable for standard infrastructure design work in a state of practice context while simpler and easier to use methods for assessing frost effects in pavements exist. Further research into developing and performing suction-controlled frost heave tests and temperature-controlled oedometer and uniaxial compression tests in Finland would benefit the future work with the Frozen and Unfrozen Soil model and its utilization into practical problems by grounding the model parameter choice in experimental results and could provide opportunities in evaluating the model performance. Another major opportunity could be developing a totally new frozen soil numerical model from the ground, which would allow greater control on and more transparent interaction with the model constitutive framework and its implementation into practice in a numerical application.

10 References

Alonso, E.E., Gens, A., Josa, A., 1990. A constitutive model for partially saturated soils. Géotechnique 40, 405–430. https://doi.org/10.1680/geot.1990.40.3.405

Andersland, O.B., Ladanyi, B., 2004. Frozen Ground Engineering. John Wiley & Sons.

Anderson, D., Williams, P., Guymon, G., Kane, D., 1984. PRINCIPLES OF SOIL FREEZING AND FROST HEAVING.

Anderson, D.M., Tice, A.R., 1972. Predicting unfrozen water contents in frozen soils from surface area measurements, in: Highway Research Record. Presented at the 51st Annual Meeting of the Highway Research Board.

Aukenthaler, M., 2016. The Frozen & Unfrozen Barcelona Basic Model.

Brinkgreve, R.B.J., Kumarswamy, S., Swolfs, W.M., 2017. Plaxis 2D Manual 2017.

Campbell, G.S., 1985. Soil Physics with BASIC: Transport Models for Soil-Plant Systems. Elsevier.

Chen, J., Wang, H., Li, L., 2015. Determination of Effective Thermal Conductivity of Asphalt Concrete with Random Aggregate Microstructure. Journal of Materials in Civil Engineering 27. https://doi.org/10.1061/(ASCE)MT.1943-5533.0001313

Cicchetti, L., 2018. Thermo-Hydro-Mechanical simulations of artificial ground freezing.

Dore, G., Zubeck, H.K., 2009. Cold Regions Pavement Engineering, 1st ed. McGraw-Hill.

Fourier, J.B.J., 1878. The Analytical Theory of Heat. Cambridge University Press, London, United Kingdom. https://doi.org/10.1017/CBO9780511693205

Gandahl, R., 1987. Tjäle och tjälskydd : Erfarenheter från FoU-verksamheten vid SVI och VTI. Statens Väg- och Trafikinstitut., VTI meddelande 546.

Gerling, B., Löwe, H., van Herwijnen, A., 2017. Measuring the Elastic Modulus of Snow. Geophysical Research Letters 44, 11,088-11,096. https://doi.org/10.1002/2017GL075110

Ghoreishian Amiri, S.A., Grimstad, G., Aukenthaler, M., Panagoulias, S., Brinkgreve, R.B.J., Haxaire, A., 2016a. The Frozen and Unfrozen Soil Model Manual.

Ghoreishian Amiri, S.A., Grimstad, G., Kadivar, M., Nordal, S., 2016b. Constitutive model for rate-independent behavior of saturated frozen soils. Canadian Geotechnical Journal 53, 1646–1657. https://doi.org/10.1139/cgj-2015-0467

Harlan, R.L., 1973. Analysis of Coupled Heat-Fluid Transport in Partially Frozen Soil. Water Resources Research 9, 1314–1323. https://doi.org/10.1029/WR009i005p01314

Heindel, Noyes, 1997. Permeability of Highway Base and Sub-base Material (Research Report). Vermont Agency of Transportation, Vermont.

Huotari, T., Kukkonen, I., 2004. Thermal Expansion Properties of Rocks: literature Survey and Estimation of Thermal Expansion Coefficient for Olkiluoto Mica Gneiss (Working report No. 2004– 04). Posiva Oy, Olkiluoto.

ISSMFE-TC8, 1989. Work report 1985-1989, in: Proceedings of the International Symposium on Frost in Geotechnical Engineering, VTT Symposium 94-95. Presented at the Frost in Geotechnical Engineering: International Symposium 1989, VTT, Saariselkä, pp. 15–70.

Jobmann, M., Polster, M., Schonebeck, M., 2007. Investigation on Thermal Expansion Effects in Clay Formations (Investigation report). DBE Technology GmbH, Peine.

Johansson, L.S., Lu, X., Isacsson, U., 1998. Ageing of road bitumens: state of the art. TRITA-IP FR 98, 45.

Johnston, G.H., 1981. Permafrost: engineering design and construction. Wiley.

Kangas, H., Onninen, H., Saarelainen, S., 2000. Testing a pavement on thawing, frost-susceptible subgrade with the heavy vehicle simulator. Tielaitos.

Kuroiwa, D., 1968. Liquid permeability of snow. Low Temperature Science A26, 29–52.

Lai, Y., Yang, Y., Chang, X., Li, S., 2010. Strength criterion and elastoplastic constitutive model of frozen silt in generalized plastic mechanics. International Journal of Plasticity 26, 1461–1484. https://doi.org/10.1016/j.ijplas.2010.01.007

Li, N., Chen, F., Xu, B., Swoboda, G., 2008. Theoretical modeling framework for an unsaturated freezing soil. Cold Regions Science and Technology 54, 19–35. https://doi.org/10.1016/j.coldregions.2007.12.001

Liikennevirasto, 2018. Liikenneviraston ohjeita 38/2018 Tierakenteen suunnittelu.

Luomala, H., Ryynänen, T., Belt, J., Alatyppö, V., Lampinen, A., 2008. Management of Pavement Service Life by Using New Technology (Research Report No. 74), Earth and Foundation Structures. Tampere University of Technology, Tampere.

Ma, B., Zhou, X., Liu, J., You, Z., 2016. Determination of Specific Heat Capacity on Composite Shape-Stabilized Phase Change Materials and Asphalt Mixtures by Heat Exchange System. Materials 9, 389–404. https://doi.org/10.3390/ma9050389

Maher, A., Bennert, T., 2008. Evaluation of Poisson's Ratio for Use in the Mechanistic Empirical Pavement Design Guide (MEPDG) (Research report No. FHWA-NJ-2008-004). Rutgers State University, Piscataway.

Minkoff, S.E., Stone, C.M., Bryant, S., Peszynska, M., Wheeler, M.F., 2003. Coupled fluid flow and geomechanical deformation modeling. Journal of Petroleum Science and Engineering 38, 37–56. https://doi.org/10.1016/S0920-4105(03)00021-4

Nishimura, S., Gens, A., Olivella, S., Jardine, R.J., 2009. THM-coupled finite element analysis of frozen soil: formulation and application. Géotechnique 59, 159–171. https://doi.org/10.1680/geot.2009.59.3.159

Nixon, J.F. (Derick), 1991. Discrete ice lens theory for frost heave in soils. Can. Geotech. J. 28, 843–859. https://doi.org/10.1139/t91-102

Nordal, R.S., Refsdal, G., 1989. Frost protection in design and construction, in: Proceedings of the International Symposium on Frost in Geotechnical Engineering, VTT Symposium 94-95. Presented at the Frost in Geotechnical Engineering: International Symposium 1989, VTT, Saariselkä, pp. 127–63.

Obrzud, R.F., Truty, A., 2018. The Hardening Soil model - a practical guidebook (Material model guide No. 100701), Z_Soil PC report. Zace Services, Preverenges.

Petersen, D.R., Link, R.E., Mamlouk, M., Witczak, M.W., 2005. Determination of Thermal Properties of Asphalt Mixtures. Journal of Testing and Evaluation 33, 12592. https://doi.org/10.1520/JTE12592

Rajaei, P., Baladi, G.Y., 2015. Frost Depth. Transportation Research Record Journal of the Transportation Research Board 74–80. http://dx.doi.org/10.3141/2510-09

Rempel, A.W., 2007. Formation of ice lenses and frost heave. Journal of Geophysical Research: Earth Surface 112. https://doi.org/10.1029/2006JF000525

RIL 218-2001, 2001. Lumirakenteiden suunnittelu- ja rakentamisohjeet, RIL Ohjeet ja normit. Suomen Rakennusinsinöörien Liitto RIL r.y.

Roberts, F.L., Kandhal, P.S., Brown, E.R., Lee, D.-Y., Kennedy, T.W., 1996. Hot mix asphalt materials, mixture, design and construction, 2nd ed. National Asphalt Pavement Association Research and Education Foundation, Lanham, Md. US.

Rostami, H., 2017. Finite Element Analysis of Coupled Thermo-Hydro-Mechanical Processes in Fully Saturated, Partially Frozen Soils 103.

Roy, M., Rochelle, P.L., Leroueil, S., Konrad, J.M., Bergeron, G., 1995. Effets de cycles de gel–dégel sur les propriétés d'une argile sensible. Can. Geotech. J. 32, 725–740. https://doi.org/10.1139/t95-070

Saarelainen, S., 1992. Modelling frost heaving and frost penetration in soils at some observation sites in Finland: the SSR model, VTT Publications. Technical Research Centre of Finland, Espoo.

Saarenketo, T., Pyhähuhta, M., Munro, R., 2012. What is permanent deformation and why we do not like it. ROADEX E-learning. URL https://www.roadex.org/e-learning/lessons/permanent-deformation/what-is-permanent-deformation-and-why-we-do-not-like-it/ (accessed 6.2.19).

Schofield, A., Wroth, P., 1968. Critical State Soil Mechanics.

Sepaskhah, A.R., Tabarzad, A., Fooladmand, H.R., 2010. Physical and empirical models for estimation of specific surface area of soils. Archives of Agronomy and Soil Science 56, 325–335. https://doi.org/10.1080/03650340903099676

Seppälä, M., 1997. Distribution of permafrost in Finland. Bulletin of the Geological Society of Finland 69, 87–96. https://doi.org/10.17741/bgsf/69.1-2.007

Shibata, T., Adachi, T., Yashima, A., Takahashi, T., Yoshioka, I., 1985. Time-dependence and volumetric change characteristic of frozen sand under triaxial stress condition. Ground freezing. Proc. 4th international conference, Sapporo, 1985 173–179.

Shirazi, M.A., Boersma, L., 1984. A unifying quantitative analysis of soil texture. Soil Science Society of America Journal 48, 142–147. https://doi.org/10.2136/sssaj1984.03615995004800010026x

Sidler, R., 2014. Snow Slab Failure Due to Biot-Type Acoustic Wave Propagation, in: International Snow Science Workshop Proceedings 2014. Presented at the International Snow Science Workshop, Banff, pp. 146–150.

Simonsen, E., 1999. On thaw weakening of pavement structures (Dissertation). KTH, Stockholm.

Sundberg, J., 1988. Thermal properties of soils and rocks. Chalmers University of Technology, Linnköping.

Taha, M.R., Hardwiyono, S., Yusoff, N.I.M., Hainin, M.R., 2013. Study of the Effect of Temperature Changes on the Elastic Modulus of Flexible Pavement Layers. Research Journal of Applied Sciences, Engineering and Technology 5, 1661–1667. https://doi.org/10.19026/rjaset.5.4920

Tarnawski, V.R., Wagner, B., 1996. On the prediction of hydraulic conductivity of frozen soils. Can. Geotech. J. 33, 176–180. https://doi.org/10.1139/t96-033

Teng, J., Shan, F., He, Z., Zhang, S., Zhao, G., Sheng, D., 2018. Experimental study of ice accumulation in unsaturated clean sand. Géotechnique 1–9. https://doi.org/10.1680/jgeot.17.P.208

Thomas, H.R., Cleall, P., Li, Y.-C., Harris, C., Kern-Luetschg, M., 2009. Modelling of cryogenic processes in permafrost and seasonally frozen soils. Géotechnique 59, 173–184. https://doi.org/10.1680/geot.2009.59.3.173

Tsytovich, N.A., 1975. The mechanics of frozen ground. Scripta Book Co.

van Genuchten, M.T., 1980. A Closed-form Equation for Predicting the Hydraulic Conductivity of Unsaturated Soils. Soil Science Society of America Journal 44, 892–898. https://doi.org/10.2136/sssaj1980.03615995004400050002x

Wagner, W., Riethmann, T., Feistel, R., Harvey, A.H., 2011. New Equations for the Sublimation Pressure and Melting Pressure of H_2O Ice Ih. Journal of Physical and Chemical Reference Data 40, 043103. https://doi.org/10.1063/1.3657937

Yang, Z., 2013. Study of Minimum Void Ratio for Soils with a Range of Grain-Size Distributions (Master's thesis). University of Massachusetts Amherst, Amherst.

Zhang, S., Teng, J., He, Z., Liu, Y., Liang, S., Yao, Y., Sheng, D., 2016a. Canopy effect caused by vapour transfer in covered freezing soils. Géotechnique 66, 927–940. https://doi.org/10.1680/jgeot.16.P.016

Zhang, X., Alonso, E.E., Casini, F., 2016b. Explicit formulation of at-rest coefficient and its role in calibrating elasto-plastic models for unsaturated soils. Computers and Geotechnics 71, 56–68. https://doi.org/10.1016/j.compgeo.2015.08.012

Zhang, Y., 2014. Thermal-Hydro-Mechanical Model for Freezing and Thawing of Soils. (Dissertation). University of Michigan, Michigan.

Zhou, G., Hu, K., Zhao, X., Wang, J., Liang, H., Lu, G., 2015. Laboratory investigation on tensile strength characteristics of warm frozen soils. Cold Regions Science and Technology 113, 81–90. https://doi.org/10.1016/j.coldregions.2015.02.003

Zohrabi, M., Temporal, J., 2001. The permeability of structural backfills (Research Report No. TRL478). TRL, Berks.